Next Generation Shade-Tolerant Reconfigurable PV Modules for Urban Landscapes

by Raoul Weegink

Graduation Project

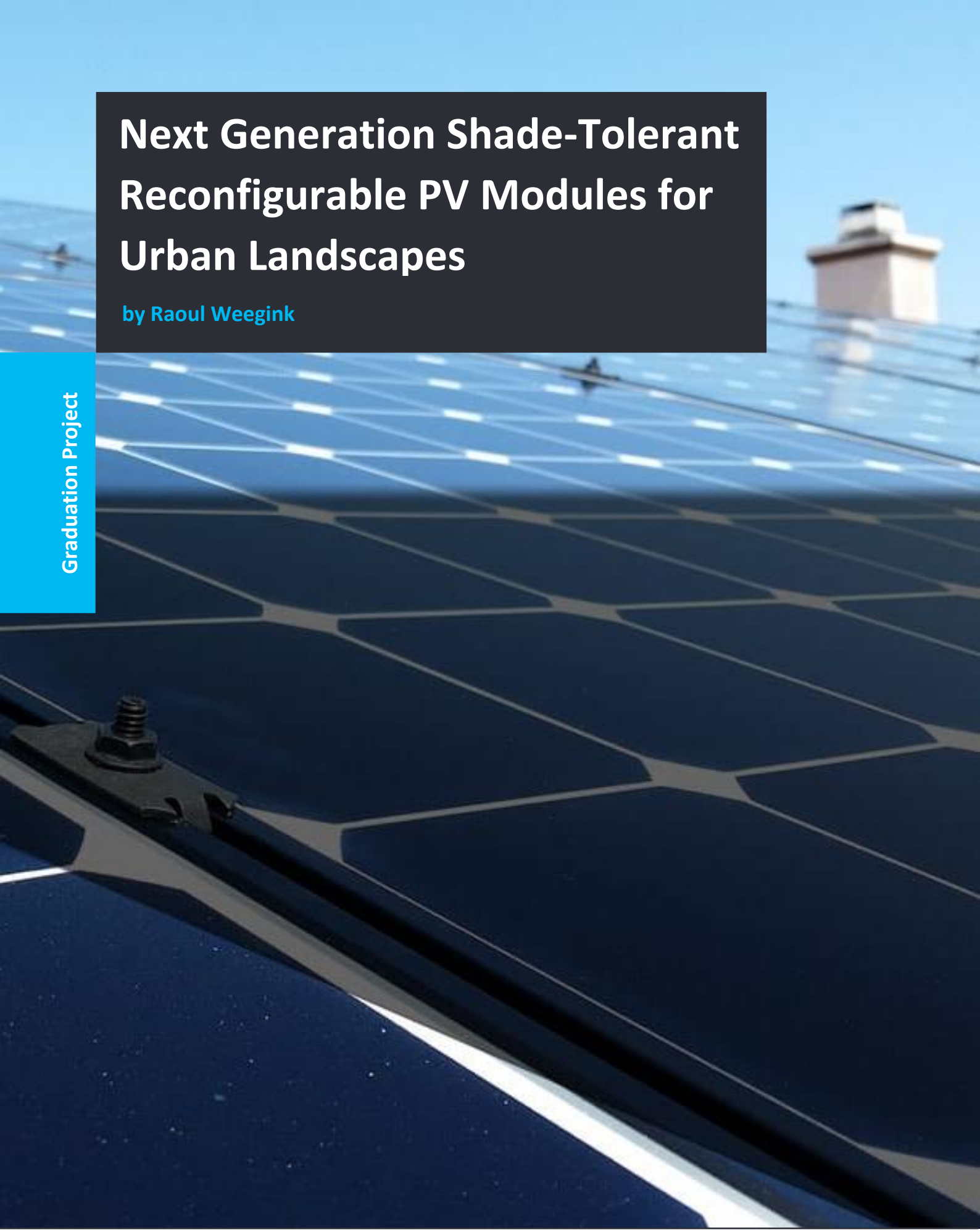

TU Delft Delft University of Technology

Challenge the future

Next Generation Shade-Tolerant Reconfigurable PV Modules for Urban Landscapes

by

Raoul Weegink

in partial fulfilment of the requirements for the degree of

Master of Science
in Sustainable Energy Technology

at Delft University of Technology,
to be defended publicly on Friday July 5, 2019 at 10:00 AM.

Supervisor:	Dr. Olindo Isabella
Thesis committee:	Prof. dr. Arno Smets
	Dr. Olindo Isabella
	Dr. Mohamad Ghaffarian Niasar
	Ir. Andres Calcabrini

An electronic version of this thesis is available at www.repository.tudelft.nl/.

TU Delft Delft University of Technology

ABSTRACT

In urban environments, more and more building added and building integrated photovoltaic (PV) systems are found. These systems use conventional PV modules which have a poor performance under non-uniform illumination conditions. When the module is partially shaded, either at least one subgroup is bypassed or the module current is limited by the current of the worst performing cell. This leads to significant and disproportionate power losses. One way to address this issue is to implement a dynamic module architecture which changes its electrical configuration depending on the shading profile.

This report evaluates the potential and performance of reconfigurable modules in urban landscapes and describes the optimal module configuration. An electrical simulation framework was developed in MATLAB to trace the current-voltage (I-V) characteristics of several static and dynamic module architectures. For a PV module with 72 solar cells, it was found that a series-parallel connected reconfigurable architecture with six subgroups is the optimal trade-off between a high shading tolerability and a simple module design. The potential of these PV modules increases for locations further away from the equator since shadows are larger and occur more frequently. The annual energy yield of a shaded module of a typical PV system in an urban landscape located in Rotterdam (the Netherlands) can increase up to 9% when replacing a conventional with a reconfigurable module. Reconfigurable modules require additional components, but the negative effect on the power output under uniform illumination conditions is marginal. Consequently, reconfigurable PV modules make complex shading analysis for PV systems superfluous.

Compared to a static parallel topology, the module current is generally much lower which in turn leads to lower power losses on system level. Other advantages of the reconfigurable PV module are the smaller seasonal fluctuations in energy yield and the absence of local maxima in P-V curves. Finally, a proof of concept was made to validate the simulation framework. Only minor deviations between the simulation results and the measurements were found. Experiments also showed that solar cells with a soft breakdown must be used to prevent the formation of hot-spots under all circumstances.

PREFACE

The basis for this research stems from my passion for contributing to a more sustainable world. Global climate change, population growth and a rapid increase in the primary energy consumption demand a transition towards renewable energy systems. Solar energy will play a crucial role in this transition as it is widely abundant and can be harvested by decentralized photovoltaic (PV) systems. Enhancing the shading tolerability of PV modules leads to a huge potential for increasing the deployment of PV systems in urban landscapes. A reconfigurable PV module changes its electrical interconnections in real-time to improve its power output in partial shading conditions, and is the focus of this report.

This graduation project is part of my master Sustainable Energy Technology at Delft University of Technology. The research was done in a nine-month project during the academic year 2018-2019 and was under the direct supervision of associate professor Olindo Isabella. Andres Calcabrini was my daily point of contact. Hereby, I would like to express my special thanks of gratitude to both supervisors for their support, advice and guidance throughout the research process and for proofreading my report.

I am also thankful to my fellow students and especially Arturo, Mario, Tijmen and Steven for giving valuable suggestions and feedback. Next, I want to thank Eternal Sun for allowing me to use their solar simulator. This has greatly improved the validation of my simulation framework. Furthermore, thanks to my colleagues at the department of Photovoltaic Material and Devices for the positive, motivating and supportive working environment. Finally, I want to thank my parents for their love and support during both my bachelor Applied Physics and master Sustainable Energy Technology. Your commitment and encouragement gave me the motivation to achieve things that I never imagined to be possible. I hope that you will enjoy reading this report.

Raoul Weegink
Delft, June 2019

TABLE OF CONTENTS

NOMENCLATURE

Abbreviations

BAPV	Building Added Photovoltaic
BIPV	Building Integrated Photovoltaic
BPD	Bypass Diode
IAM	Incident Angle Modifier
IBC	Interdigitated Back Contact
LASS	Large Area Solar Simulator
MPP	Maximum Power Point
MPPT	Maximum Power Point Tracker
PV	Photovoltaic
RB	Reverse Bias
SP	Series-Parallel
STC	Standard Test Conditions
TCT	Total Cross-Tied

Symbols

a_{m}	Module altitude [°]
a_{s}	Solar altitude [°]
A	Area [m^2]
A_{m}	Module azimuth [°]
A_{s}	Solar azimuth [°]
c	Speed of light $= 2.998 \cdot 10^8$ m/s
COI	Configurations of Interest
d	Thickness [m]
DHI	Diffuse horizontal irradiance [W/m^2]
DNI	Direct normal irradiance [W/m^2]
EQE	External quantum efficiency
FF	Fill factor
G	Solar irradiance [W/m^2]
h	Planck's constant $= 6.626 \cdot 10^{-34}$ m^2 kg/s
I	Current [A]
I_0	Saturation current [A]
I_{MPP}	Current at maximum power point [A]
I_{PH}	Photogenerated current [A]
I_{SC}	Short-circuit current [A]
k	Boltzmann's constant $= 1.380 \cdot 10^{-23}$ J/K
K	Extinction coefficient [m^{-1}]
l	Length [m]
n	Ideality factor
n	Refractive index
N	Total number of units in a PV module
p	Number of units connected in parallel
P	Power [W]
P_{in}	Incident irradiance [W]

P_{MPP}	Power at maximum power point [W]
q	Charge of an electron $= 1.602 \cdot 10^{-19}$ C
R	Resistance [Ω]
R_{S}	Series resistance [Ω]
R_{SH}	Shunt resistance [Ω]
s	Number of units connected in series
S	Number of switches
SF	Shading factor
SIF	Shade impact factor
SR	Spectral response [A/W]
T	Module temperature [K]
T_0	Reference temperature [K]
V	Voltage [V]
V_{MPP}	Voltage at maximum power point [V]
V_{OC}	Open-circuit voltage [V]
α	Temperature coefficient [%/K]
η	Efficiency [%]
θ_{i}	Angle of incidence [°]
θ_{r}	Angle of refraction [°]
λ	Wavelength [m]
ρ	Resistivity [Ωm]
τ	Transmittance

LIST OF FIGURES

LIST OF TABLES

1

INTRODUCTION

A rapidly increasing energy consumption and the impact of global climate change demand a transition towards renewable energy systems. Solar energy has a high potential because it can be harvested by decentralized systems and is widely abundant. However, there are still some challenges such as a poor energy yield under partial shading conditions. This chapter addresses the relevance and trends in solar energy research as well as the current challenges and ends with an overview of the aim and outline of this report.

1.1. ENERGY DEMAND AND CLIMATE CHANGE

Population growth resulted in a massive increase in the global energy consumption. Moreover, higher living standards resulted in an increase of the energy demand per capita [1]. Although energy efficiencies have improved, the global energy consumption has doubled in the past 40 years as shown in Figure 1.1. The large majority of the primary energy is generated from fossil fuels such as coal, crude oil and natural gas. Burning these fossil fuels caused a drastic increase in the atmospheric carbon dioxide (CO_2) concentration to over 400 ppm [2]. Global warming is a direct consequence and leads to rising sea levels and more extreme weather conditions.

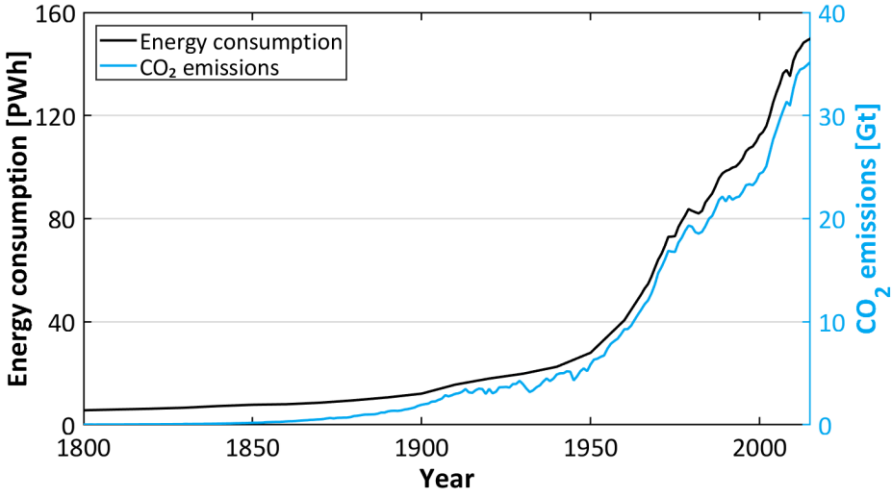

Figure 1.1: *Primary energy consumption [1] and carbon dioxide emissions [3] between 1800 and 2017.*

If these trends continue, the world will run out of fossil fuels in a few decades and the impact of the greenhouse effect might be irreversible [4]. Clean and widely abundant renewable energy sources are essential to meet the future energy demand, while limiting global warming. Photovoltaic technologies use sunlight for energy extraction and have by far the largest potential in terms of capacity. Furthermore, utilizing solar energy is non-polluting and cheap, it can be harvested by decentralized systems and requires little maintenance because of the absence of moving parts [5]. The most important challenges are its relatively low conversion efficiency, the daily and seasonal fluctuations in energy yield and the electrical mismatch losses due to non-uniform operating conditions. Wind, hydro and biomass are other important renewable energy sources which each have their own advantages and disadvantages.

1.2. TRENDS IN SOLAR RESEARCH

Solar energy can be used for electricity or heat production. The most common method for harvesting solar energy is the direct conversion of sunlight into electricity using a photovoltaic (PV) cell. The operation of a solar cell is based on the photovoltaic effect. Electron-hole pairs are generated in the semiconductor of the solar cell when exposed to light. However, only photons with an energy higher than the bandgap energy of the semiconductor contribute to this process. Separating these charge carriers with a p-n junction and using metal contacts for collection, results in a current. The operating principles of solar cells will be discussed in more detail in the next chapter. The energy of sunlight can also be absorbed in a thermal collector to heat up water for a variety of purposes. A more advanced approach uses mirrors to concentrate sunlight on a small area to obtain very high temperatures and then use a steam turbine to convert the heat into electricity.

The photovoltaic effect was first demonstrated by Edmond Becquerel in 1839. In his experiment, he submerged two platinum electrodes in an electronically conducting solution and measured a current under illumination. The first solar cell was made by Charles Fritts in 1883 using selenium as semiconductor which was coated with a thin layer of gold. The cell had a conversion efficiency of about 1% [6]. In 1905, Albert Einstein explained the principles behind the photoelectric effect and was later awarded the Nobel prize in physics. In 1954, researchers at Bells Laboratory discovered that silicon is more efficient than selenium in electron-hole generation and resulted in the first practical solar cell with an efficiency of 6% [7]. The combined effort of universities and businesses resulted in significant technological improvements and costs reductions ever since.

Nowadays, cells can be made from a wide variety of semiconductor materials. Most common is monocrystalline and multi-crystalline silicon. These solar cell are referred to as first generation PV technologies which have a conversion efficiency that has steadily increased up to 25.3% [8]. Second generation technologies are also extensively used and comprises thin-film cells made of cadmium telluride (CdTe), copper indium gallium selenide (CIGS) or amorphous silicon (a-Si). Although their conversion efficiency is generally lower, these cells require significantly less material and can therefore potentially be manufactured at much lower costs. Finally, third generation solar cells use special techniques such as multi-junctions or light concentration to overcome the Shockley Queisser limit, which is the maximum theoretical efficiency of a single bandgap solar cell [5]. Third generation solar cells are currently only cost-effective in specific circumstances such as space applications. Other emerging cell concepts include dye-sensitised, organic, perovskite and quantum dot solar cells. These are still extensively being researched.

Mass production and improved production methods significantly reduced the costs of solar cells. The price of conventional crystalline silicon solar cells has dropped exponentially from almost $100/W in the mid-1970s to less than a dollar per Watt today [9]. The costs are expected to decrease even further which stimulates the deployment of photovoltaic energy systems. These systems already contributed to 45% of all new installed power generation capacity in 2017 [10]. Moreover, the International Renewable Energy Agency projects that in 2020 the electricity of PV systems is cheaper than electricity from conventional sources [11].

1.3. PROBLEM STATEMENT

Growing awareness about climate change leads to rapid developments in the energy sector. In 2017, more than 400 GW of PV was deployed worldwide [12]. This is an increase of 95 GW (31%) year-on-year as shown in Figure 1.2. Approximately a quarter of this new capacity is installed in residential PV systems (generally up to 10 kW) and around 18% in PV systems on commercial rooftops (generally between 10 kW and 2 MW) [10]. Retail grid parity in many countries allowed building owners to also invest in PV systems at non-ideal locations which do not have an optimal tilt or orientation, or suffer from partial shading which is inevitable in urban environments [13]. Shading is often caused by clouds, bird droppings and static objects such as trees, chimneys, dormers and surrounding buildings.

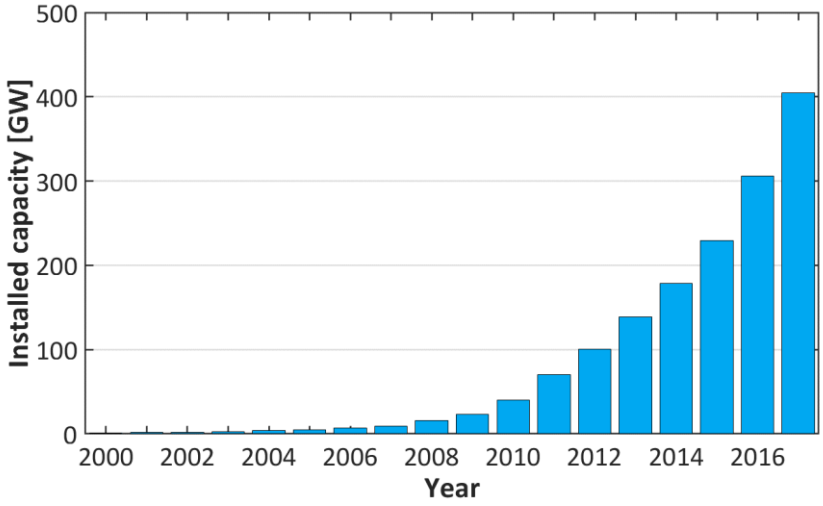

Figure 1.2: *Cumulative global installed PV capacity between 2000 and 2017 [10].*

A conventional PV module (used in utility scale projects) consists of multiple solar cells connected in series. The PV module is generally divided into three subgroups, each with a bypass diode connected in parallel. Bypass diodes are mainly used to prevent hot-spot formation which can permanently damage the module. In the ideal case, the reduction in the output power is equal to the reduction in the irradiation incident on the module, and is known as shading linearity or the optimal shading tolerability. In partial shading conditions, the irradiation incident on a PV module is not uniformly distributed. Due to the series connection of solar cells and the limited number of bypass diodes in a conventional PV module, current mismatch leads to significant and disproportionate power losses. Shading only a small fraction of a module can reduce the power output with more than 30%. This is because either at least one subgroup is bypassed or the module current is limited by the current of the worst performing (i.e. most shaded) cell.

Improving the shading tolerability of modules increases the performance of PV systems in urban landscapes. Additionally, the potential of indoor, façade and other novel PV concepts can be explored. These applications help buildings to meet their energy demand and can be divided into building added photovoltaic (BAPV) and building integrated photovoltaic (BIPV) systems. It is widely acknowledged that shading in urban landscapes has a huge impact on the performance of these systems. Most research is currently focused on improving the conversion efficiency and reducing the costs of PV modules [14]. Leading-edge research looks into reconfigurable modules. These dynamic PV modules change their cell interconnections in real-time to improve the power output under electrical mismatch conditions, which are often caused by partial shading. Although a conventional module has all its individual cells connected in series for practical reasons, shade-tolerant module topologies such as the reconfigurable module are essential to further increase the deployment of PV energy systems in urban landscapes.

1.4. RESEARCH GOAL AND OUTLINE

The aim of this report is to evaluate the potential and performance of reconfigurable PV modules and to find the optimal module configuration. This objective can be subdivided into the following research questions:

1. What is the ultimate potential of reconfigurable PV modules in urban landscapes?
2. Which reconfigurable PV module topology is the optimal trade-off between high shading tolerability and a simple module design with minimal losses under uniform conditions?
3. How does the performance of the reconfigurable PV module compare with other series and parallel connected module layouts?

These questions will be answered by creating an equivalent mathematical and electrical model of the reconfigurable PV module which will be validated with measurements of a prototype. The model will be simulated for a typical PV system in an urban landscape. The simulation results are used to determine the potential and performance of the reconfigurable PV module. Finally, a sensitivity analysis is performed on all parameters affecting the performance of the PV module.

This report addresses both the existing and proposed methodologies to improve the shading tolerability of PV modules, and is structured as follows. Chapter 2 gives a brief introduction on the operating principles of photovoltaic technologies. This chapter also introduces an equivalent mathematical model to simulate the electrical behaviour of solar cells. Chapter 3 provides a detailed overview of existing approaches to reduce mismatch power losses under partial shading conditions as well as their limitations. Chapter 4 addresses the architecture of the proposed reconfigurable module and its potential in a typical urban landscape. A comparative performance study between conventional, reconfigurable and several other reference PV modules will be presented and discussed in detail in chapter 5. The manufacturing process of the prototype and the validation of the simulation model is addressed in chapter 6. Finally, chapter 7 provides conclusions and recommendations for further research to substantially improve the potential of PV modules in the urban environment.

2

PHOTOVOLTAIC TECHNOLOGY

The main component of these systems are PV modules which consist of multiple solar cells. This chapter addresses the operating principles of solar cells as well as an equivalent mathematical model to simulate the electrical behaviour of solar cells. Finally, relevant parameters describing the performance of a solar cell are given, including their dependence on the irradiance and cell temperature.

2.1. SOLAR CELL OPERATION

Solar cells form the basis of a photovoltaic (PV) module. A solar cell is able to convert light into electricity using the photovoltaic effect. Here, generation, separation and collection of charge carriers occur in a semiconductor material when exposed to light [5]. When a photon is incident on a solar cell and its energy is larger than the bandgap of the semiconductor, an electron-hole pair will be formed. These charge carriers can be separated by the p-n junction and results in an electrical current. Spectral mismatch, recombination and others losses should be minimized to ensure high efficiencies. The current density of a single junction solar cell is usually between 25 and 45 mA/cm^2 which yield currents up to 10 A with 6-inch solar cells. However, the voltage of a solar cell is independent of the cell's area and is in the order of 0.6-0.7 V which is too low for many applications. Therefore, cells in a module are connected in series to obtain a higher voltage. The electrical behaviour of a module is similar to individual cells.

A solar cell can operate in forward and reverse bias. This can be explained by looking at the p-n junction. Doping causes an excess of free holes in the p-type semiconductor and a surplus of free electrons in the n-type semiconductor. At the junction, holes will diffuse into the n-layer leaving behind a negatively charged ion in the p-region and vice versa. Consequently, all free charge carriers near the p-n junction will recombine and result in a depletion region which functions as a potential barrier. Due to thermal generation, there are always some electrons in the p-type region and holes in the n-type region. These minority carriers result, under the influence of the electric field in the depletion region, in a drift current opposite to the diffusion current. In equilibrium, both currents are equal and the net current is zero. When the cell is in complete darkness and a positive voltage is applied to the p-type semiconductor, holes in the p-type are repelled towards the junction whereas electrons in the n-type semiconductor are attracted

towards the junction. As a result, the depletion region becomes narrower and free charge carriers can move more easily across the junction. The diffusion current increases and leads to a net positive current. When the voltage is sufficiently high, the depletion layer almost completely vanishes and the diode starts conducting. This operating condition is known as forward bias and is shown in Figure 2.1a. In normal conditions, a solar cell operates in forward bias.

When the solar cell is in the dark and a negative voltage is applied to the p-type semiconductor, the opposite occurs and the potential barrier increases as shown in Figure 2.1b. This operating principle is known as reverse bias. Due to the larger width of the depletion region, the diffusion current becomes negligible. Consequently, the net current is negative and equal to the relatively small current of the minority carriers and is known as the saturation current. However, when the reverse voltage is high enough, the kinetic energy of a minority carrier is sufficient to break covalent bonds when the particle hits an atom. This results in the formation of an electron-hole pair. The charge carriers set free in the collision can in turn be accelerated by the electric field causing a chain reaction that leads to an excessively high flow of electrons through the junction known as breakdown. Although there are also other breakdown mechanisms present in solar cells, localized avalanche multiplication in micro-plasma regions is the dominant process in front-back contact monocrystalline silicon and polycrystalline silicon solar cells [15].

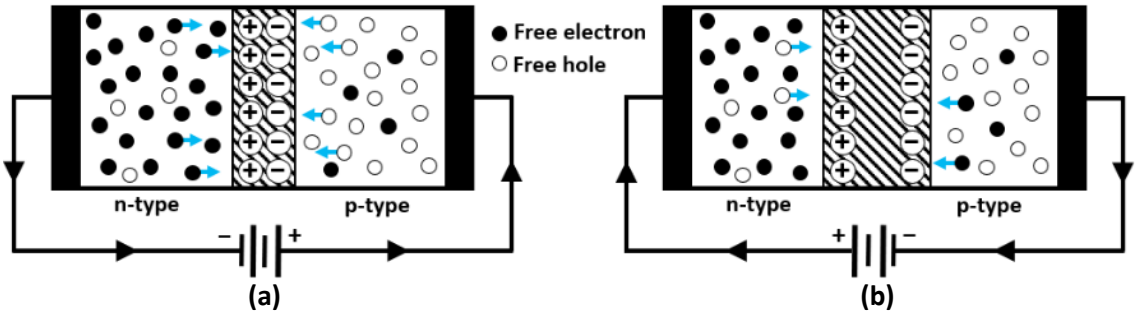

Figure 2.1: *Solar cell operating in (a) forward and (b) reverse bias.*

2.2. EQUIVALENT CIRCUIT OF A SOLAR CELL

Tracing the current-voltage (I-V) curve of a solar cell is a fast and reliable method to determine its performance. It is achieved by measuring the voltage across and current through the solar cell while changing the value of the series connected resistive load. However, experiments are often subjected to changes in measurement conditions such as fluctuations in the irradiation and cell temperature. Therefore, a mathematical model which is electrically equivalent to the solar cell is often simulated. An ideal solar cell can be modelled as a current source in parallel with a diode. Since losses are inevitable, a shunt resistance and series resistance are added to the model. This equivalent circuit is often referred to as the single diode or five-parameter solar cell model and is schematically shown in Figure 2.2.

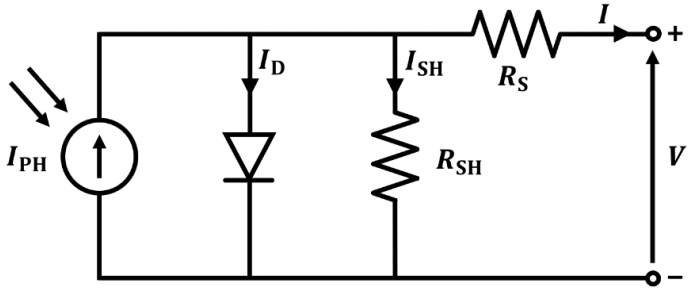

Figure 2.2: *Equivalent circuit of the single diode solar cell model.*

The shunt resistance is caused by manufacturing defects and provides an alternative path for current between the positive and negative terminals of the solar cell. The series resistance comes from the bulk resistance of the p-n junction, the contact resistance between the junction and electrodes and the resistance of the electrodes [5]. Ideally, the shunt resistance should be infinite and the series resistance should be zero. The current generated by the solar cell can be derived using Kirchhoff's law and is given by

$$I = I_{\mathrm{PH}} - I_{\mathrm{D}} - I_{\mathrm{SH}} \tag{2.1}$$

where I is the output current of the solar cell, I_{PH} is the photogenerated current, I_{D} is the diode current and I_{SH} is the current through the shunt resistance. The voltage across both the diode and shunt resistance is the sum of the output voltage of the solar cell and the voltage across the series resistance and equals $V + IR_{\mathrm{S}}$. Substituting this in the Shockley diode equation gives

$$I_D = I_0 \left(\exp\left[\frac{q(V + IR_{\mathrm{S}})}{nkT} \right] - 1 \right) \tag{2.2}$$

where I_0 is the saturation current, q is the charge of an electron, n is the diode ideality factor, k is the Boltzmann constant and T is the temperature of the solar cell. The ultimate equation for the single diode solar cell model is given by

$$I = I_{\mathrm{PH}} - I_0 \left(\exp\left[\frac{q(V + IR_{\mathrm{S}})}{nkT} \right] - 1 \right) - \frac{V + IR_{\mathrm{S}}}{R_{\mathrm{SH}}} \tag{2.3}$$

The main challenge of modelling a solar cell is to find representative values for the parameters such as the saturation current and ideality factor. In literature, there are many other models proposed, including the two diode solar cell model. This is a more advanced model and allows to separate different recombination processes [16]. Each of these solar cell models have their own advantages and drawbacks.

2.3. I-V CURVE AND EXTERNAL PARAMETERS

An I-V curve shows all possible operating points of a PV cell, module or array. The current-voltage relation can be used to derive a number of important parameters which are used to describe the performance. The I-V and corresponding P-V curve of a typical PV cell is shown in Figure 2.3.

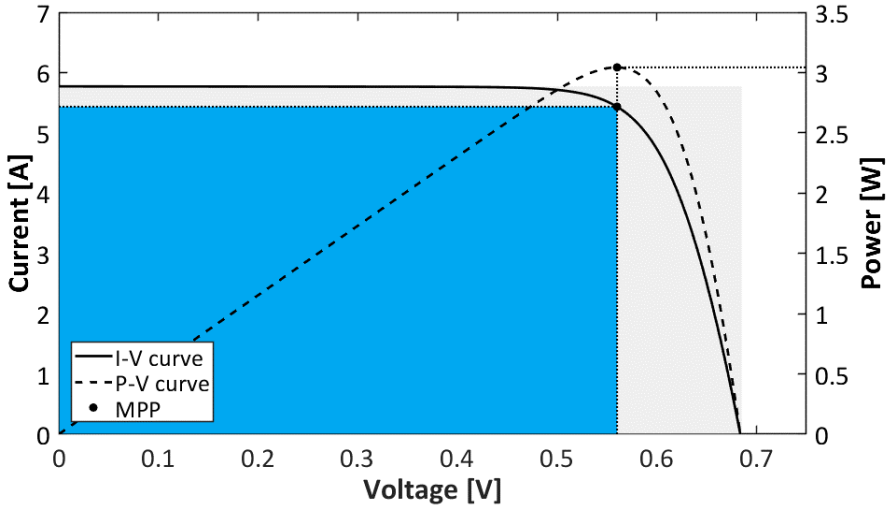

Figure 2.3: *I-V and P-V curve of a typical solar cell.*

These curves allow to determine the short-circuit current, open-circuit voltage, maximum power point, fill factor and efficiency. The short-circuit current (I_{SC}) and open-circuit voltage (V_{OC}) are respectively the maximum current through and maximum voltage across the solar cell. Since these operating points are either in short-circuit conditions (i.e. when the voltage is zero) or in open-circuit conditions (i.e. when the current is zero), the generated power is zero. The point where the product of current times voltage reaches a maximum is known as the maximum power point (MPP) and is indicated in Figure 2.3. The mathematical expression to find the maximum power point uses the derivative with respect to the voltage and is given by

$$\frac{\mathrm{d}P}{\mathrm{d}V} = \frac{\mathrm{d}(IV)}{\mathrm{d}V} = 0 \tag{2.4}$$

Note that power is only generated when both the current and voltage are positive. The solar cell will dissipate power when either the current or voltage is negative. The fill factor (FF) is defined as the ratio between the maximum power of the PV cell and the product of I_{SC} and V_{OC}.

$$FF = \frac{P_{\mathrm{MPP}}}{I_{\mathrm{SC}}V_{\mathrm{OC}}} = \frac{I_{\mathrm{MPP}}V_{\mathrm{MPP}}}{I_{\mathrm{SC}}V_{\mathrm{OC}}} \tag{2.5}$$

where P_{MPP}, I_{MPP} and V_{MPP} are respectively the power, current and voltage in the maximum power point. The fill factor can be visualized as the ratio between the blue and grey rectangles in Figure 2.3. Here, the blue area is the largest possible rectangle that fits within the I-V curve. The efficiency reflects the performance of the solar cell and is given by

$$\eta = \frac{P_{\mathrm{MPP}}}{P_{\mathrm{in}}} = \frac{I_{\mathrm{SC}}V_{\mathrm{OC}}FF}{P_{\mathrm{in}}} \tag{2.6}$$

where P_{in} is the irradiance incident on the solar cell in Watt. Since the performance of a cell is dependent on both the irradiance and temperature as will be explained in the next section, tests are usually performed at standard test conditions (STC). These conditions require an irradiance of 1000 W/m^2 using the AM1.5 spectrum and a cell temperature of 25°C.

The I-V curve also gives an indication of the shunt and series resistance. A smaller slope at short-circuit conditions corresponds to a higher shunt resistance and a smaller slope at open-circuit conditions means a higher series resistance. These parameters strongly affect the fill factor.

2.4. IRRADIANCE AND TEMPERATURE DEPENDENCE

Most external parameters of a solar cell are dependent on both the irradiance and temperature. The photogenerated current depends linearly on the irradiance. It is assumed that the spectral distribution of the solar radiation is maintained. Since the diode current and the current through the shunt resistance are much smaller than the photogenerated current in equation (2.1), the short-circuit current can be approximated with

$$I_{\mathrm{SC}}(G, T_{\mathrm{STC}}) \approx \frac{G}{G_{\mathrm{STC}}} I_{\mathrm{SC,STC}} \tag{2.7}$$

where G is the irradiance, G_{STC} is 1000 W/m^2 and $I_{\mathrm{SC,STC}}$ is the short-circuit current at standard test conditions. Since both the current and incident irradiance change equally, this will not affect the efficiency. The open-circuit voltage on the other hand depends logarithmically on the solar irradiation and is given by

$$V_{\mathrm{OC}}(G, T_{\mathrm{STC}}) = \frac{nkT}{q}\ln\left(\frac{I_{\mathrm{PH}}}{I_0} + 1\right) \approx V_{\mathrm{OC,STC}} + \frac{nkT}{q}\ln\left(\frac{G}{G_{\mathrm{STC}}}\right) \tag{2.8}$$

where $V_{\mathrm{OC,STC}}$ is the open-circuit voltage at standard test conditions and $I_{\mathrm{PH}} \approx I_{\mathrm{SC}} \gg I_0$. The I-V curves for a range of irradiation intensities are shown in Figure 2.4a. From the graph it is clear that the maximum power point voltage slightly increases with light intensity.

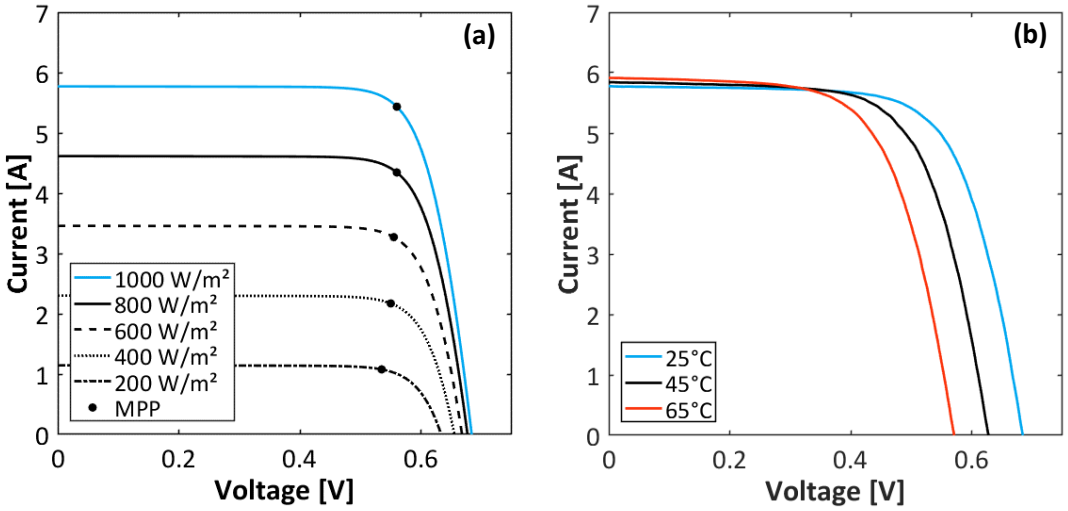

Figure 2.4: *Impact of (a) the irradiance intensity and (b) the cell temperature on the I-V curve of a solar cell.*

Since multiple solar cell parameters are temperature dependent, the overall impact of the cell temperature requires a more thorough approach. When temperature increases, the bandgap of the semiconductor decreases. This increases the photogenerated current because more photons have enough energy to create electron-hole pairs. The overall effect of temperature on the short-circuit current can be approximated by

$$I_{\mathrm{SC}}(G_{\mathrm{STC}}, T) \approx I_{\mathrm{SC}}(G_{\mathrm{STC}}, T_0)\left(1 + \alpha_{I_{\mathrm{SC}}}(T - T_0)\right) \tag{2.9}$$

where $\alpha_{I_{\mathrm{SC}}}$ is the temperature coefficient of I_{SC} and is positive and T_0 is the reference cell temperature and often equals 25°C [17]. Equation (2.8) suggests that the open-circuit voltage should increase with temperature. However, the saturation current drastically increases with the cell temperature and therefore the overall effect on the open-circuit voltage is given by

$$V_{\mathrm{OC}}(G_{\mathrm{STC}}, T) \approx V_{\mathrm{OC}}(G_{\mathrm{STC}}, T_0)\left(1 + \alpha_{V_{\mathrm{OC}}}(T - T_0)\right) \tag{2.10}$$

where $\alpha_{V_{\mathrm{OC}}}$ is the temperature coefficient of V_{OC} and is negative. Since the relative temperature coefficient of V_{OC} has the largest magnitude, the maximum power point power decreases with increasing temperature. The I-V curves for a range of cell temperatures are shown in Figure 2.4b.

3

EXISTING METHODOLOGIES

In conventional photovoltaic (PV) modules, solar cells are connected in series. Since the current in a series connection is limited by the worst performing cell, current mismatch causes significant power losses under non-uniform illumination conditions. A combined effort of universities and businesses resulted in the development of techniques to improve the shading tolerability. In this chapter, commercially applied methodologies are discussed as well as methodologies that are still in a research phase. The focus is on the module level rather than the system level.

3.1. BYPASS DIODES

A conventional commercial PV module has all its solar cells connected in series. The module is usually divided into three subgroups, each with a bypass diode connected in parallel as shown in Figure 3.1. The blue solar cells indicate the size and orientation of a single subgroup.

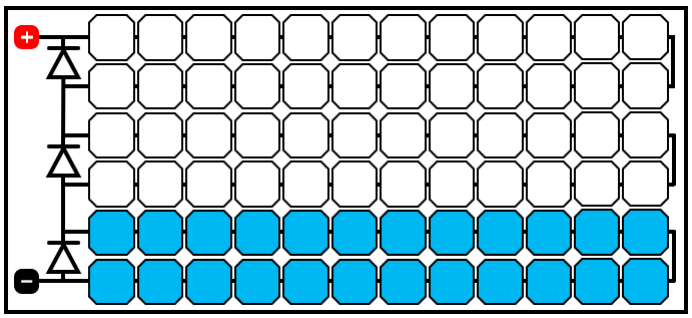

Figure 3.1: *Conventional PV module with 72 series connected solar cells and three bypass diodes.*

Hot-spot heating occurs when a large number of series connected solar cells force a shaded cell to operate in high reverse bias. A detailed explanation of the hot-spot phenomenon is given in Appendix A. Bypass diodes provide an alternative path for current to flow around the shaded cell(s), but are mainly used to prevent hot-spot formation. These diodes are placed in parallel with a certain number of solar cells. The maximum number of solar cells a bypass diode should be connected across to prevent these cells from operating in high reverse bias is given by

$$n_{\max} < 1 + \frac{V_{\mathrm{BD}} - V_{\mathrm{BPD}}}{V_{\mathrm{OC}}} \tag{3.1}$$

where $n_{\max}$ is the maximum number of cell per bypass diode, V_{BD} is the breakdown voltage of the solar cell, V_{BPD} is the forward voltage across the bypass diode. Equation (3.1) shows that $n_{\max}$ depends on the characteristics of the solar cells, but is in the order of 20 cells for a typical breakdown voltage of 15 V. Consequently, a conventional PV module has three bypass diodes.

Under uniform illumination, all solar cells generate power and a positive potential difference arises between the p-type contact and n-type contact of each cell. Bypass diodes are connected in anti-parallel to the solar cells and will therefore be reverse biased and act as an open-circuit. If a shaded cell is forced to operate in low reverse bias (see appendix A), the current would be limited by this solar cell and causes the bypass diode to conduct. Once a bypass diode is activated, the current will pass through the diode and the power potential of bypassed cells is lost. Since bypass diodes are intended to prevent the formation of hot-spots by ensuring low bias operation, shading one cell would already activate the bypass diode. Therefore, the I-V curve under different shading intensities as shown in Figure 3.2 is almost independent of the number of shaded cells which share the same bypass diode. Whether the module is placed in landscape or portrait orientation has a tremendous impact on the performance of the module due to the connection of the bypass diodes.

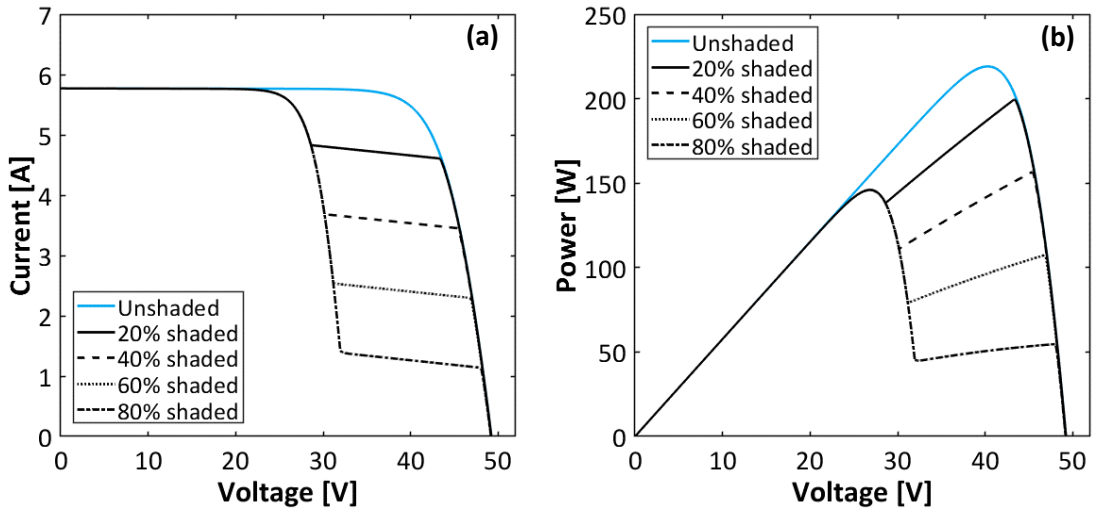

Figure 3.2: *Impact of the shading factor on (a) the I-V curve and (b) the P-V curve of the conventional PV module when a single solar cell is shaded.*

Under uniform operating conditions, the P-V curve only shows one maximum power point (MPP). Maximum power point tracking (MPPT) algorithms are used to ensure that modules operates at their MPP. Common MPPT algorithms include the 'perturb and observe' and the 'incremental conductance' method. As shown in Figure 3.2, bypass diodes alter the P-V curve drastically under non-uniform illumination conditions. Shaded cells lead to multiple peaks of which only one is the global maximum. It is important to note that bypass diodes of strings containing shaded cells are not necessarily activated in the global maximum power point. In order to find the global rather than local maximum power point, advanced MPPT is required. The MPPT algorithm should be selected based on its accuracy, tracking speed, simplicity and costs. The power increment or load-line techniques provide a good trade-off, and can be adopted for global MPPT [18].

Although the power of bypassed cells is lost, the module's output is generally higher with respect to a PV module without bypass diodes. This is because in most situation the shaded cells will not limit the current of the solar cells under a different bypass diode. Consequently, bypass diodes improve the shading tolerability of a PV module especially when multiple cells within the same subgroup are shaded. Since a bypassed string will probably contain unshaded or partially shaded

cells which still produce power, there is a huge potential to improve the shading linearity [19]. Increasing the number of bypass diodes decreases the power loss of bypassed cells and therefore increases the shading tolerability. However, adding bypass diodes increases the manufacturing costs and potentially leads to many local maxima in the P-V curve [20]. Furthermore, each activated bypass diode has conduction losses due to the voltage drop across the diode.

Not all PV modules require bypass diodes to prevent hotspots. Chu et al. have reported that some indigitated back contact (IBC) solar cells can safely operate in reverse bias for a prolonged period of time without having a significant effect on the performance of a solar cell [21]. Nevertheless, commercially available modules made of this type of solar cells do contain bypass diodes. In this case, these diodes are only used to improve the shading tolerability rather than to prevent the formation of hotspots. Consequently, the limit defined in equation (3.1) is not valid anymore. When more cells than $n_{\max}$ share the same bypass diode, shaded cells might be forced to operate in high reverse bias when the fraction of shaded cells within the subgroup is relatively small. The current is then not limited by the shaded cells and hence the bypass diode will not be activated. Increasing the number of shaded cells within the subgroup moves the operating point from high to low reverse bias and the bypass diode will still activate as shown in Figure 3.3.

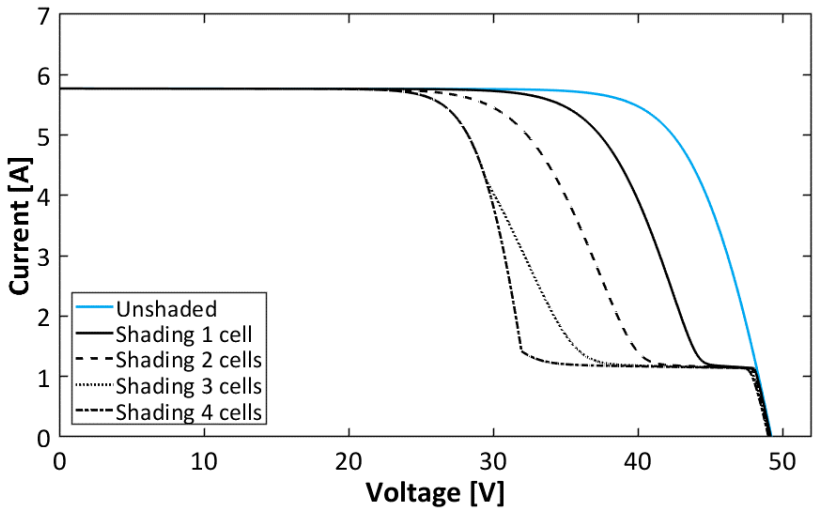

Figure 3.3: *Impact of shading on the I-V curve of a conventional PV module when solar cells have a low breakdown voltage. All shaded cells belong to the same subgroup and receive an 80% lower irradiation.*

3.1.1. Smart bypass diodes

When a conventional bypass diode is activated it will generally dissipate a couple of Watt. This power loss is proportional to the forward voltage across the bypass diode. A normal silicon diode has a typical forward voltage of 600 mV, whereas the conventional Schottky bypass diode has a forward voltage around 400 mV. Although adding more bypass diodes would in principle improve the shading tolerability, a larger number of bypass diodes also implies higher conduction losses in partial shading conditions and therefore a reduction in the output power of the module under non-uniform illumination conditions. Several companies such as Texas Instruments developed a new bypass diode which has a 10 times lower forward voltage [22]. Consequently, the power loss of these so-called smart or active bypass diodes is drastically reduced. This allows to implement more bypass diodes while the conduction losses remain acceptable. Less power dissipation will also result in less heating of the bypass diode and improves the reliability of the module.

Smart bypass diodes contain a body diode, MOSFET, capacitor, charge pump, controller and FET driver. When shaded solar cells activate a smart bypass diode, current will initially flow through

the body diode and will enable the charge pump to charge the capacitor. When the voltage of the capacitor reaches a certain level (i.e. fully charged), the controller activates the MOSFET and the charge pump is switched off. The activated MOSFET provides a low resistive path resulting in marginal power dissipation. The stored energy in the capacitor is used to power the controller while the MOSFET is active. When the capacitor is completely discharged, the MOSFET is deactivated and the cycle repeats. The power dissipation in a smart bypass diode is minimized by maximizing the duty cycle of the MOSFET. The main disadvantage is that smart bypass diodes are currently too expensive to implement on large scale. The costs of a Schottky diode is $0.16 whereas a smart bypass diode is around $1.50 [13]. However, significant cost reductions seem realistic when these smart diodes are manufactured in mass production.

3.1.2. Overlapping bypass diodes

Besides the number and distribution of bypass diodes within a module, their configuration is also relevant. It is important to distinguish between PV modules without and with overlapping bypass diodes. In non-overlapping bypass diodes, each solar cell can be bypassed by only one bypass diode as shown in Figure 3.4. This is the most common configuration.

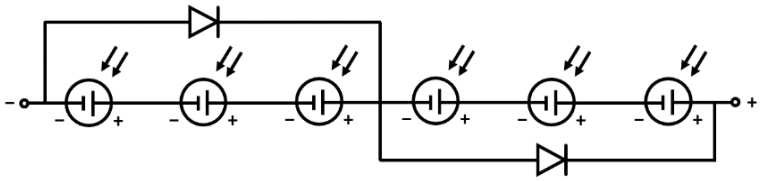

Figure 3.4: *Non-overlapping bypass diodes.*

If bypass diodes overlap, there are two alternative paths for current to flow around shaded cells. Silvestre et al. described how overlapping bypass diodes alter the I-V curve of a PV module [23]. An example of the connection of overlapping bypass diodes is schematically shown in Figure 3.5. When any of the two central solar cells are shaded, both bypass diodes are activated. As a result, the power of only two cells is lost and the shading tolerability is improved. There are two disadvantages. First, overlapping bypass diodes can potentially lead to overcurrent production [24]. This is because the current of the four outer solar cells will now flow through each of the two bypass diodes and results in current accumulation at the PV module terminals. Second, the power of four rather than three solar cells is lost, in case only one bypass diode is activated. As a result, the overall impact on the shading tolerability is hard to determine.

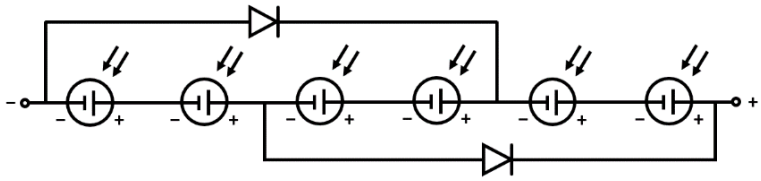

Figure 3.5: *Overlapping bypass diodes.*

3.2. STATIC CONNECTION TOPOLOGIES

A PV module consists of a certain number of interconnected solar cells. The way in which these cells are connected is described by their topology or architecture. The most common topologies are series, parallel, series-parallel, total cross-tied, bridge-linked and honeycomb [25]. Currently, most of these topologies are used to interconnect modules at system level rather than solar cells

at module level. Cells in commercial PV modules are usually connected in series. These strings carry the same current which cannot exceed the current of a single cell and the module voltage is the sum of the individual cell voltages as shown in Figure 3.6a. In contrast, cells connected in parallel operate at the same voltage and the module current is the sum of the individual cell currents as shown in Figure 3.6b. Power losses in cell interconnections can be calculated with

$$P = I^2 R \tag{3.2}$$

where R is the wire resistance. Consequently, connecting all cells in series would result in the best performance under uniform irradiance, because the resistive power losses are minimized.

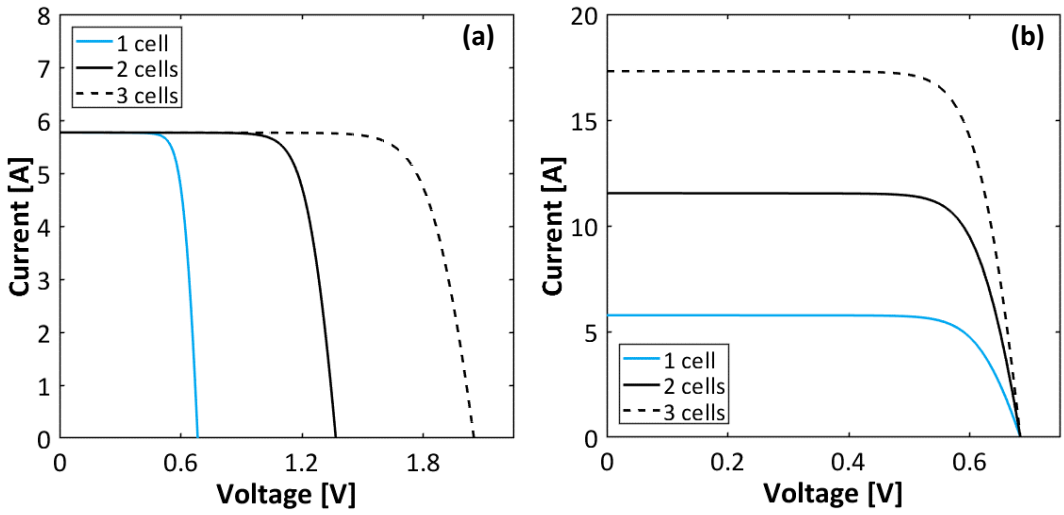

Figure 3.6: *I-V curve of (a) series and (b) parallel connected solar cells.*

As mentioned in section 2.4, the current changes linearly and the voltage logarithmically with irradiance. In absence of bypass diodes, the current through a series connected string is limited by the worst performing cell, as shown in Figure 3.7a. As a result, the series architecture is hardly resilient to partial shading. Connecting all cells in parallel provides maximum shading tolerability, because shaded solar cells cannot limit the current of unshaded cells and the voltage does hardy vary with irradiance.

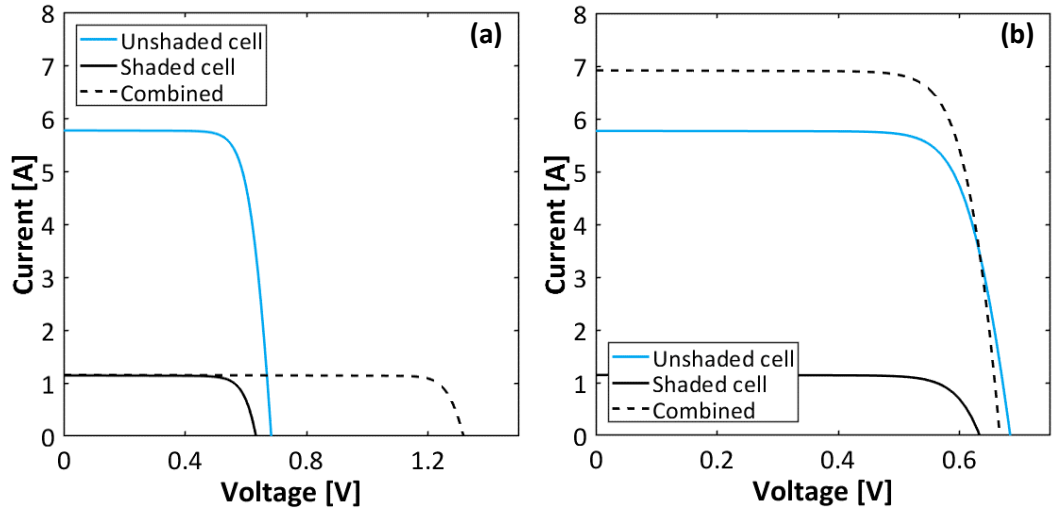

Figure 3.7: *Impact of current and voltage mismatch on the I-V curve when a shaded and unshaded solar cell are connected in (a) series and (b) parallel.*

The main disadvantage of a parallel connection is that it significantly increases the current and therefore the resistive power losses and cable costs. Series-parallel (SP) and total cross-tied (TCT) architectures provide better solutions for an urban environment.

3.2.1. Series-parallel

The series-parallel (SP) topology is a middle ground between connecting all cells in series or parallel. The aim is to minimize the power losses while maximizing the shading tolerability. In this topology, cells are connected in series to form strings and multiple strings are then connected in parallel [26]. As an example, a module of 16 cells with 4 parallel strings of each 4 cells in series is schematically shown in Figure 3.8a. Non-uniform irradiance will now only affect the current of the strings containing the (partial) shaded cells. Compared to connecting all cells in parallel, the current and therefore the resistive power losses will be lower. For a given number of cells within a module, several SP topologies exist. In the example with a PV module of 16 cells, the other configurations are 2 strings of 8 cells in series (8x2 SP) and 8 strings of 2 cells in series (2x8 SP). The optimal configuration depends on the shading conditions and system requirements.

3.2.2. Total cross-tied

The total cross-tied (TCT) topology is another module architecture to balance between shading tolerability and power losses [27]. This topology is derived from the SP architecture by connecting ties across the different strings. In other words, cells are connected in parallel to form rows and multiple rows are then connected in series as schematically shown in Figure 3.8b. Compared to a SP topology, TCT can mitigate mismatch problems for a wider range of partial shading profiles. As a result, research showed that PV modules in urban landscapes which have a TCT topology generally outperform a SP architecture [28], [29].

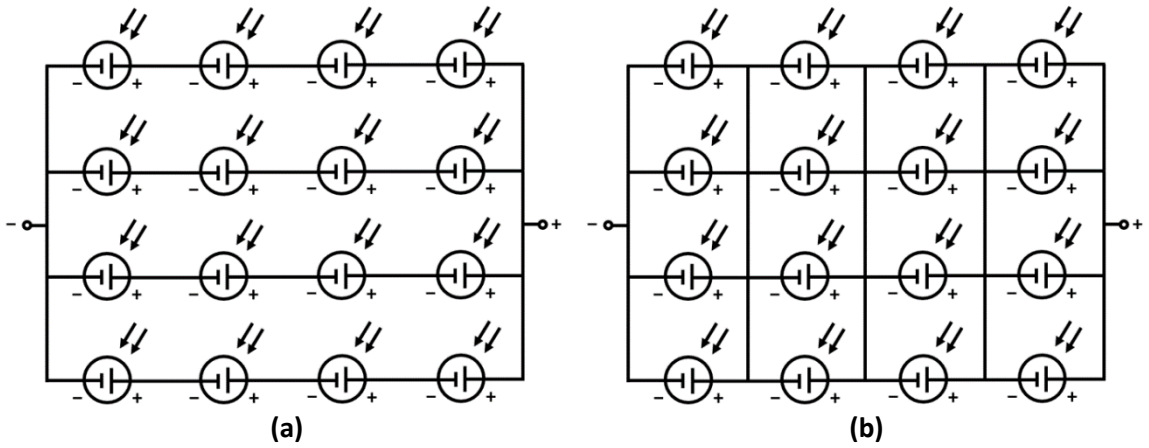

Figure 3.8: *(a) Series-parallel and (b) total cross-tied topology.*

The most important drawback of a TCT configuration is the increased complexity due to the large number of ties. Bridge-linked and honeycomb architectures require even more complex wiring and are outside the scope of this report.

3.3. DYNAMIC CONNECTION TOPOLOGIES

Bypass diodes and parallel topologies are static techniques to improve the shading tolerability and have hardwired interconnections. In dynamic topologies, interconnections can be changed in real-time using switches. The switching moments can be at regular or variable time intervals and should be chosen carefully to minimize mismatch losses. Algorithms are used to find the optimal configuration for a specific shading pattern. Depending on the degree of flexibility (i.e. the number of configurations provided by the switches), dynamic topologies can result in a much higher shading tolerability compared to static techniques. Several dynamic topologies exist and are mostly implemented on system level. The operating principles, advantages and drawbacks of different dynamic topologies will be addressed below.

3.3.1. Irradiance equalization

The irradiance equalization method enables changing the interconnections between individual solar cells. It is commonly implemented and investigated on system level [30], [31]. It can also be implemented on module level. In this case solar cells are connected in total cross-tied through a switching matrix [32]. Each row generally contains an equal number of solar cells. This is referred to as 'exact row sizing'. The current produced by a row is proportional to the sum of its parallel connected cell irradiances. Cells will be relocated to ensure that each row receives almost the same irradiance as shown in Figure 3.9. It is important to realize that only cell interconnections are changed and that the physical location of these solar cells remain the same.

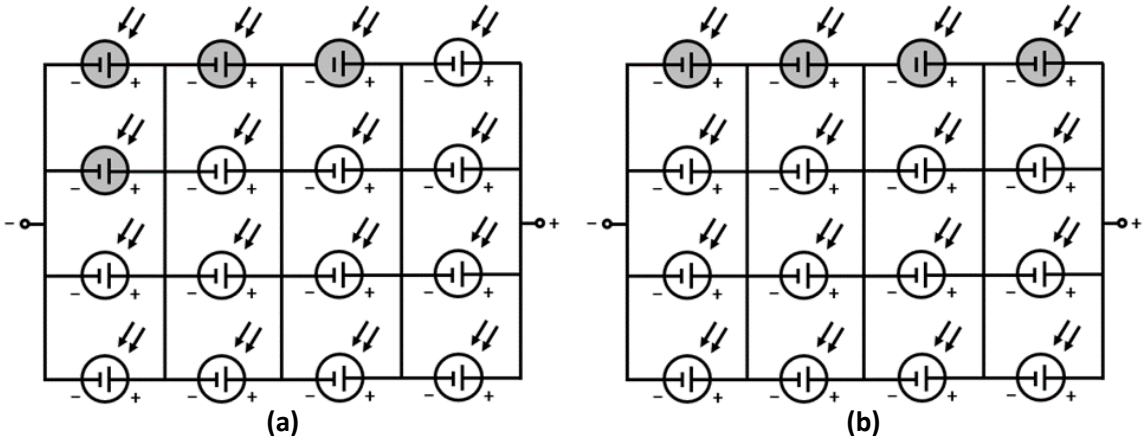

Figure 3.9: *Irradiance equalization (a) before and (b) after reconnection. The switching matrix is hidden for simplicity. The cell interconnections are changed while the physical location of each solar cell within the module is maintained.*

Since each solar cell can potentially be relocated to each row of the TCT topology, many switches are required to enable the large amount of possible configurations. This drastically increases resistive power losses and costs. The optimal topology is found by determining the power of each possible configuration. However, this requires an impractical number of calculations. Storey et al. found a more efficient method in which solar cells are sorted based on the irradiance incident on cells [33]. This array is then converted into a matrix with a size corresponding to the TCT topology. Next, matrix transformations are used to equalize the available power in each row. As a result, the current mismatch losses between the series connected rows are minimized. The researchers also proved that the output power will increase if the switching matrix is able to dynamically change the dimensions of the TCT topology, but this requires a more complex control algorithm.

3.3.2. Adaptive banking

The adaptive banking technique is a variant of the irradiance equalization method and is also mainly implemented on system level [25], [30]. In this case, the PV module is divided into a fixed and adaptive bank. Only solar cells in the adaptive bank can be relocated [34]. The two parts are connected through a switching matrix. Under uniform illumination conditions, the solar cells of the adaptive bank are equally distributed across the rows of the fixed part. Therefore, it is essential that the number of cells in the adaptive bank is a multiple of the number of rows in the TCT topology. Under partial shading conditions, cells from the adaptive bank are relocated to compensate for the shaded cells. This leads to a TCT topology with an arbitrary row size [35]. Obtaining the optimal configuration is an iterative process where the most illuminated cell of the adaptive bank is connected in parallel to the poorest performing row as shown in Figure 3.10b. Here, the current is initially limited by the left row which only contains one unshaded solar cell and therefore receives most cells from the adaptive bank. It should be noted that the adaptive bank can also contain shaded cells which will be connected to non or less shaded rows.

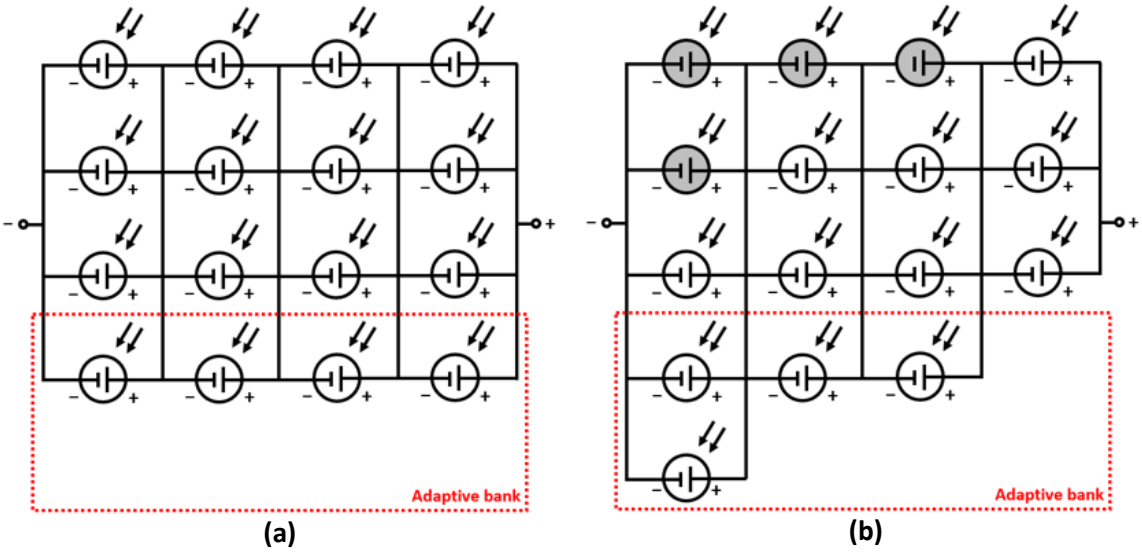

Figure 3.10: *Adaptive banking under (a) uniform illumination and (b) partial shading conditions. Only solar cells within the adaptive bank can electrically be relocated.*

The optimal size of the adaptive bank is a trade-off between high shading tolerability and system complexity. A small adaptive bank allows to drastically reduce the number of switches, resistive power losses and costs with respect to the irradiance equalization method. However, when the adaptive bank is too small, the mismatch losses cannot be sufficiently mitigated. The adaptive banking technique provides a relatively high shading tolerability when the adaptive bank is larger than the number of shaded cells [36].

3.3.3. Other concepts

Irradiance equalization and adaptive banking are the most common dynamic topologies. There are several other dynamic module layouts which also increase the shading tolerability. These architectures generally require less switches, but only allow to switch between a limited number of configurations.

Snake-like SP topology

The snake-like topology proposed by Baka et al. uses 10 subgroups of 6 series connected solar cells [37]. The PV module can only switch between two configurations: all subgroups are either connected in series or in parallel. Due to the snake-like wiring between cells within the module, the additional resistive wiring losses are minimized. This is especially the case when elongated (*I-type*) subgroups are used at the sides as shown in Figure 3.11b. In partial shading conditions, the module will generally switch to its parallel configuration. Note that it is impossible to prevent current mismatch losses within a subgroup. Since hot-spot formation cannot occur in the parallel configuration and the interconnections are updated in real-time, no bypass diodes are required across the subgroups.

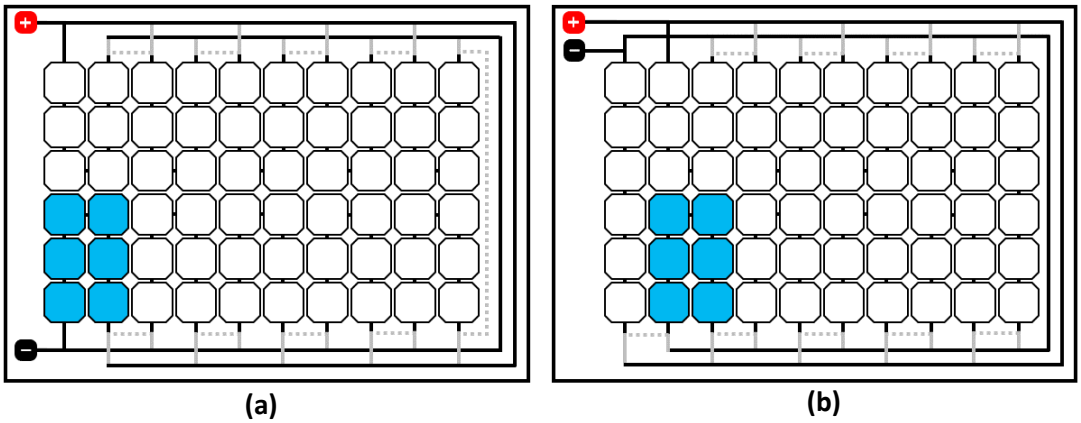

Figure 3.11: *Simplified schematic of the (a) U-type and (b) I-type snake-like SP topologies. The subgroups are either connected all in series (dotted grey lines) or all in parallel (solid grey lines).*

Switches are always present in the current path of this architecture. Low on-resistance switches are used to ensure high performance under uniform illumination conditions. Compared to the conventional PV module, the power loss of the snake-like topology is only 0.4% at STC. Multiple local DC-DC converters are integrated within the module to boost the voltage and to reduce the impact of current accumulation in the parallel configuration. Baka et al. discovered that dynamic PV modules outperform conventional PV modules at locations where partial shading is dominant. The gain increases with irradiation intensity and shading factor [38], [39]. The disadvantage of this topology is the limited amount of possible configurations. When partial shading occurs, the module can only switch to a parallel configuration and still requires 29 switches. Baka et al. did not compare the performance of the snake-like topology with a static parallel architecture and the size of the subgroups is not optimized.

Dynamic TCT topology

Series-parallel (SP) and total cross-tied (TCT) are two static topologies. As discussed in section 3.2, TCT is derived from the SP architecture by connecting ties across the different strings. Chao et al. proposed a dynamic TCT interconnection where switches are installed in each tie [25]. The optimal position of the switches is found by a particle swarm optimization algorithm and depends on the shading pattern. Under uniform irradiance, all switches are open leading to a conventional series-parallel topology. However, in partial shading conditions, this reconfiguration method can result in asymmetric and unpredictable configurations as shown in Figure 3.12. Although its effectiveness is only demonstrated on system level, an equivalent methodology can be applied on module level. The disadvantage is that it would again require a large amount of switches which affects the resistive power losses, costs and reliability of the module.

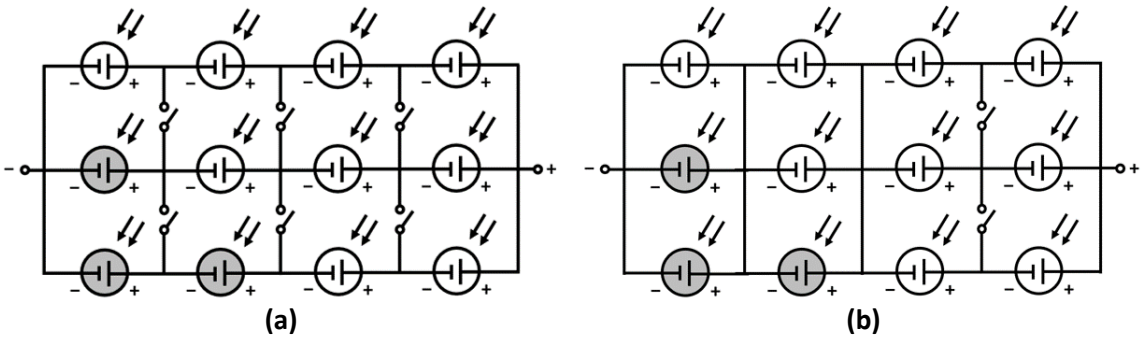

Figure 3.12: *Dynamic TCT topology (a) before and (b) after reconnection.*

Mini solar cells

All of the above mentioned methodologies connect solar cells or strings of series connected cells in parallel to increase the shading tolerability. The most important drawback is the higher output current which leads to larger resistive power losses. Cutting standard solar cells (i.e. 125x125 mm or 156x156 mm) into smaller pieces reduces the photocurrent of individual cells. Therefore, more solar cells can be connected in parallel while the current still remains within an acceptable range. These mini solar cells can be used in both static and dynamic topologies.

Carr et al. designed a static shade robust PV module in which each solar cell was cut into 16 mini cells [40]. These sub-cells are connected in series and bypassed by a low current Schottky diode to form a building block. The short-circuit current of the cell is now reduced to roughly 0.6 A. The use of back contact cells allows to connect these solar cells on the backside which reduces the complexity. The PV module has a series-parallel topology with 15 parallel strings of 4 blocks in series. Their research showed that an annual yield gain of around 4% can be achieved in urban environment [41]. The main disadvantages are that more material is wasted, the spacing between mini solar cells is relatively large and the cells have a relatively large perimeter to area ratio and therefore suffer from larger edge recombination which leads to a lower cell efficiency.

Q Cells recently developed and commercialized a shade tolerant DUO/Twin Peak PV module [42]. The PV module is divided into six subgroups of 20 series connected half cells. The subgroups are connected in a total cross-tied topology where each row contains two subgroups as shown in Figure 3.13. Furthermore, a bypass diode is placed across each of the three rows. Since only two subgroups are connected in parallel and the cell current is halved, the resistive power losses remain roughly the same. Due to its architecture, the module will outperform the conventional PV module especially when shading occurs on only one of the two parallel connected sides of the module. However, a detailed performance analysis in partial shading conditions is not available.

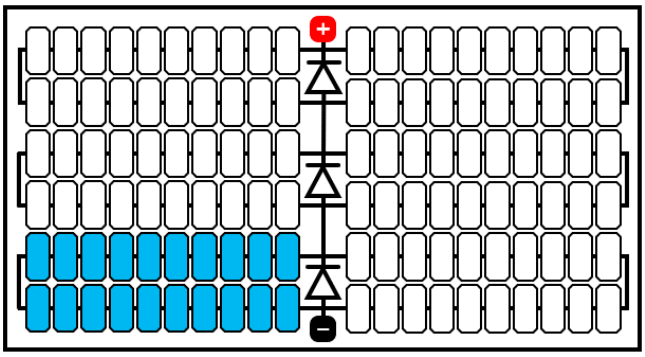

Figure 3.13: *DUO PV module with 120 half cells and three bypass diodes.*

4

POTENTIAL OF SERIES-PARALLEL RECONFIGURABLE PV MODULES

The proposed reconfigurable topology combines the strengths of several existing methodologies and is a trade-off between high shading linearity and a simple module design with minimal losses under uniform illuminations conditions. A detailed description of the module layout will be given in this chapter. Furthermore, an urban landscape scenario is introduced to evaluate the potential of such reconfigurable modules in locations where partial shading conditions are dominant.

4.1. RECONFIGURABLE UNITS AND SWITCH MATRIX

Partial shading causes a non-uniform irradiance on PV modules. In a reconfigurable module, the interconnections between solar cells can be changed in real-time using switches to mitigate the negative effect of shading. A *reconfigurable unit* is defined as the smallest group of cells in a PV module which can be electrically relocated. The electrical connection between solar cells within a reconfigurable unit is fixed. The most elementary reconfigurable unit consists of a single solar cell, but reconfigurable units can be made of multiple solar cells. Each reconfigurable unit within a PV module should have the same interconnection topology and number of solar cells to avoid current and voltage mismatch [31]. A PV module with reconfigurable units consisting of a single cell is referred to as a fully reconfigurable module. There are $N!$ different ways of connecting N reconfigurable units. Since conventional modules generally consist of 60, 72 or 96 solar cells, a fully reconfigurable PV module can adopt decillions of configurations. Fortunately, the majority of these configurations are equivalent from an electrical point of view.

The configurations of interest (COI) are only those that under a certain shading pattern result in different I-V curves. An example with 4 reconfigurable units in a series-parallel (SP) connection shows how the configurations of interest can be obtained. The units can be connected all in series (4x1 SP), all in parallel (1x4 SP) or as two parallel strings of each two units in series (2x2 SP). Swapping units within the same string or changing the order in which strings are connected in parallel does not affect the output of the module. Therefore, the 2x2 SP configurations shown in Figure 4.1 are electrically equivalent.

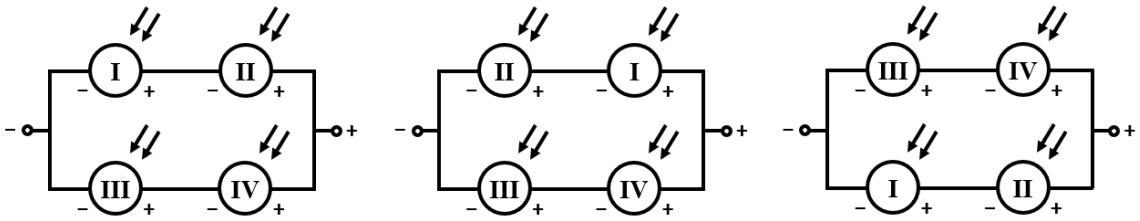

Figure 4.1: *Equivalent configurations in a 2x2 SP connection.*

For the 2x2 SP connection, there are three configurations of interest (i.e. unique configurations) as shown in Figure 4.2. When all reconfigurable units are either connected in series or parallel, there is only one unique configuration. As a result, there are in total 5 configurations of interest for a module with 4 reconfigurable units in a series-parallel connection.

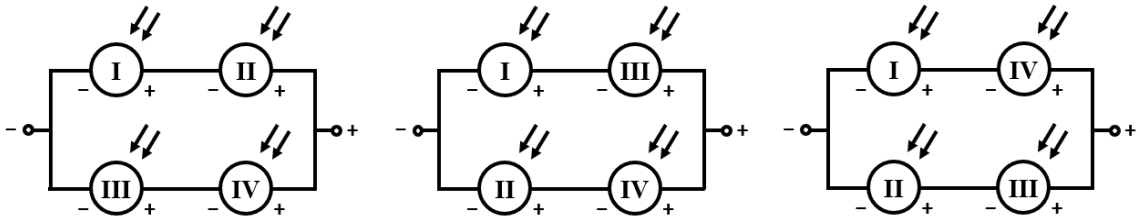

Figure 4.2: *Unique configurations in a 2x2 SP connection.*

Using this methodology, the initial $N!$ possible configurations is reduced to

$$COI = \frac{N!}{p!\,(s!)^p} \tag{4.1}$$

where s is the number of series connected units per string and p is the number of parallel strings and equals N/s [31], [43]. The result for a module with 72 reconfigurable units is shown in Figure 4.3. By summing the configurations of interest of all possible SP combinations, the total number of unique configurations can be obtained.

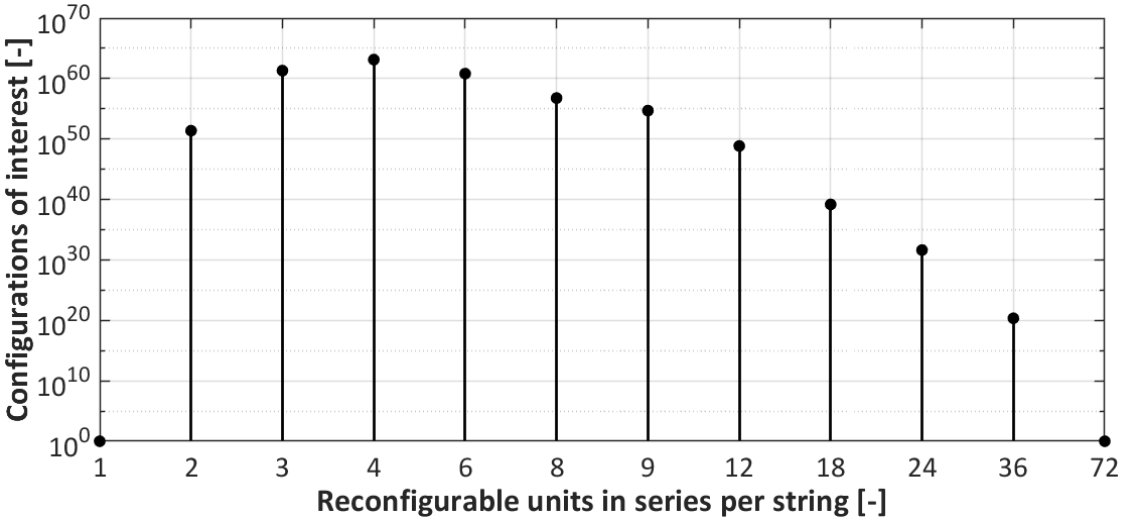

Figure 4.3: *Number of unique configurations for a SP connected reconfigurable PV module with 72 units.*

A reconfigurable PV module requires switches to change from one configuration into another. The switching matrix defines the switch positions for each configuration of interest. For the PV module with 4 reconfigurable units in a series-parallel connection, the configurations of interest can be obtained using the layout shown in Figure 4.4.

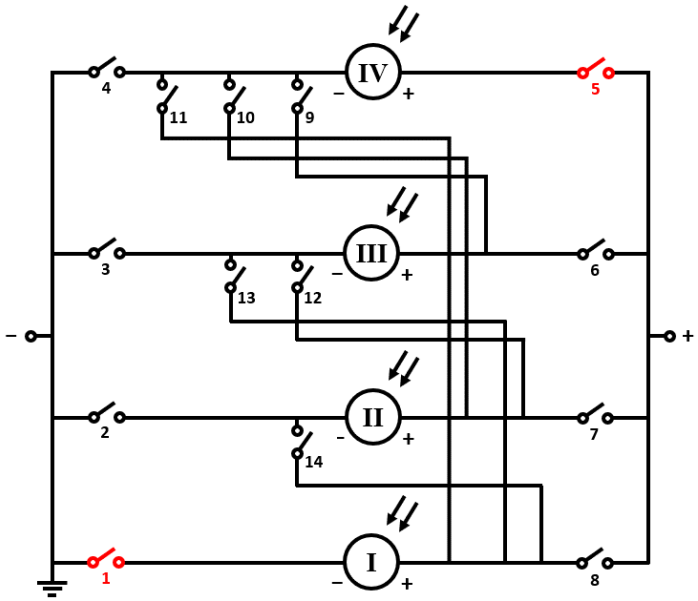

Figure 4.4: *SP connected reconfigurable PV module with 4 units. The red switches are always closed and can therefore be omitted.*

As discussed before, the output power is independent of the order in which units are connected in series or strings are connected in parallel. Therefore, the 'first' and 'last' unit can always be connected to the negative and positive terminal respectively and consequently switch 1 and 5 can be omitted. The total number of required switches can now generally be calculated with

$$S = 2(N-1) + \sum_{i=1}^{N-1} i = \frac{1}{2}(N^2 + 3N - 4) \tag{4.2}$$

It is obvious that for a module consisting of a prime number of units, these can only be connected all in series or all in parallel. In this specific case, the number of switches is given by

$$S = 3(N-1) \tag{4.3}$$

Using equation (4.1) to (4.3), the number of unique configurations as well as the required number of switches can be calculated for a variety of unit and module size combinations as shown in Figure 4.5.

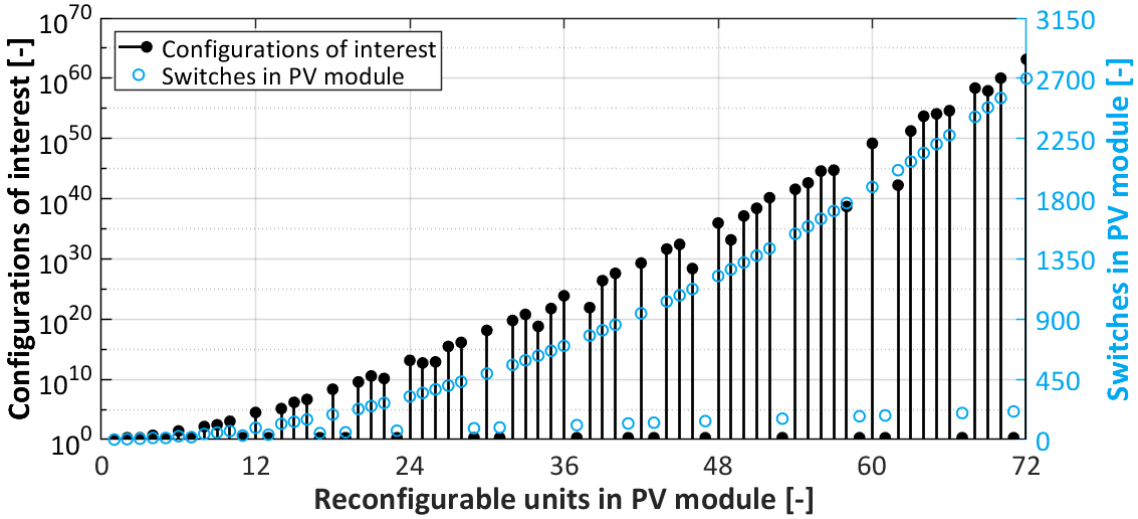

Figure 4.5: *Total number of unique configurations and switches in a SP connected reconfigurable PV module for a range of unit and module size combinations.*

Similar equations can be derived for other PV module topologies, such as total cross-tied (TCT). Although TCT has the same number of unique configurations, it requires many more switches. In an example of a TCT connected reconfigurable PV module with four units, the configurations of interest can be obtained using the layout shown in Figure 4.6. This PV module architecture is also capable of switching to SP interconnections and therefore has twice as many configurations of interest. Switches 1 and 20 can be omitted, because the 'first' unit can always be connected to the negative terminal, while the 'last' two units can directly be connected to the positive terminal when these units are connected in parallel. It is important to realize that for several unit and module size combinations, some additional switches can be neglected. When units II and IV or III and IV in this example are connected in parallel, these units can also directly be connected to the positive terminal and therefore switches 17 and 19 are superfluous.

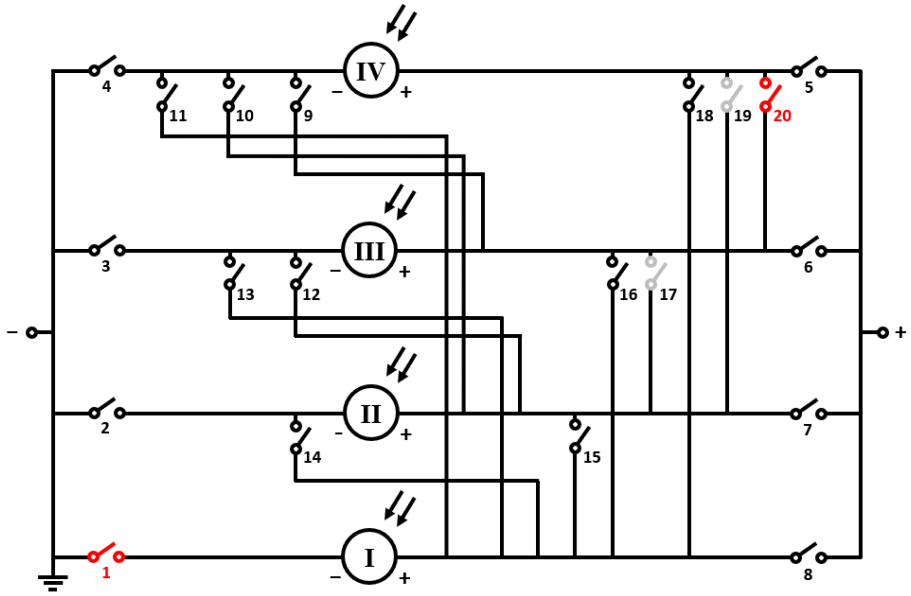

Figure 4.6: *TCT connected reconfigurable PV module with 4 units. The red and grey switches are superfluous.*

As mentioned in section 3.2.2, a static TCT configuration generally outperforms a SP connection. However, in a reconfigurable SP connected PV module, units with similar shading conditions are grouped together in a string to prevent these units from limiting the current of the other units. Since interconnections in a reconfigurable SP connected PV module are already optimized with respect to the shading conditions, the additional gain of a TCT architecture is assumed to be very limited and will be verified in the next chapter. The units in the proposed reconfigurable module will therefore only be connected in SP configurations. Furthermore, since resistive power losses increase with the number of units connected in parallel and the number of unique configurations and switches is unmanageable for a fully reconfigurable module, the interconnections between subgroups of series connected solar cells rather than individual cells are changed. This reduces the system complexity drastically.

4.2. URBAN LANDSCAPE

The potential of reconfigurable PV modules and their optimal subgroup size can be determined by estimating the maximum amount of solar radiation that a module can convert as a function of its layout. Therefore, different module architectures are simulated in the urban landscape shown in Figure 4.7a. The landscape represents a street where a shading study is performed on the marked rooftop of the middle house. The roof is facing south and has a tilt of 30°.

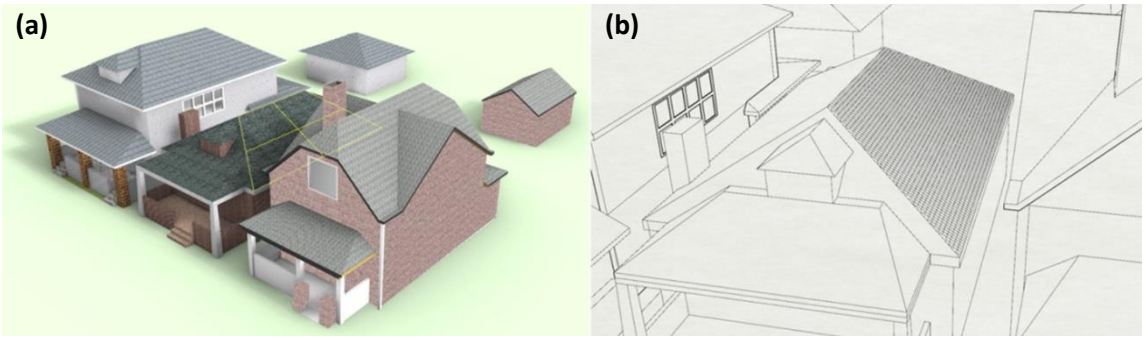

Figure 4.7: *(a) 3D urban landscape where PV modules will be placed on the marked roof of the middle house. The roof is facing south and tilted 30 degrees. (b) Projected grid on the roof to evaluate the irradiance throughout the year.*

To obtain the irradiance profile on the roof, sensitivity and sky maps should be combined [44]. The first step is to create a 3D building model of the urban landscape and includes surrounding obstacles which can directly or indirectly affect the irradiance incident on the selected rooftop. Then, a grid is created on the rooftop with a size of 125x125 mm as shown in Figure 4.7b and is equal to the area of a solar cell.

By means of ray tracing, sensitivity maps are obtained for each cell on the roof. These maps show the sensitivity of a surface to light incident from all possible directions. For a single cell, the sensitivity to light from one specific direction can be calculated by illuminating the whole urban landscape from that direction and taking the reflections from the surroundings into account. The sensitivity is then the absorbed ray intensity at the cell divided by the radiative power of the light source. The obtained sensitivity maps for two cells on the rooftop are shown in Figure 4.8. It is clear that the cell high up the rooftop is less shaded throughout a year and will therefore generally receive a higher irradiance. Note that the sensitivity is independent of the geographical location of the urban landscape and can be larger than one due to light reflection.

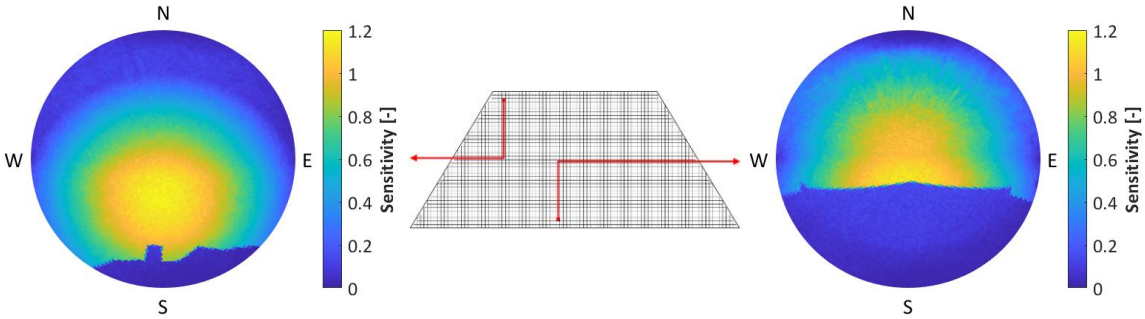

Figure 4.8: *Sensitivity maps of two cells on the rooftop of the urban landscape. The dark blue area in the south is due to the shadow caused by the neighbour's house.*

In the next step, climate data and the Perez luminance model are used to obtain sky maps. The Perez model uses the Direct Normal Irradiance (DNI), Diffuse Horizontal Irradiance (DHI) and the sun's position to reconstruct the luminance distribution across the sky [45]. Sky maps combine the direct irradiance with the diffuse sky irradiance. In the simulation, Rotterdam was chosen as the location of the urban landscape. The sky maps are generated for each 10-minute interval during an entire year. Multiplying the sensitivity and sky maps, gives the irradiance on each cell on the roof. As an example, the sky maps and irradiance profiles on the rooftop for a sunny and cloudy day are shown in Figure 4.9.

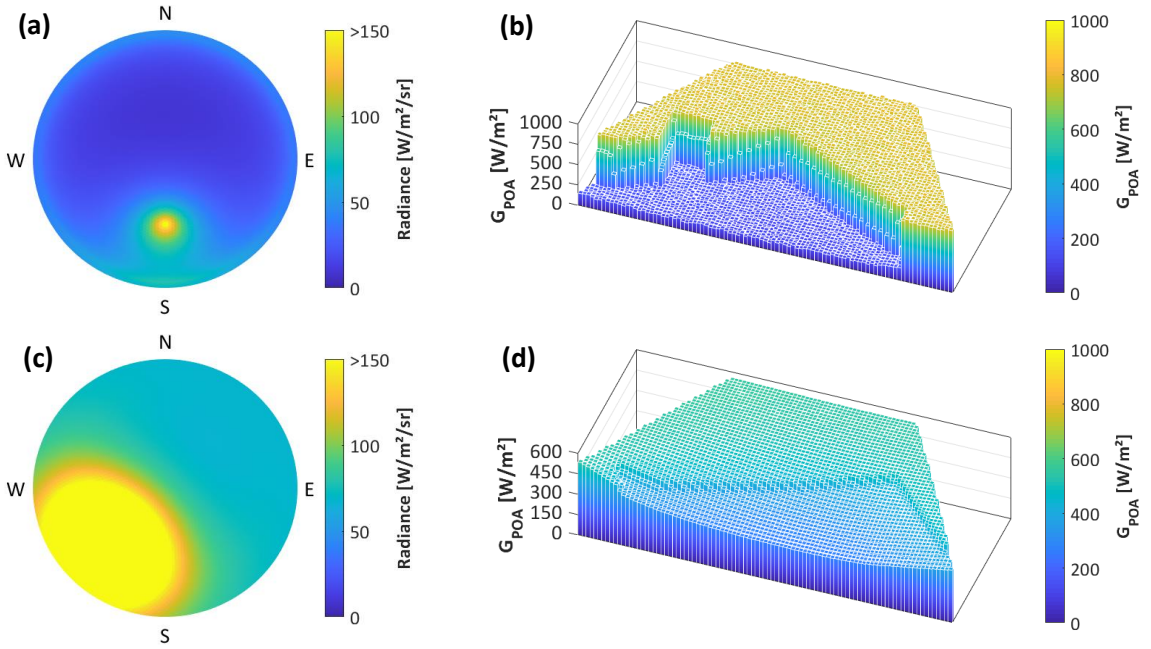

Figure 4.9: *(a) Sky maps for a sunny day (DNI = 600 W/m², DHI = 80 W/m²) when the sun is in the south ($A_s = 180°$) and 45° above the horizon ($a_s = 45°$). (b) Irradiance profile on the roof for the sunny case. (c) Sky maps for a cloudy day (DNI = 60 W/m², DHI = 400 W/m²) when the sun is in the southwest ($A_s = 225°$) and 35° above the horizon ($a_s = 35°$). (d) Irradiance profile on the roof for the cloudy case.*

4.3. OPTIMAL SUBGROUP SIZE AND ORIENTATION

The irradiance on each cell throughout an entire year is obtained by combining sensitivity and sky maps. A PV system is then created by accommodating as many 72-cell modules on the roof as possible. For conventional PV modules, a landscape orientation is generally preferred over a portrait orientation, because of the positioning of the three bypass diodes. Consequently, the PV system consists of 31 modules which are positioned in landscape mode as shown in Figure 4.10a. to allow a fair comparison. Each PV module can be divided into a fixed number of subgroups (i.e. reconfigurable units). Lefevre et al. defines several criteria to consider when selecting a module architecture [46]. It is important that all subgroups have an equal number of cells to prevent mismatch losses under uniform irradiation and that the shape is rectangular and consistent to enhance the manufacturing process. Consequently, there are 24 possible subgroup size and orientation combinations which can be separated into four families as shown in Figure 4.10b.

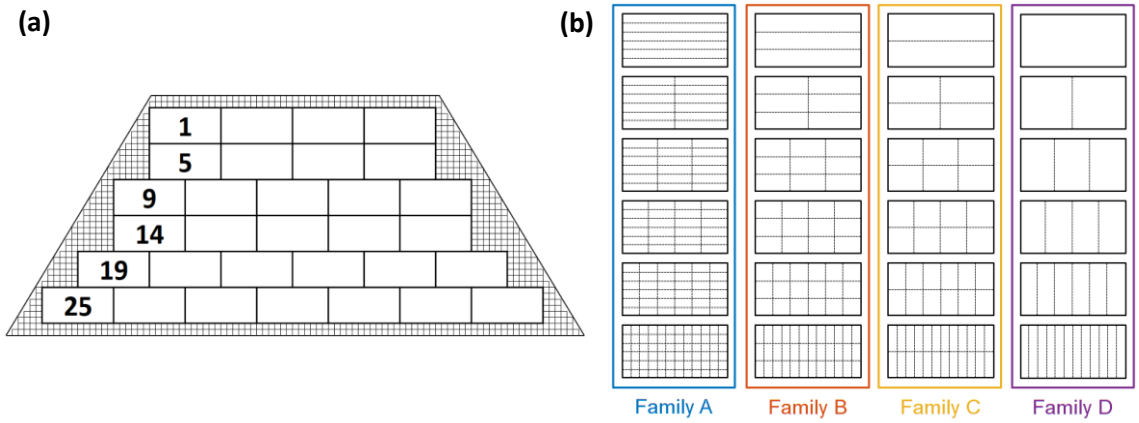

Figure 4.10: *(a) Accommodation of 31 PV modules on the rooftop of the urban landscape. (b) Division of the 24 possible subgroup size and orientation combinations for 72-cell PV modules into four families.*

Most of these layouts vary in their subgroup size and therefore require a different amount of switches as derived in section 4.1. Solar cells within a subgroup are connected in series. The subgroup current is therefore limited by its worst performing cell. Since the current of a solar cell changes linearly with irradiation while the voltage remains almost constant, the solar radiation could be used as indicator for the potential of each of the 24 module layouts. Hence, a good estimation of the maximum amount of solar radiation that a module can convert (i.e. effective irradiation), is using the minimum cell irradiation within a subgroup as the solar radiation incident on the whole subgroup. The results are shown in Figure 4.11 for the entire PV system as well as the modules which suffer the least and the most from partial shading. Note that these modules will have the lowest and highest gain respectively when switching to a reconfigurable PV module and do not necessarily receive the highest and lowest irradiation. It can be observed that smaller subgroups have a higher effective irradiation and that layouts within Family D perform worst.

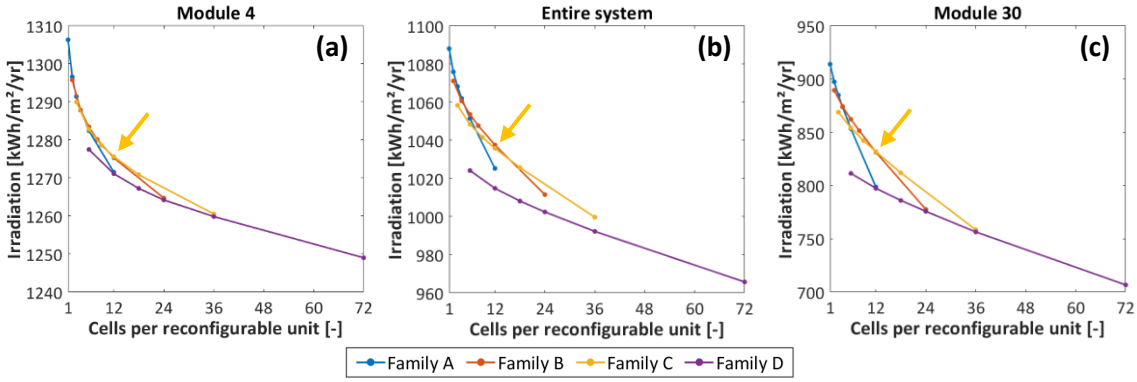

Figure 4.11: *Maximum harvestable solar irradiation in Rotterdam (the Netherlands) for each of the 24 module layouts when considering (a) only the module which suffers least from partial shading, (b) the entire PV system and (c) only the module which suffers most from partial shading. The yellow arrow indicates the selected module layout.*

Smaller subgroups seem beneficial and also allow more possible configurations, but require more components and complex wiring which results in power losses. The number of switches increases drastically when decreasing the subgroup size. The optimal size of the subgroups is therefore a trade-off between shading linearity, resistive power losses, complexity, costs and reliability. The simulations showed that the optimal layout for a 72-cell module contains 6 reconfigurable units, each with 12 series connected cells. This means that there are four possible subgroup shapes of which family B and C both provide an optimal output. Family C is preferred, because it would perform more equally in the case of row, column and corner shading. Figure 4.12 visualizes the proposed reconfigurable module. For illustration purposes, the terminals are drawn at the sides, whereas the actual terminals are located at the centreline of the module to reduce wire losses. The proposed reconfigurable module can switch between 27 unique configurations and requires 25 switches. A complete list of these configurations is presented in appendix B.

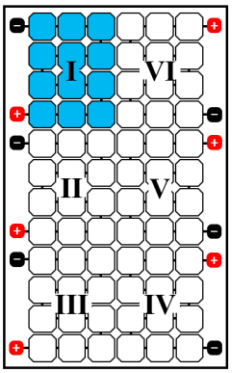

Figure 4.12: *Proposed PV module layout with 6 reconfigurable units of 12 series connected solar cells each. The module can adopt 27 unique configurations using 25 switches.*

4.4. WORLDWIDE POTENTIAL

To determine the potential of the proposed reconfigurable module, its effective irradiation is compared with the conventional PV module for different climates around the world as shown in Figure 4.13. The methodology is slightly modified for the conventional module, because a subgroup will not produce any power when a bypass diode is activated. Hence, the effective irradiation is calculated for each combination of activated and deactivated bypass diodes and the maximum value is used. It should be noted that for locations on the southern hemisphere, the urban landscape is rotated to ensure that the considered rooftop is facing north. It appeared that module 4 and 30 (almost) always have the lowest and highest gain respectively and is irrespective of the latitude of the location. The module which suffers most from partial shading has a global average annual irradiation increment of roughly 11%. This would mean that a reconfigurable PV module with 20% efficient solar cells would produce as much energy as conventional PV modules with 22% efficient solar cells. Furthermore, it can be concluded that the gain is larger for location further from the equator, because the average sun's position is lower and therefore shadows caused by surrounding objects are generally larger and occur more frequently.

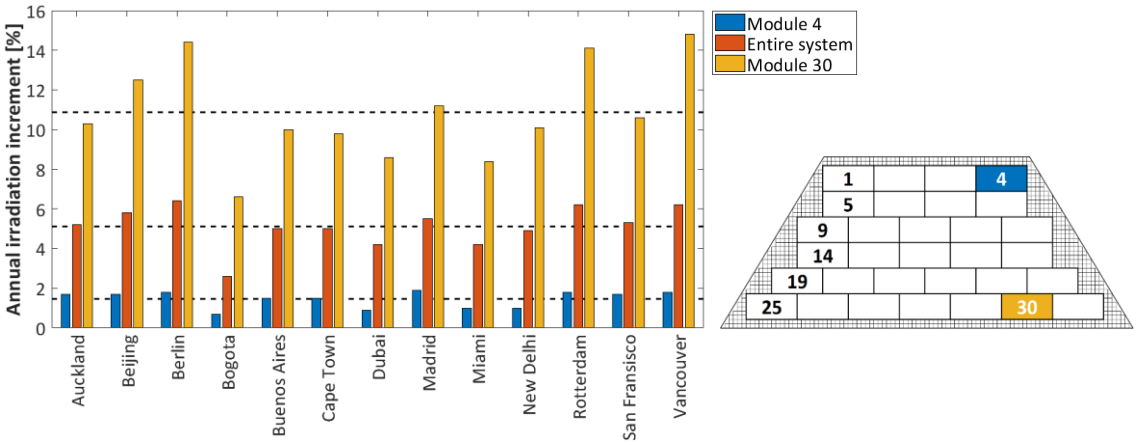

Figure 4.13: *Annual irradiation increment of the proposed reconfigurable module layout with respect to the conventional PV module.*

5

COMPARITIVE PERFORMANCE ANALYSIS OF PV MODULES

In this chapter, electrical simulations of the reconfigurable PV module are discussed to evaluate the module performance. The chapter starts by introducing relevant reference topologies and an overview of the parameters used in the simulation framework. Next, a case study is presented in which the performance of the reference and reconfigurable modules is compared. This done for several static shading patterns as well as the earlier introduced urban landscape. A detailed sensitivity analysis is carried out to analyse the validity of the results in the presence of design uncertainty. Finally, the practical implementation of a reconfigurable PV module is addressed.

5.1. REFERENCE TOPOLOGIES

To put the proposed reconfigurable module into perspective, its performance is compared with several relevant reference topologies shown in Figure 5.1. The blue solar cells represent the size and orientation of a single subgroup.

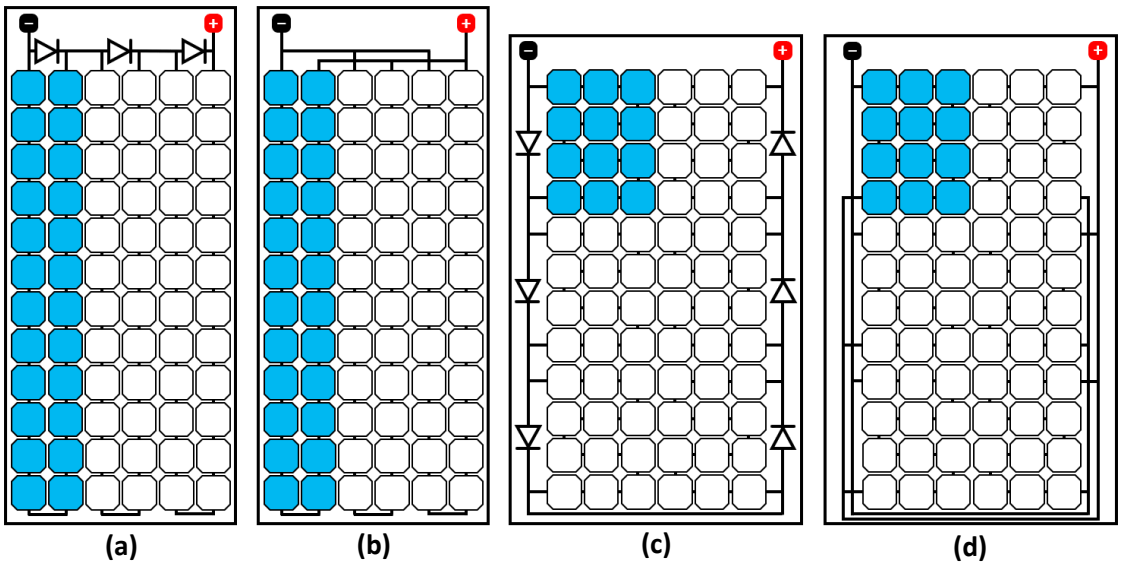

Figure 5.1: *Reference topologies: a) three series connected subgroups with bypass diodes, b) three parallel connected subgroups, c) six series connected subgroups with bypass diodes and d) six parallel connected subgroups.*

The four relevant reference topologies are referred to as *3 series*, *3 parallel*, *6 series* and *6 parallel* respectively. Most important is the *3 series* architecture, because it is the standard in commercial PV modules. In this topology, a bypass diode is connected in parallel with each of the three series connected subgroups. The *3 parallel* architecture is the parallel equivalent of the conventional module and has no bypass diodes. Two similar reference topologies are obtained when switching to six subgroups with the same shape as used within the reconfigurable PV module. In Figure 5.1, the subgroup interconnections for these last two topologies are drawn at the sides for illustration purposes. In reality, these interconnections are located at the centreline of the PV modules. Furthermore, subgroups in the fixed parallel topologies are in reality connected at the junction box and therefore current accumulation does not occur in wires within a module.

5.2. SIMULATION PARAMETERS AND LOSSES

Simulations of the reference and reconfigurable modules are performed in MATLAB Simulink [47]. The PV modules considered in this report contain 72 solar cells with a size of 125x125 mm. The single diode solar cell model in Figure 2.2 is adjusted to include the reverse characteristics associated with shading. This is done by connecting the combination of a voltage source, resistor and diode in parallel with the current source [48]. The values used in this eight-parameter model are given in Table 5.1. Both solar cells with a low and high reverse bias voltage are considered.

Table 5.1: *Parameters in the modified single diode solar cell model.*

Parameter	Symbol	Value
Series resistance	R_S	6.4 mΩ
Shunt resistance	R_{SH}	64 Ω
Saturation current	I_0	1.56 nA
Ideality factor	n	1.2
Photogenerated current	I_{PH}	5.78 A
Saturation current (reverse)	$I_{0,RB}$	0.01 A
Ideality factor (reverse)	n_{RB}	10
Reverse bias voltage	V_{RB}	-2.5 V **or** -15 V

The I-V curves of these solar cells in both reverse and forward bias are shown in Figure 5.2. All simulations are performed at a cell temperature of 25°C which corresponds to the standard test conditions (STC). In the electrical simulations, the temperature effects described in section 2.4 are not taken into account, because these would drastically increase the computation time.

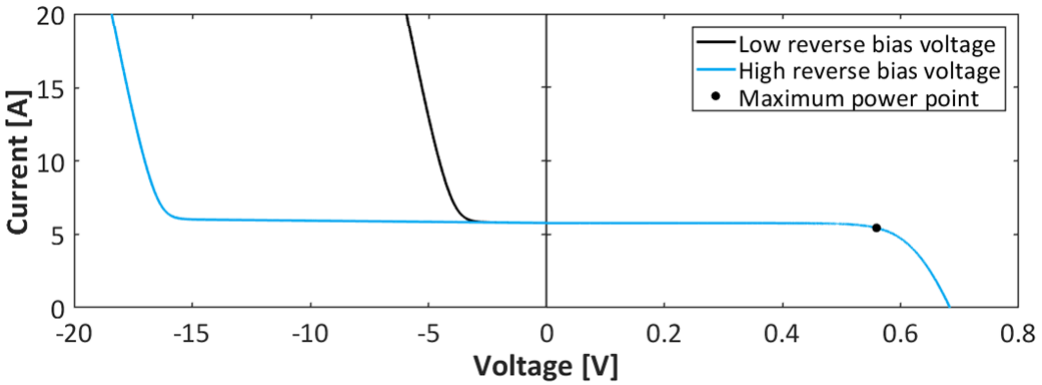

Figure 5.2: *I-V curve of a solar cell at standard test conditions in both reverse ($V < 0$) and forward ($V > 0$) bias operation. Note that the scale on the horizontal axis is not linear.*

The I-V curve under forward bias can be used to determine the external parameters of the solar cells. These are listed in Table 5.2. The power produced by each solar cell at STC is around 3 W.

Table 5.2: *External solar cell parameters.*

Parameter	Symbol	Value
Open-circuit voltage	V_{OC}	0.69 V
Short-circuit current	I_{SC}	5.78 A
Power in MPP	P_{MPP}	3.04 W
Voltage in MPP	V_{MPP}	0.56 V
Current in MPP	I_{MPP}	5.43 A
Fill factor	FF	0.76
Efficiency	η	19.5%

Wiring losses

It is assumed that all solar cells in the reference and reconfigurable modules have these electrical properties and are therefore identical. The modules contain 72 solar cells which are connected using flat tabbing wire made of tin coated copper. The power dissipation in these wires can be calculated with equation (3.2) in which the resistance is given by

$$R = \rho \frac{l}{A} \tag{5.1}$$

where ρ is the resistivity and equals $1.68 \cdot 10^{-8}$ Ωm for copper, l is the length of the wire and A is its cross-sectional area. Conventional solar cells have both front contacts (fingers and busbars) and rear contacts. Solar cells are tied together by connecting the front contacts of one cell to the rear contacts of another cell as shown in Figure 5.3. Narrow tabbing wires are used to minimize the inactive (i.e. shaded by metal) area of cells. Due to the use of multiple busbars, the current through each of these wires is only a fraction of the cell current. As a result, the relatively high resistance of narrow tabbing wires does not cause significant power losses. Thicker wires would further reduce the losses, but are stiffer and therefore can easily lead to cell breakage [49].

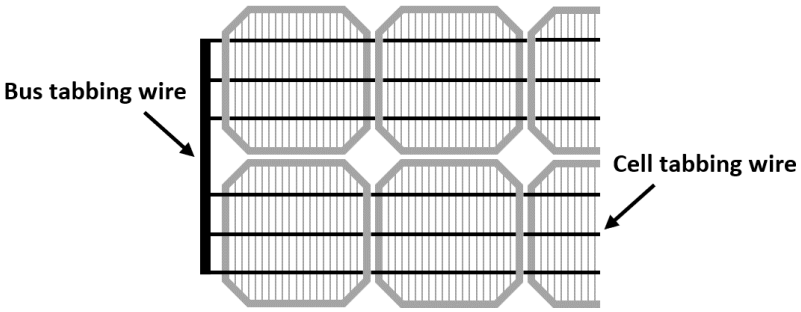

Figure 5.3: *Solar cell interconnections with tabbing wire.*

The narrow solar cell tabbing wires on each busbar are brought together at the end of a string via a bus tabbing wire. This wider tabbing wire carries the whole cell current and is used for all other interconnections within a PV module, such as to connect side-to-side strings or subgroups to the junction box. The width and thickness of the used wires are listed in Table 5.3.

Table 5.3: *Tabbing wire parameters for solar cell interconnections.*

Parameter	Value
Cell tabbing width	2.0 mm
Cell tabbing thickness	0.2 mm
Bus tabbing width	6.0 mm
Bus tabbing thickness	0.3 mm

Each of the reference and reconfigurable modules differ in their interconnections and hence also in their wiring losses. These losses can be attributed to solar cell or subgroup interconnections. Modules with an identical subgroup size require the same wiring within a subgroup. It is assumed that the solar cells have a perfect square shape and contain three busbars and that its current is uniformly generated. As a result, the current through each of the busbars is one third of the cell current. To account for the subgroup losses in the simulations, a single resistor is modelled in series to each subgroup. Its resistance is the sum of the resistance of all wires within a subgroup. Since the current through this resistor equals the whole cell current, an equivalent resistance should be used to compensate for the lower current in cell tabbing wires. It is assumed that the type of cell interconnections are independent of the reverse bias voltage of solar cells.

To account for the losses in the wires for subgroup interconnections, several additional resistors are added to the equivalent models of the modules. Most of these wires are connected between subgroups and the junction box as shown in detailed schematics in appendix C. The length of these wires is therefore dependent on the position of the subgroups with respect to the junction box. The junction box is generally positioned at the backside of a module near the edge of the short side. The required wire length in modules with three subgroups is therefore relatively small, but increases significantly for PV modules with six subgroups. Whether a current flows through a wire in the *3 series* and *6 series* topologies, depends on the activation of bypass diodes. Since the diodes are located inside the junction box, the relatively long wires only carry a current when one or more bypass diodes are activated. Series connected modules therefore have lower wiring losses compared to their parallel counterparts. Placing the junction box in the centre of a module would reduce the wiring losses in modules with six subgroups. However, in reality this leads to a higher temperature of the junction box. This in turn leads to a lower performance of the solar cells behind the junction box. When wires are connected to the junction box, there is a small contact resistance of 0.5 mΩ/contact which is also taken into account in the simulations [50].

Other losses

In the reconfigurable module, metal-oxide-semiconductor field-effect transistors (MOSFETs) are used as electric switches. These transistors have the ability to change their conductivity with the applied voltage. A MOSFET has four terminals: source, drain, body and gate. The body is always directly connected to the source. When the applied voltage at the gate of a standard MOSFET is below a certain threshold, the transistor will not conduct and the switch is turned off and vice versa. These transistors can only block current in one direction. To block current in both directions, two MOSFETs must be connected in series and in opposite polarity [51]. Since both transistors should operate synchronously, their gates are connected. The back-to-back n-channel MOSFET as shown in Figure 5.4 is an example of a suitable switch for the reconfigurable module. It is assumed that each switch has a resistance of 10 mΩ when closed.

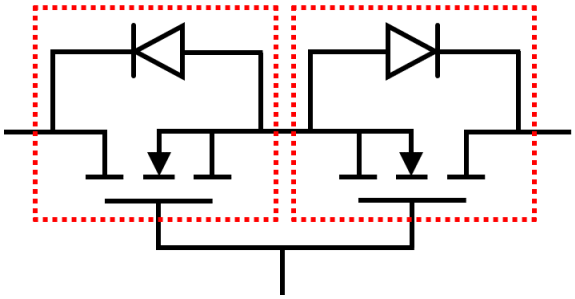

Figure 5.4: *Schematic overview of the switch in a reconfigurable module.*

The reconfigurable PV module requires 25 switches to change between all unique configurations. These switches are positioned on a central switchboard close to the junction box. Under uniform irradiance, the PV module will operate in its series configuration and only 5 switches are closed. In partial shading conditions, the module will likely operate in another configuration. When the module is in a 3x2, 2x3 or 1x6 SP configuration, there are respectively 6, 7 and 10 switches closed. Switches are non-ideal components that contribute to the power losses, especially when closed. The total power loss in the switchboard therefore depends on the selected configuration.

In the series connected reference topologies, bypass diodes are connected in parallel with each subgroups. SM74611 Smart Bypass Diodes of Texas Instruments are used. The specifications of these diodes are listed in Table 5.4 [22]. Smart bypass diodes are preferred over conventional Schottky diodes, because the power losses are much smaller when activated. This allows for a comparison between the optimal conventional module and the reconfigurable module.

Table 5.4: *Overview of the smart bypass diode parameters.*

Parameter	Symbol	Value
Activated diode resistance	R_{BPD}	3.2 mΩ
Saturation current	$I_{0,\mathrm{BPD}}$	0.10 nA
Ideality factor	n_{BPD}	0.02

The I-V curve of the smart bypass diode is shown in Figure 5.5. When only one diode is activated and the other subgroups operate at STC, the maximum power point current is around 5.4 A. The smart bypass diode will then dissipate approximately 0.16 W.

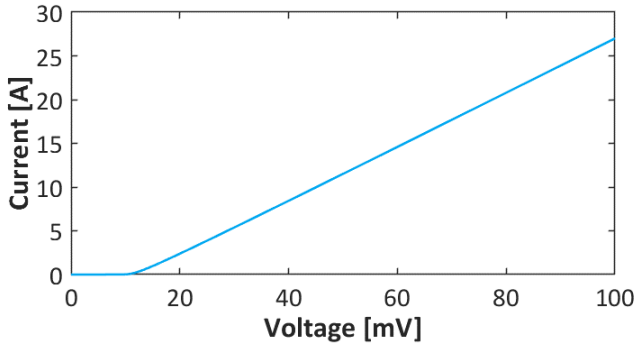

Figure 5.5: *I-V curve of the smart bypass diode.*

Finally, each module has a DC-DC power converter. The converters optimize the output power by constantly tracking the maximum power point of each individual PV module. The performance of a PV module is thus independent of other modules in the PV system. This allows comparing different module architectures in partial shading conditions rather than the system performance. The losses of the DC-DC converter are neglected for the time being.

5.3. PERFORMANCE IN STATIC SHADING PROFILES

A PV module can operate under uniform and non-uniform conditions. In uniform conditions, each solar cell has identical electrical and physical properties and therefore all cells produce the same output power. Non-uniform operating conditions lead to mismatch losses. These can be caused by a wide range of both internal and external factors. Manufacturing defects, malfunctioning and faulty solar cells are known as internal causes of variations in electrical properties between solar cells [14]. External factors include degradation of solar cells, dirt deposition, non-uniform surface

temperatures and partial shading. Shading is often caused by clouds or row-to-row shading of modules. In the urban environments, there are significantly more contributors to partial shading conditions. Partial shading is primarily due to static objects such as surrounding buildings, trees, chimneys and dormers. It can also be cause by soiling, bird droppings and fallen leaves. Some of these causes are unpredictable due to their random occurrence. As a result, the direction, shape and density of shadows cannot be fully known beforehand [37]. The proposed reconfigurable PV module was designed to improve the performance under quasi-static shading conditions. Nevertheless, its output power would definitely be higher than the conventional module in case of fixed random shading due to its smaller subgroup size.

First, the performance of the reference and reconfigurable modules are analysed for a variety of static partial shading conditions. Representative and commonly occurring shading patterns in the building environment are considered, including row, column and corner shading. It is obvious that the output power of a module does not only depend on the shading pattern, but also on the shading intensity. The shading factor is used to quantify the shading intensity and varies between 0 (non-shaded) and 1 (completely shaded). Shading patterns do not respect the borders of solar cells and results in partial shading of individual cells. It is important to realize that shading 10% of a solar cell with a shading factor of 1 is almost equivalent to shading the entire cell with an effective shading factor of 0.1 [52]. This is because the same energy is incident on the solar cell and the effect of the series resistance is negligible under normal irradiation concentrations. In the simulations of static shading profiles, a typical shading factor of 0.8 is used.

5.3.1. Row shading

The performance of the reference and reconfigurable PV modules is analysed by tracing the I-V curve and finding the maximum power point for all reference topologies and each configuration of the reconfigurable PV module (see appendix B). Power losses in wires are hereby neglected to facilitate the explanation of the results. First, solar cells with a high reverse bias voltage are considered. The simulation results for row shading are shown in Figure 5.6.

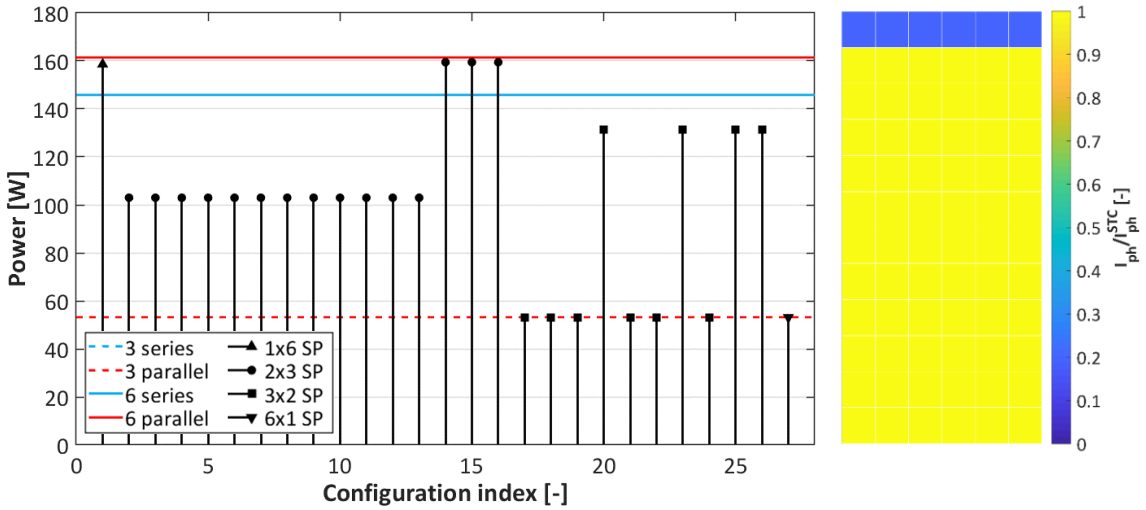

Figure 5.6: *Maximum power point power for the reference and reconfigurable PV modules under row shading.*

When one row of cells is shaded, each subgroup in the *3 series* and *3 parallel* topologies contains two shaded solar cells. The current through and voltage across the three subgroups are therefore identical. As a result, no bypass diodes are activated. Moreover, since current and voltage mismatch losses do not occur between subgroups, the *3 series* and *3 parallel* architectures result in the same output power. Switching from three to six subgroups increases the output power of the module by a factor larger than two. The gain is both due to the size and shape of the subgroups. In the *6 series* topology, the bypass diodes of the two partially shaded subgroups are conducting. It is important to realize that whether a bypass diode is active in the maximum power point depends on the shading factor as shown in Figure 3.2. Due to the activation of the two bypass diodes, the power potential of 24 solar cells is lost. In contrast, each subgroup in the *6 parallel* topology contributes to the output power. The voltage mismatch losses caused by the partially shaded subgroups are marginal. This is because the voltage depends logarithmically on the irradiance whereas the current has a linear dependence. As a result, parallel topologies generally outperform series connections.

The maximum power point power of each of the 27 configurations of the reconfigurable module is also shown in Figure 5.6. The highest power is obtained when subgroups with very similar I-V curves are connected in series to prevent current mismatch losses. Consequently, the 1x6 SP and three 2x3 SP configurations in which the equally shaded subgroups are connected in series (i.e. configurations 14 to 16) perform best. The main advantage of these last three configurations is that the module current is two times lower compared to the *6 parallel* topology while its output power is almost identical. The lower module current significantly reduces the power losses at system level and the costs of converters and cables. Note that the three 2x3 SP configurations perform slightly better than the 1x6 SP configuration since less switches are closed resulting in lower resistive losses.

5.3.2. Column shading

Column shading is the most common shading profile in large PV power plants. A conventional PV module has elongated subgroups and is optimized for this type of shading. Column shading also frequently occurs in urban landscapes and is often due to surrounding buildings and row-to-row shading of modules. The simulation results for column shading are shown in Figure 5.7.

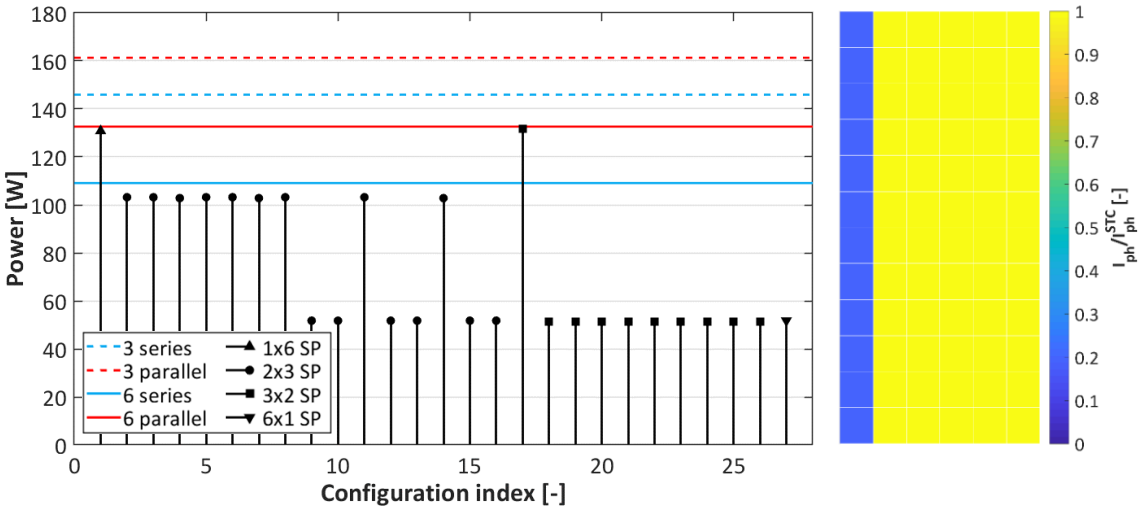

Figure 5.7: *Maximum power point power for the reference and reconfigurable PV modules under column shading.*

The most important observation is that modules with three subgroups now outperform the other topologies. The reason is that a smaller fraction of the module is affected due to the shape of the subgroups. Independent of the size of the subgroups, there is a gain when switching from a series to a parallel architecture. The gain is largest for a topology with six subgroups, because a smaller fraction (one third rather than half) of the solar cells within the shaded subgroups are shaded and therefore voltage mismatch losses are smaller too. As in the case of row shading, the reconfigurable PV module can achieve roughly the same output power as the *6 parallel* topology, but with a current that is three times lower.

5.3.3. Corner shading

Corner shading is characteristic for urban landscapes and can be caused by a wide range of static objects such as chimneys and dormers. In this case, shaded subgroups do not contain the same number of shaded solar cells. The simulation results for corner shading are shown in Figure 5.8.

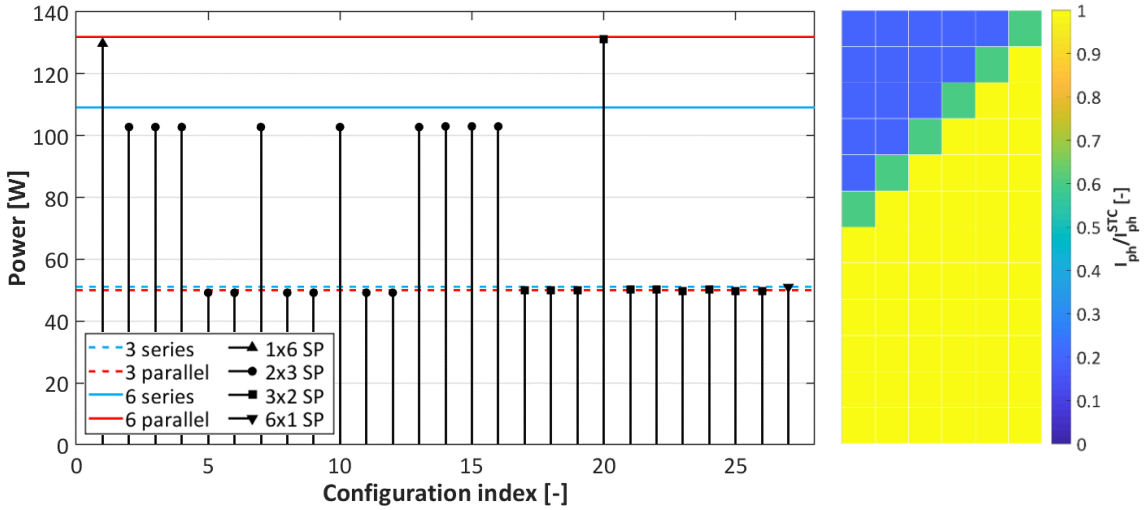

Figure 5.8: *Maximum power point power for the reference and reconfigurable PV modules under corner shading.*

When solar cells with a *high reverse bias voltage* are used, shading only one solar cell within a subgroup is already sufficient to limit the entire subgroup current and activate its bypass diode. As a result, the current of each shaded subgroups is equal, but the voltages differ. In the *3 series* topology, the maximum power point occurs when no bypass diodes are activated. This module topology slightly outperforms the *3 parallel* architecture, because the parallel connection suffers from voltage mismatch losses. Finally, the power output can be doubled when a module with six subgroups is used. The current of the reconfigurable module is again three times lower.

Impact reverse bias voltage

When solar cells with a *low reverse bias voltage* are used, the results change slightly. When only a small fraction of the solar cells within a subgroup is shaded, the shaded solar cells will not limit the subgroup current in the maximum power point. Series connected reconfigurable units should here be considered as one subgroup. Consequently, several configurations of the reconfigurable PV module as well as reference topologies with three subgroups can produce a noticeable higher power in row and corner shading scenarios as shown in Figure 5.9. One of the reasons why PV modules with these cells produce a higher power is because partial shading does not necessarily lead to the activation of bypass diodes as demonstrated in Figure 3.3. It should be noted that the gain decreases when smaller subgroups are used, because the probability that a small fraction of a subgroup is shaded is reduced.

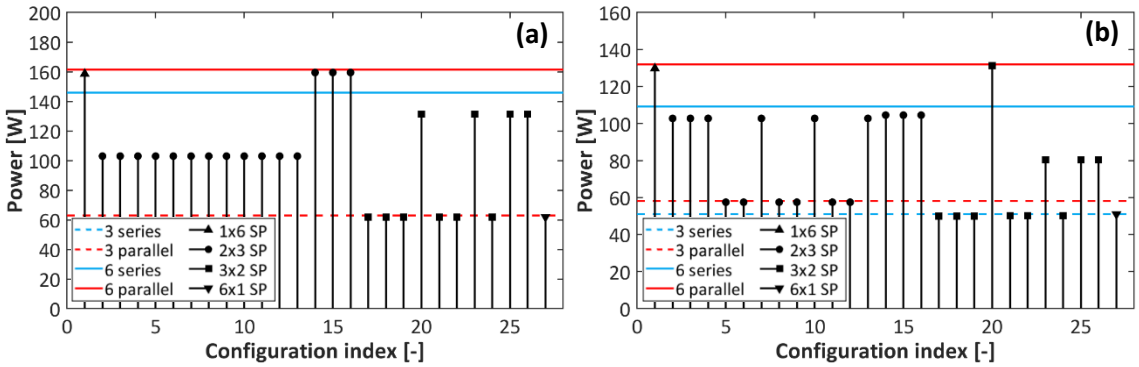

Figure 5.9: *Maximum power point power for the reference and reconfigurable PV modules under (a) row and (b) corner shading when the solar cells have a low reverse bias voltage.*

Reconfigurable TCT topologies

The proposed reconfigurable module can adopt 27 unique series-parallel configurations using 25 switches. A reconfigurable module which can adopt total-cross tied configurations requires many more switches as explained in section 4.1. Although static TCT configurations are generally more shade tolerant than static SP connections, the gain in reconfigurable modules was assumed to be limited since the interconnections are already optimized with respect to the shading pattern. To verify this claim, the output power of a reconfigurable PV module with TCT interconnections is analysed for both row, column and corner shading. As an example, the results for row shading are shown in Figure 5.10. Note that when two reconfigurable units are connected in parallel to form a row and three rows are connected in series, it is referred to as a 2x3 PS configuration. These configurations do not correspond to the configurations in appendix B.

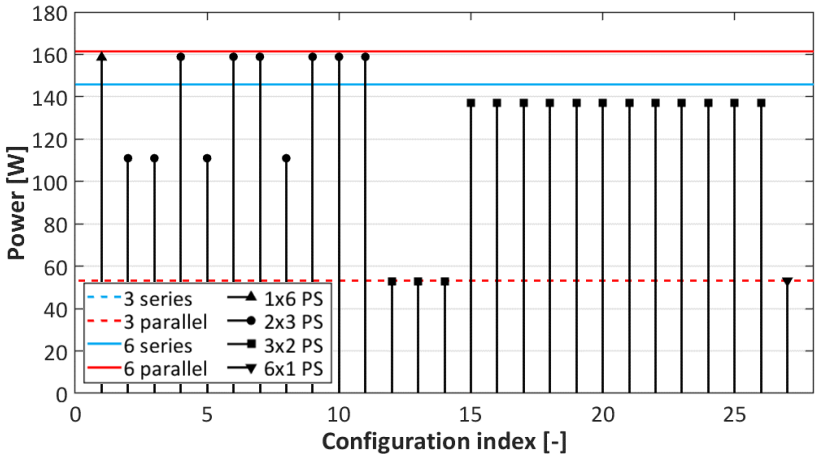

Figure 5.10: *Maximum power point power for the reference and TCT (i.e. PS) connected reconfigurable PV modules under row shading.*

The highest maximum power point power of the TCT connected reconfigurable PV module never exceeds the optimal power of the SP connected reconfigurable module. The main difference is that more configurations can achieve the maximum power. It should be mentioned that for some shading patterns, the SP connected reconfigurable module only produces optimal power when all subgroups are connected in parallel, while its equivalent TCT topology has the option to obtain the same power at a lower current. This is the case when the current of each parallel row is almost the same and there is always one subgroup receiving an unique shading intensity. Most of these scenarios are however very unlikely and do not compensate for the additional module complexity and costs due to the extra required switches.

5.3.4. Ultimate performance

Similar simulations can be performed taking into account wiring losses. To analyse how much power is lost in the wires, the module topologies are also simulated under uniform illumination conditions. As a reference, the power in the maximum power point when losses are neglected is 219.08 W and 41.53 W at an uniform irradiation of 1000 W/m^2 and 200 W/m^2 respectively. The output power for each topology is shown in Table 5.5.

Table 5.5: *Maximum power point power [W] for the reference and reconfigurable modules for uniform conditions and several partial shading scenarios. The output power for PV modules containing solar cells with a low reverse bias voltage and distributed switches are shown in red and blue respectively.*

Module topology	1000 W/m^2	200 W/m^2	Row	Column	Corner
3 series	216.23	41.42	53.11 61.00	144.00	50.93
3 parallel	216.08	41.41	53.10 60.92	159.20	49.84 57.55
6 series	215.74	41.40	143.35	107.12	107.14 107.29
6 parallel	213.42	41.31	156.78	129.30	128.28
6 reconfigurable	212.06 214.26	41.25 41.34	154.88 156.25	128.32 129.16	127.29 128.78

The maximum power point power at uniform illumination conditions clearly shows the higher wiring losses for modules with six parallel or reconfigurable connected subgroups. Since power losses increase quadratically with current, the losses in the reference and reconfigurable module topologies are much smaller at a lower irradiation. Subgroups containing shaded cells generally conduct a lower current and hence contribute less to the wiring losses. Consequently, the output power of modules with six subgroups slightly differs when the modules are rotated 180°. This is due to the fact that the junction box is not placed symmetrically with respect to the subgroups. The impact of the position of the junction box will be discussed in the sensitivity analysis.

As explained earlier, when only a small fraction of the solar cells within a subgroup is shaded, the output power of a PV module depends on the reverse bias voltage. In these cases, the red value in Table 5.5 corresponds to PV modules with cells with a low reverse bias voltage. In the standard reconfigurable module, switches are placed at a central switchboard for simplicity and reliability. However, when each switch is located at its optimal position, the wire lengths and therefore the power losses can be minimized. The maximum powers of the reconfigurable PV module with distributed switches are presented in blue in Table 5.5. It is clear that the reconfigurable module can now outperform the PV module with a *6 parallel* topology. The impact of distributed switches will also be discussed in more detail in the sensitivity analysis.

5.3.5. Shading tolerability

It is shown that the reference and reconfigurable modules have a different output power for the considered static shading scenarios and hence have a different shading tolerability. A measure to quantify the shading linearity is the Shading Impact Factor (SIF) and is given by

$$SIF = \left(1 - \frac{P}{P_{\mathrm{STC}}}\right)\frac{1}{SF} \tag{5.2}$$

where P is the actual power in the maximum power point, P_{STC} is the power output at standard test conditions (i.e. without shading) and SF is weighted shading factor of the module [13]. A SIF of 4 means that the mismatch losses are 4 times larger than the power reduction that the shading profile would suggest. A SIF of 1 is unfeasible, because there is always a difference between the incident and actual solar energy that can be harvested under partial shading conditions. The shade impact factors for each of the three partial shading scenarios are given in Table 5.6 when solar cells with a high reverse bias voltage are used. It can be concluded that a PV module with the *6 parallel* topology and the reconfigurable PV module have the highest shading tolerability.

Table 5.6: *Shade impact factor of the reference and reconfigurable modules for several partial shading scenarios.*

Module topology	Row	Column	Corner	Average
3 series	11.32	2.51	3.82	5.88
3 parallel	11.31	1.97	3.85	5.71
6 series	5.03	3.78	2.52	3.78
6 parallel	3.98	2.96	1.99	2.98
6 reconfigurable	4.04	2.96	2.00	3.00

5.4. ANNUAL ENERGY YIELD COMPARISON

Partial shading and uniform illumination conditions often alternate. To compare the annual yield of the reference and reconfigurable modules, the irradiation data of the aforementioned urban landscape in Rotterdam (the Netherlands) is used as input. Simulations are performed for an entire year using 10-minute interval data to obtain the annual energy yield. It is important to note that the reference topologies responds immediately to changing shading conditions. However, the reconfigurable PV module only changes its configuration at a specified switching interval. Between these time instants, the reconfigurable module might be in a non-optimal configuration due to changes in the shading conditions. Furthermore, the reconfigurable PV module cannot produce any useful power during the switching process. It is assumed that the switching interval and process are sufficiently short that these power losses can be neglected. These practical implementation issues will be discussed in more detail in section 5.6.

To reduce the simulation time, several simplifications are made. These affect the performance of the PV modules almost equally. First, it is assumed that the solar cells have a perfect square shape rather than the conventional octagonal shape. This makes raytracing simulations much less complex. Second, the margin between adjacent solar cells is neglected, because the margin is much smaller than the size of a solar cell. Finally, optical gains and losses in the module are neglected. Even with these simplifications, the computation time is too long to simulate each PV module in the urban landscape. Therefore, only the modules which suffer the least or the most from partial shading (i.e. module 4 and 30 respectively) are considered. An overview of the annual energy yield of the reference and reconfigurable topologies is given in Table 5.7.

The simulations are performed for both solar cells with a high and low reverse bias voltage. The results show that modules with six parallel or reconfigurable connected subgroups can increase the annual energy yield with around 9% when partial shading occurs frequently. Furthermore, modules which are hardly partially shaded lose less than 0.5% when switching from a conventional *3 series* to another module topology. Finally, the impact of the reverse bias voltage on the energy yield is hardly noticeable. Therefore, the remaining results are only discussed for PV modules containing solar cells with a high reverse bias voltage.

Table 5.7: *Annual energy yield [kWh] for the reference and reconfigurable topologies of the least (4) and most (30) partially shaded modules in the urban landscape in Rotterdam. Solar cells with a high and low reverse bias voltage are considered.*

Module topology	High RB voltage		Low RB voltage	
	4	30	4	30
3 series	273.86	164.10	274.03	164.85
3 parallel	+0.26%	+4.33%	+0.21%	+3.91%
6 series	+0.21%	+2.96%	+0.16%	+2.61%
6 parallel	-0.04%	+9.26%	-0.10%	+8.77%
6 reconfigurable	-0.45%	+8.70%	-0.51%	+8.21%

As an example, the power output for the different topologies of the most partially shaded PV module is shown in Figure 5.11 for a sunny day. It clearly illustrates that the gain of reconfigurable module only occurs during partial shading conditions (i.e. grey marked periods). Under uniform conditions, the module slightly underperforms due to the switches and longer wires. This effect is strongest around noon, because of the high irradiance which results in a higher current.

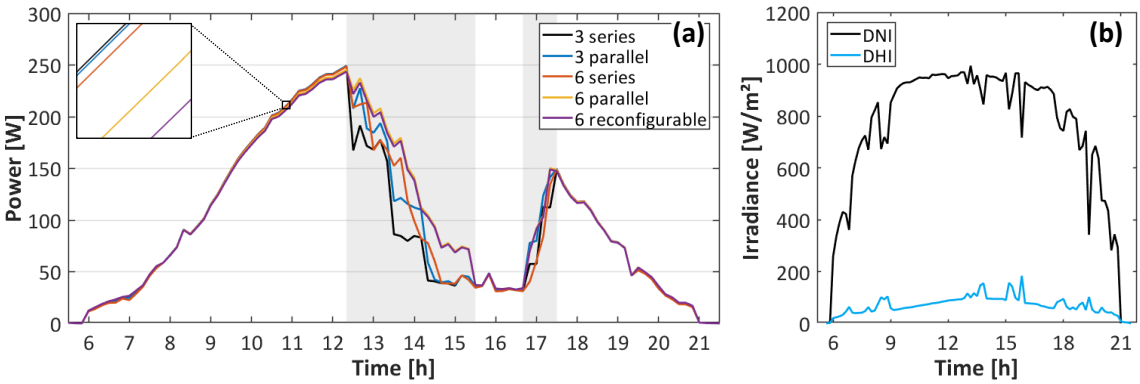

Figure 5.11: *(a) Power output of the most partially shaded module in the urban landscape throughout a sunny day. The grey areas mark the partial shading periods. (b) Direct and diffuse irradiation during the considered sunny day.*

5.4.1. Contribution of configurations

The reconfigurable PV module can adopt 27 unique configurations which can be divided into four categories: 1x6, 2x3, 3x2 and 6x1 SP. The reconfigurable module updates its configuration once per switching interval. Under uniform irradiance, the module operates in its series configuration. In partial shading conditions, other configurations will most likely provide a higher power. The least partially shaded PV module in the urban landscape is therefore most of the time in its series configuration, while the most partially shaded module is in its parallel configuration as shown in Figure 5.12. Both modules are also around 20% of the year in a 2x3 or 3x2 SP configuration.

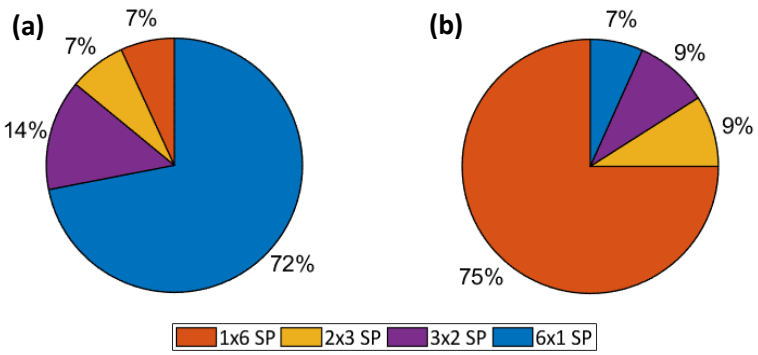

Figure 5.12: *Optimal configuration division throughout a whole year for the reconfigurable topology of (a) the least and (b) the most partially shaded modules in the urban landscape.*

The contribution of each category to the monthly energy yield is shown in Figure 5.13. Although the least partially shaded PV module is 72% of the year in its series configuration, it contributes to 90% of the annual energy yield. This is because the series configuration is preferred at uniform illumination conditions which is generally related to a relatively high output power. Likewise, the most partially shaded PV module is 75% of the year in its parallel configuration, while it only contributes to 57% of the annual energy yield.

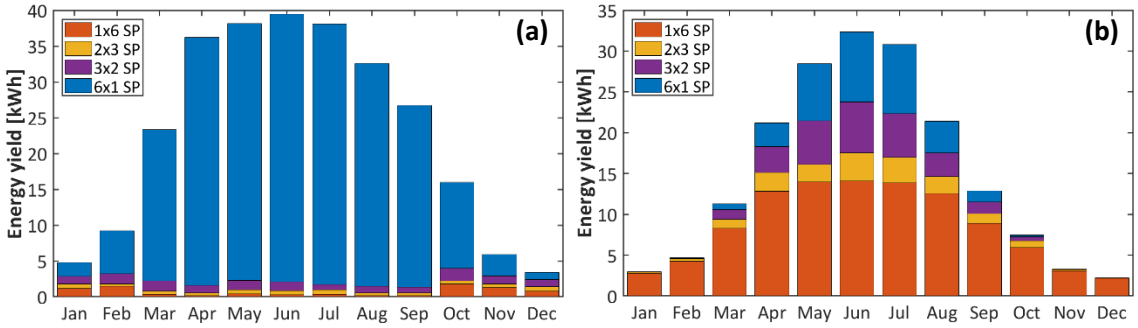

Figure 5.13: *Monthly energy yield for the reconfigurable topology of (a) the least and (b) the most partially shaded modules in the urban landscape.*

The results also show that the energy yield in summer is more than 8 times higher compared to winter months. This large difference is both due to the higher irradiation in summer as well as a longer time from dusk till dawn. An important remark is that these seasonal fluctuations would even be higher for conventional PV modules. As an example, the energy yield of the least partially shaded module is slightly reduced (<1%) in summer months, whereas the energy yield in winter months increases up to 7%. The monthly energy yield of the most partially shaded module always increases. The gain in summer months is around 7% and increases up to 20% in winter months. Consequently, the difference between the maximum and minimum monthly energy yield for the least and the most partially shaded modules is reduced by 5% and 9% respectively. This has a positive effect on energy storage requirements.

5.4.2. Module current distribution

The results presented in Table 5.7 show that a PV module with the *6 parallel* topology slightly outperforms the reconfigurable PV module. Furthermore, this architecture is less complex, more reliable and easier to manufacture. This may sound like there is no point in having reconfigurable PV modules. However, losses in the DC-DC power converter, losses in the cables at system level and the costs of the PV module are not yet taken into account. The main advantage of the reconfigurable module is that it can produce roughly the same output power as the fixed parallel topology with six subgroups, but at a much lower current. Power converters with a large current range are either less efficient or more expensive. Furthermore, lower currents result in less cable losses at system level when cables with the same cross-sectional area are used.

Since modules with six parallel connected subgroups or six reconfigurable units have the highest potential by far, the current distribution of these modules will be analysed and compared with the conventional PV module. The power generated by a PV module changes more or less linearly with the current. The proportionality factor depends on the layout of the PV module and is affected by the activation of bypass diodes in the series connected PV modules or switching between the configuration categories in the reconfigurable PV module. The relation between the maximum power point power and current for all time instants is shown in Figure 5.14.

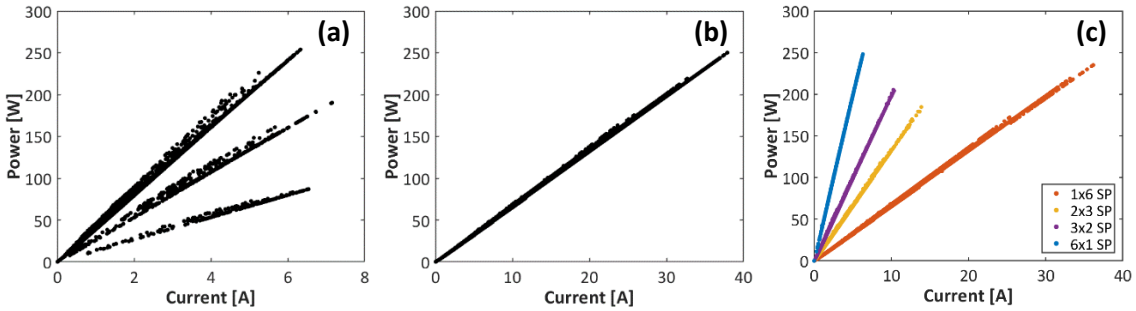

Figure 5.14: *Power against current in the maximum power point of the most partially shaded module in the urban landscape with (a) three series connected subgroups, (b) six parallel subgroups and (c) six reconfigurable units.*

For the *3 series* topology, the results show three slopes. This is due to the activation of zero, one or two bypass diodes. Some points have an offset from the linear trends. This is the case when only a small fraction of cells within a subgroup is shaded. This is more likely to occur in a larger subgroup and results in a relatively high maximum power point voltage. The non-linear part of the I-V curve near the MPP will then show a sharp rather than a smooth transition. The current distribution of the same three topologies is shown in Figure 5.15. It is obvious that the *3 series* and *6 parallel* topologies have the smallest and largest current range respectively. The relatively high probability of low currents is caused by (partial) shading as well as the lower irradiation in winter months and around sunrise and sunset.

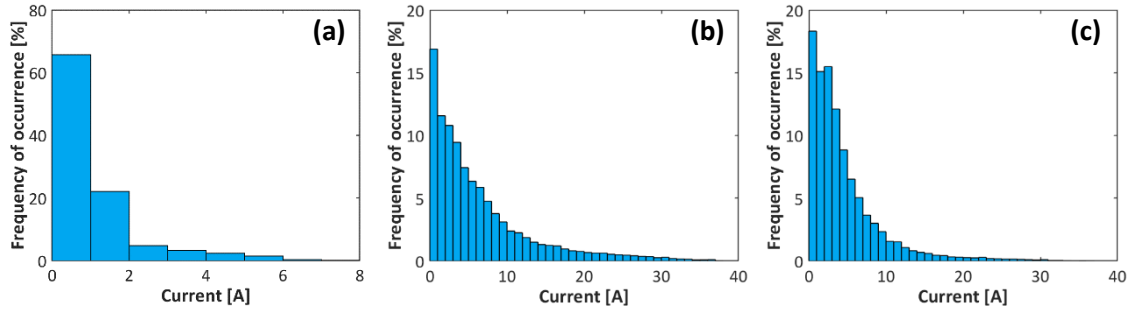

Figure 5.15: *Histogram of the current in the maximum power point of the most partially shaded module in the urban landscape with (a) three series connected subgroups, (b) six parallel subgroups and (c) six reconfigurable units.*

Smaller current range

It is also observed that the current range of the reconfigurable module is almost the same as the current range of the module with a *6 parallel* topology. However, the probability of high currents is smaller. To relax the requirements of the DC-DC power converter, two options are investigated to reduce the current range of the reconfigurable PV module. First, the 1x6 SP configuration is discarded as shown in Figure 5.16a. At least two subgroups have to be connected in series and therefore the maximum module current can be reduced with a factor two. However, higher mismatch losses are inevitable and drastically affect the annual energy yield (-1.74%).

The second option is based on the ability of the reconfigurable PV module to operate in another configuration when the output current exceeds a certain threshold. The module is then forced to operate in its second best or an even worse configuration. This methodology limits the current range to the set threshold. The impact on the annual energy yield is now much smaller, because the 1x6 SP configuration is only disregarded at high currents. The relation between the maximum power point power and current when the current is limited to 15 A is shown in Figure 5.16b.

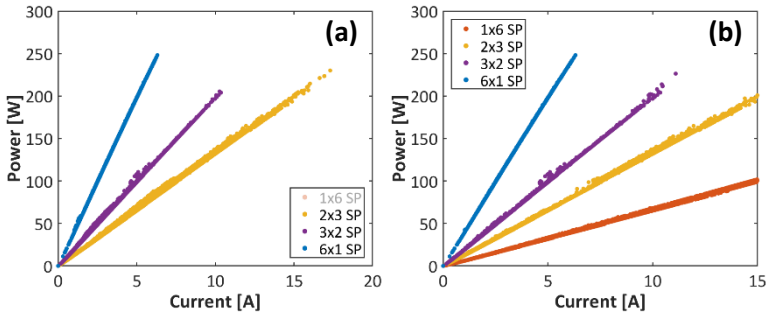

Figure 5.16: *Power against current in the maximum power point of the most partially shaded module in the urban landscape with six reconfigurable units discarding (a) the 1x6 SP configuration and (b) currents above 15 A.*

When the current is limited to 15 A, approximately four percent of the 1x6 SP configurations are substituted with mostly 2x3 SP configurations. Although the maximum current is even smaller than in the first option, the annual energy yield only decreases with 0.61%. The impact of both options on the current distribution is shown in Figure 5.17.

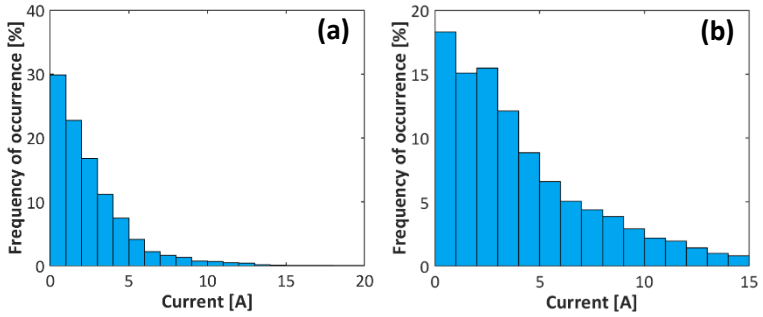

Figure 5.17: *Histogram of the current in the maximum power point of the most partially shaded module in the urban landscape with six reconfigurable units without (a) the parallel configuration and (b) currents above 15 A.*

Similar results can be obtained for the least partially shaded PV module in the urban landscape. Since this PV module is in its 6x1 SP configuration most of the time, the current range is already much smaller without implementing any restrictions.

5.5. SENSITIVITY ANALYSIS

Many parameters are defined in the simulation framework and assumptions were made. In a sensitivity analysis, the impact of changes in these input parameters is studied and often serves as a what-if analysis. To determine the robustness of the simulation results, a sensitivity analysis is performed for the most relevant parameters of the reference and reconfigurable topologies.

5.5.1. Absorption and reflection

It is assumed that the irradiation incident on a PV module is completely absorbed. In reality, a fraction of the light is reflected on the protective glass encapsulation layer and depends on the angle of incidence. Research performed by De Soto et al. uses Snell's and Beer-Lambert's laws to obtain an incident angle modifier (IAM) which is multiplied with the irradiation [53]. It should be noted that all light incident on the module is treated as direct irradiation. Therefore, the IAM is zero when the sun is behind the PV module. The method uses the sun's position to calculate the angle of incidence on the roof for each time instance with

$$\cos(\theta_{\mathrm{i}}) = \cos(a_{\mathrm{m}})\cos(a_{\mathrm{s}})\cos(A_{\mathrm{m}} - A_{\mathrm{s}}) + \sin(a_{\mathrm{m}})\sin(a_{\mathrm{s}}) \qquad (5.3)$$

where θ_i is the angle of incidence, a_m is the module altitude and equals 90° minus the roof tilt, a_s is the altitude of the sun and A_m and A_s are the azimuth of the module and sun respectively. Given the index of refraction of the glass layer n, the angle of refraction can be calculated with

$$\theta_r = \arcsin\left(\frac{1}{n} sin(\theta_i)\right) \tag{5.4}$$

The refractive index of glass is around 1.5. The incidence angle modifier can now be obtained by

$$IAM = \frac{\tau(\theta_i)}{\tau(0)} \tag{5.5}$$

where τ is the transmittance of the glass encapsulation layer of the module and is given by

$$\tau(\theta_i) = e^{-\frac{Kd}{\cos(\theta_r)}}\left[1 - \frac{1}{2}\left(\frac{\sin^2(\theta_r - \theta_i)}{\sin^2(\theta_r + \theta_i)} + \frac{\tan^2(\theta_r - \theta_i)}{\tan^2(\theta_r + \theta_i)}\right)\right] \tag{5.6}$$

where K is the glazing extinction coefficient and d is the glazing thickness. The transmittance at normal irradiation can be rewritten into

$$\tau(0) = \lim_{\theta_i \to 0} \tau(\theta_i) = e^{-Kd}\left[1 - \left(\frac{1-n}{1+n}\right)^2\right] \tag{5.7}$$

A typical glazing extinction coefficient is 4 m^{-1} and a common thicknesses is 2.0 mm. The incident angle modifier can be plotted for all possible angles of incidence as shown in Figure 5.18.

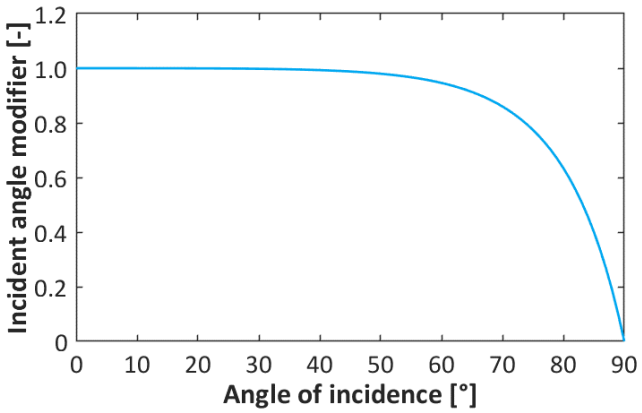

Figure 5.18: *Incidence angle modifier as a function of the angle of incidence.*

When this correction factor is applied to the irradiation data of the urban landscape, the annual energy yield of the least and the most partially shaded PV modules is reduced with around 4% and 6% respectively. The difference between both modules is caused by shading which alters the relative yield contribution at large angles of incidence. The IAM does not change the uniformity of the irradiation incident on the module and hence each topology is similarly affected. Strobach et al. found that the IAM for diffuse irradiation is around 95% and only depends on the module tilt [54]. Hence, the reflection of diffuse irradiation is overestimated for large angles of incidence and vice versa. Since the urban landscape is facing south, the highest irradiation and therefore the largest contribution to the annual energy yield occurs for relatively small angles of incidence. The impact of the IAM of the diffuse irradiation is therefore marginal.

Optical gains and losses due to for example reflection of light on the back sheet of a PV module or shading caused by tabbing wires are neglected. Complex raytracing simulations are required to account for these factors and this would significantly increase the simulation time. The solar cells in each topology are affected in almost the same way.

5.5.2. Interconnection wires

In the reference and reconfigurable topologies, both narrow and wide tabbing wires are used. The wider tabbing wires have a lower resistance and therefore cause smaller power losses. These wires are used for subgroup interconnections. When only narrow tabbing wires are used in the PV module, the power losses can significantly increase. The impact of the wire dimensions on the performance of the most partially shaded PV module in the urban landscape is shown in Figure 5.19a. The annual yields when losses in wires are completely neglected, are given as a reference.

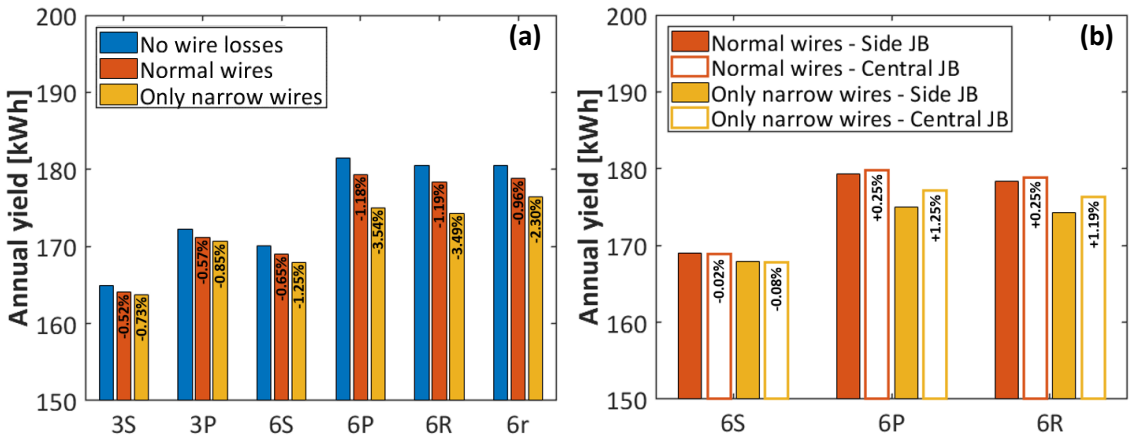

Figure 5.19: *Annual energy yield of the most partially shaded module in the urban landscape when changing (a) the dimensions of the tabbing wires and (b) the position of the junction box. The reference topologies are indicated with 3S, 3P, 6S and 6P. The reconfigurable topologies with central and distributed switches are referred to as 6R and 6r.*

Since PV modules with three subgroups hardly contain wide tabbing wires, the additional loss is relatively small when narrow wires are used instead. It is observed that the annual energy yield reduces the most for the *6 parallel* topology. The reason is that PV modules with six subgroups require longer wires due to the larger distance between subgroups and the junction box. Furthermore, current mismatch in these architectures is lower due to the smaller subgroup size. This leads to a higher average current through the subgroups. Finally, wires in the *6 parallel* topology always conduct a current, whereas most long wires in the *6 series* topology only conduct a current when one or more bypass diodes are activated. The losses in the reconfigurable module with a central switchboard are similar to the fixed parallel topology with six subgroups. However, the length of wires can significantly be reduced when distributed switches are used. As a result, replacing wide with narrow tabbing wires has a much smaller impact on this reconfigurable module. The same conclusions are valid for the least partially shaded PV module in the urban landscape, although the annual yield reductions are even larger due to the higher currents.

Solar cell size

The resistive power losses in wires depend quadratically on the current. The current density of a solar cell is usually between 25 and 45 mA/cm^2. The size of a solar cell is typically 125 x 125 mm^2 or 156 x 156 mm^2. The current of the latter cell size is therefore significantly higher. In contrast, the voltage of a solar cell is almost independent from the cell's area. As a result, modules containing larger solar cells produce roughly the same output power per square meter, but result in a much higher current. The power losses in both cell and subgroup interconnections therefore increase. Since the module topologies with six subgroups require most wiring, the gain of these architectures will partially be negated. This is especially the case for the *6 parallel* topology and reconfigurable module. The impact can be limited by using solar cells with more busbars, cutting cells in half or increasing the dimensions of the tabbing wires for subgroup interconnections.

Position junction box

The junction box is positioned at the backside of a PV module near the edge of the short side. For modules with six subgroups, the wire lengths for the subgroups closest to the junction box are therefore much shorter than for those further away. As a result, the annual energy yield differs slightly when these modules are rotated 180°. When the module has a *6 series* topology, the optimal performance is achieved when the junction box side of the module has the highest shading probability. The reason is that current will only flow through certain wires when one or more bypass diodes are activated. The power losses are therefore minimized when the shaded subgroups are closest to the junction box. The opposite is valid for the *6 parallel* topology. Each wire always conducts a current. Therefore, the current though the longest wires should be minimized. This is the case when the subgroups furthest away from the junction box are most shaded. The gain of changing the module orientation is especially noticeable when only narrow tabbing wires are used and is the largest for the *6 parallel* topology.

When the junction box is centred in modules with six subgroups, the wire lengths and therefore power losses can be reduced. The main reason not to implement a central junction box is the increase in its operating temperature which leads a lower performance of the solar cells behind the junction box. Nevertheless, the impact of the position of the junction box on the annual yield is analysed and shown in Figure 5.19b. A central junction box only increases the yield for the *6 parallel* or reconfigurable topology. The annual energy yield is now independent of the previous mentioned module rotation. When only narrow tabbing wires are used, the gain is much larger.

5.5.3. Switches and bypass diodes

The switch resistance directly affects the power output of the reconfigurable PV module, because there are always switches present in the active current path. The output power of the module is analysed for a sunny day and a switch resistance of 0, 1, 5, 10 and 25 mΩ as shown in Figure 5.20. The losses in wires are neglected in these simulations.

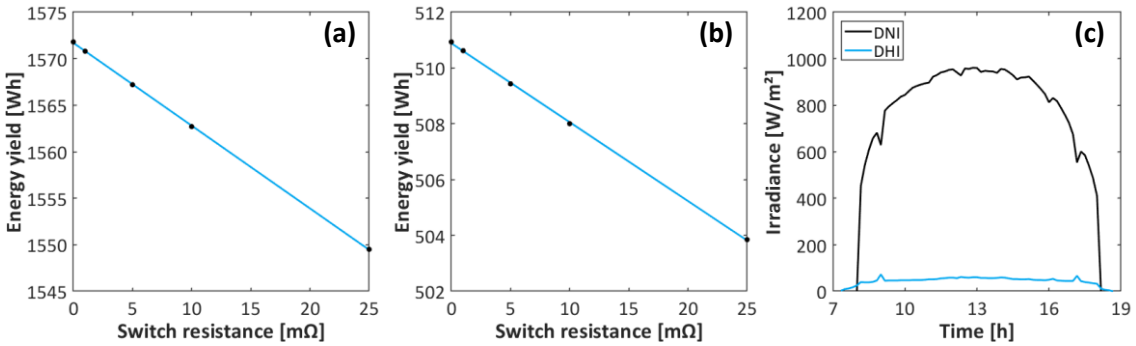

Figure 5.20: *Daily energy yield of (a) the least and (b) the most partially shaded modules in the urban landscape as a function of the closed switch resistance. (c) Direct and diffuse irradiation during the considered sunny day.*

It is observed that the power decreases almost linearly when increasing the switch resistance. The slope of the most partially shaded PV module is the smallest, because the current and power losses are generally lower. The linear fit for the PV modules in the urban landscape which suffer the least and the most from partial shading have a standard deviation of respectively 0.80% and 1.45%. The small deviation from the linear trend is due to changes in the preferred configuration. When more subgroups are connected in series, less switches are closed which contribute to the module resistance. For the series configuration in the reconfigurable module, higher switch resistance results in higher energy yield compared to other configurations, when subgroups receive almost the same irradiance.

The shift in the optimal configuration while increasing the closed switch resistance is shown in Figure 5.21. Due to the almost uniform irradiation incident on the least partially shaded module, the optimal configuration changes significantly when the switch resistance becomes non-zero. The series configuration is preferred for a typical closed switch resistance of 10 mΩ. When partial shading occurs frequently, the module is less sensitive to the switch resistance. Even for a closed switch resistance of 25 mΩ, the parallel connection still provides optimal power during most time instants. Consequently, there is a clear distinction between the optimal configuration of modules which suffer the least and the most from partial shading. Although only one day is considered in this analysis, the division for a switch resistance of 10 mΩ is similar to the results in Figure 5.12.

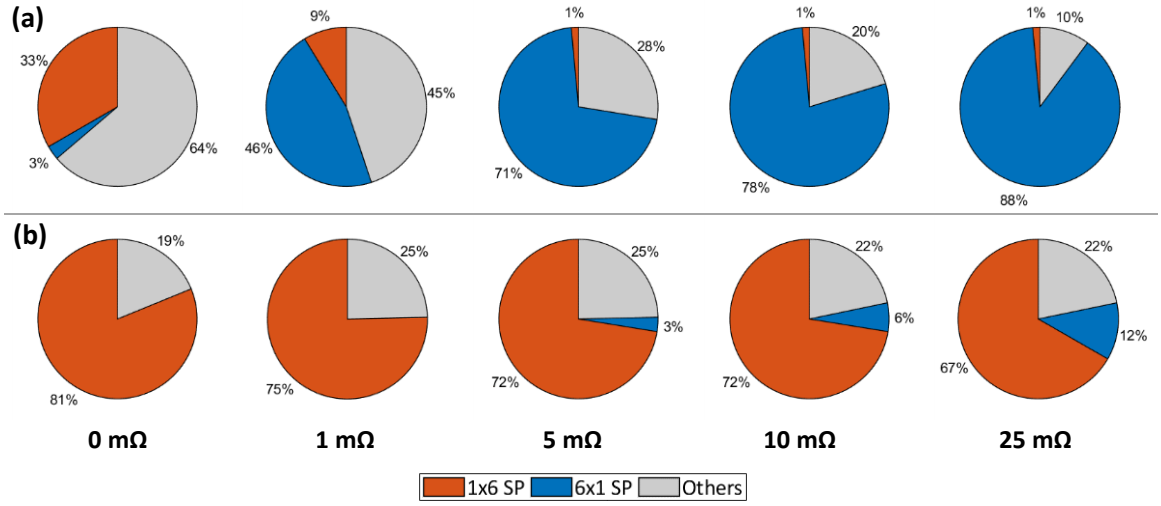

Figure 5.21: *Optimal configuration division during the sunny day of (a) the least and (b) the most partially shaded modules in the urban landscape when the closed switch resistance is increased (0, 1, 5, 10 and 25 mΩ).*

When conventional Schottky bypass diodes are used rather than state-of-the-art smart bypass diodes, the power losses increase by approximately 2 W per activated bypass diode when the other subgroups operate at STC. For example, in the case of column shading, the modules with three and six subgroups will then generate 141.96 W (-1.4%) and 101.03 W (-5.7%) respectively. Since partial shading conditions alternated with uniform illumination conditions, the annual energy yield in the urban landscape is only reduced with less than 0.4%. The impact is the largest for the module with a *6 series* topology, because generally more bypass diodes are activated.

5.6. PRACTICAL IMPLEMENTATION

The fixed series and fixed parallel topologies are relatively easy to implement. The reconfigurable module has a dynamic topology and is therefore more complex. In the simulations, the maximum power point power of each of the 27 configurations was determined and the configuration which provides the highest power was selected. However, this approach cannot be applied in reality, because tracing the I-V curve of each configuration requires a substantial time during which the PV module cannot generate any useful power. The power losses during this selection process are referred to as reconnection losses. It is thus essential that the number of traces is minimized.

5.6.1. Optimal configuration

The optimal power of a reconfigurable module is obtained when only subgroups with very similar I-V curves are connected in series to prevent current mismatch losses. Comparing short-circuit

currents of subgroups is a simple method to predict relevant configurations. As a result, current sensors are connected in series to each subgroup. In the example of the PV module with four reconfigurable units in Figure 4.4, the short-circuit current of unit II can be measured by closing only switches 2, 3 and 12. When subgroups are sorted based on these currents, the I-V curves only have to be traced for one configuration of each of the four series-parallel configuration categories (i.e. 1x6, 2x3, 3x2 and 6x1 SP). For both the 2x3 and 3x2 SP configurations, the optimal configurations can be predicted by connecting respectively the two or three subgroups in series with the highest short-circuit currents as well as the subgroups with the lowest short-circuit currents. The two remaining subgroups of the 2x3 SP configuration are also connected in series. This approach decreases the number of traces from 27 to 4. Simulations show that the optimal configuration is in 97.4% of the switching instant a member of the four selected configurations. Furthermore, the reduction in the annual yield is less than 0.01% when this method is applied.

It is possible to totally prescind from I-V curve tracings. This is done by applying a relatively simple algorithm which estimates the current mismatch for series connected subgroups. It is an iterative process in which the 6x1 SP configuration is considered first. If the relative difference between the highest and lowest short-circuit current of individual subgroups is below a specified first threshold, this configuration is selected. However, if the first threshold is exceeded, the 3x2 SP configuration is investigated. The relative difference is calculated for each of the two parallel connected strings. The 3x2 SP configuration is selected if the maximum of these two values is smaller than a specified second threshold. Otherwise, the 2x3 SP configuration will be examined. If the third threshold for this configuration is also exceeded, the 1x6 SP configuration is chosen. The order in this iterative process is important to minimize the output current of the reconfigurable module. Simulations show that the annual energy yield is reduced with roughly 0.04% if the three thresholds are set to 3, 2 and 1% respectively. Figure 5.22 shows an example of the operation of the algorithm. It should be noted that other relatively low thresholds give similar results. The small deviation in annual energy yield is due to the time instants when the irradiation is almost uniform. It is then very hard to estimate the current mismatch losses with the short-circuit currents. As a result, the division of the optimal configurations can then significantly change without affecting the yield.

Step 1: *measure current*

Unit	Current [A]
I	0.73
II	4.64
III	4.87
IV	4.79
V	1.07
VI	0.76

Step 2: *sort subgroups*

Unit	Current [A]
III	4.87
IV	4.79
II	4.64
V	1.07
VI	0.76
I	0.73

Step 3: *find relevant COI*

Category	COI index
1x6 SP	#1
2x3 SP	#16
3x2 SP	#26
6x1 SP	#27

Step 4: *calculate relative difference in short-circuit currents*

Category	Relative current mismatch [%]	Maximum mismatch [%]	Threshold exceeded?	Selected COI
6x1 SP	85.1	85.1	Yes	N.A.
3x2 SP	4.7	32.3	Yes	N.A.
	32.3			
2x3 SP	1.8	76.9	Yes	#1
	76.9			
	3.8			

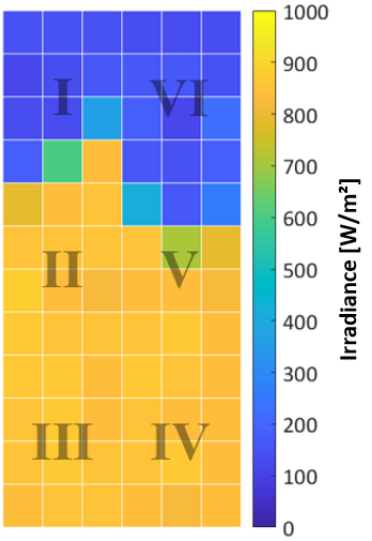

Figure 5.22: *Selection process of the algorithm to find the optimal configuration of the PV module with six reconfigurable units.*

In the example in Figure 5.22, the algorithm selects the 1x6 SP configuration. The study of the performance in static shading conditions in section 5.3 suggests that the 3x2 SP configuration would be most optimal. However, this configuration is discarded due to the small irradiation differences within the shaded and unshaded areas. These are mainly caused by the limited accuracy of the ray tracing simulations. When the irradiance within the shaded and unshaded regions is more uniform, the division of the optimal configurations will slightly change. Moreover, several 1x6 SP configurations are substituted by configurations in which multiple subgroups are connected in series. The impact on the annual energy yield is assumed to be negligible, although the module current can significantly decrease.

5.6.2. Switching interval

Since the shading conditions change in real time, the configuration should be updated frequently to ensure optimal performance. If the switching interval is too long, the gain of the reconfigurable PV module can decrease significantly. The recommended switching interval is therefore between 1 and 5 minutes for quasi-static shading conditions [55]. Instead of a regular update time, also a variable switching interval can be used. The interval is extended when the optimal configuration remained the same for a prolonged period of time.

It is important to realize that the irradiance incident on the module can drastically change within the switching interval. When the reconfigurable module is uniformly illuminated and therefore in its series configuration, hot-spot heating might occur if a single solar cell is suddenly heavily shaded by a bird dropping for example. If heating continues for a prolonged period, this can lead to irreversible damage as explained in appendix A. As a result, a relatively short switching interval or solar cells with a soft breakdown must be used to prevent hot-spots or rapid cell degradation.

6

PROTOTYPE AND MODEL VALIDATION

To demonstrate the feasibility of module architectures and to verify that the MATLAB Simulink model is performing as expected, an adjustable prototype is made. Using this prototype, the I-V curve under a range of partial shading patterns is determined and compared with simulations. The simulations show that PV modules with six parallel subgroups or reconfigurable units have the highest performance in urban landscapes. This chapter addresses the manufacturing process of the prototype and the measurement set-up, and investigates the deviations between the measurements and simulations.

6.1. MANUFACTURING PROCESS

The prototype contains six subgroups with a total of 72 mini solar cells and can switch between the fixed series, fixed parallel and the reconfigurable module topology. To create mini cells, monocrystalline silicon solar cells of 156 by 156 mm^2 are cut with a fibre laser scriber into cells of 39 by 39 mm^2 as shown in Figure 6.1. Note that each mini solar cell must contain both a front and rear contact, ideally centred in the cell.

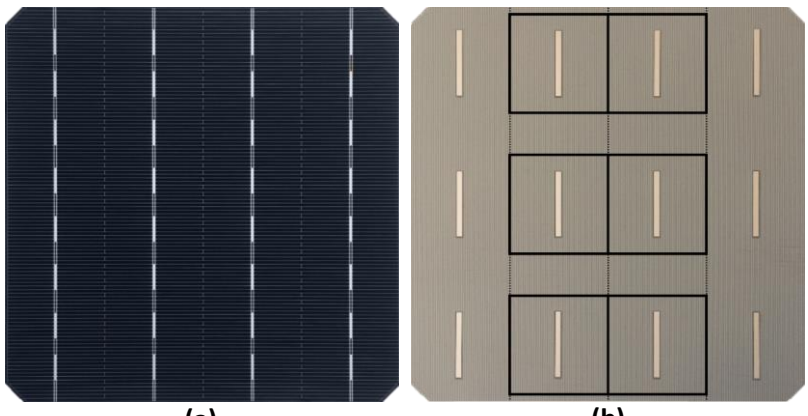

(a) (b)

Figure 6.1: *(a) Frontside and (b) backside of a monocrystalline silicon solar cell with four busbars and a size of 156 by 156 mm^2. The black squares mark the mini solar cells of 39 by 39 mm^2.*

The laser beam is directed using adjustable mirrors. It is possible to control the power, scanning speed, frequency, pulse width and the number of scans. The high energy density in the focus point of the laser beam causes the material to melt and evaporate. It should be noted that the laser only marks the solar cell. The actual cut is achieved by breaking the solar cell along the marked lines. Cells are marked from the backside to minimize the impact of the cutting process on the cell performance. The cuts can be visualized using a microscope as shown in Figure 6.2b.

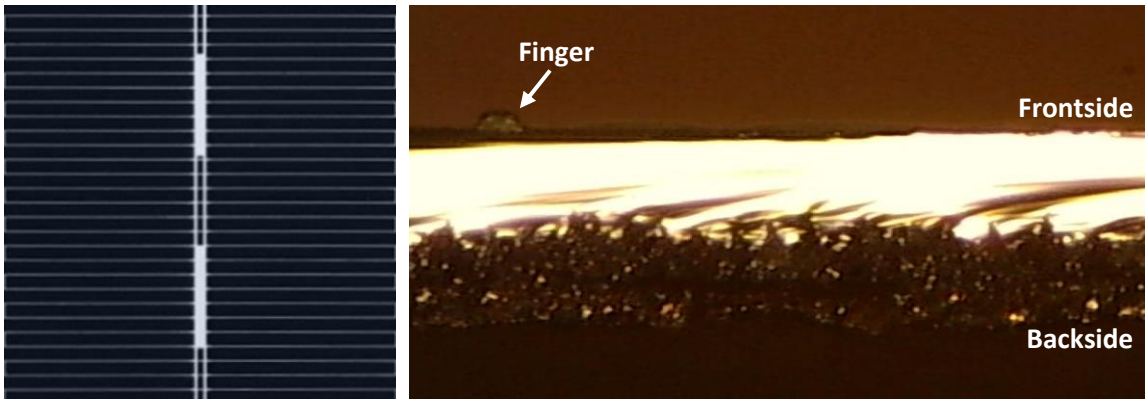

Figure 6.2: *(a) Mini solar cell with a size of 39 by 39 mm^2. (b) Cross-sectional microscope image of the mini solar cell in the direction parallel to the busbar. The dark porous structure corresponds to the molten metallization layer of the solar cell whereas the bright strip corresponds to the broken silicon layer.*

Next, the external parameters of the mini solar cell are determined by tracing its I-V curve under a solar simulator. A solar simulator approximates natural sunlight and allows measuring under standard test conditions. It should be noted that for an accurate measurement, a tabbing wire has been soldered on top of the entire busbar. This lowers the series resistance which is caused by the non-continuous busbar. Rosin flux was used to facilitate the soldering process by removing the oxidation from the metals to be joined. The I-V curve of each mini solar cell is very similar and is shown in Figure 6.3.

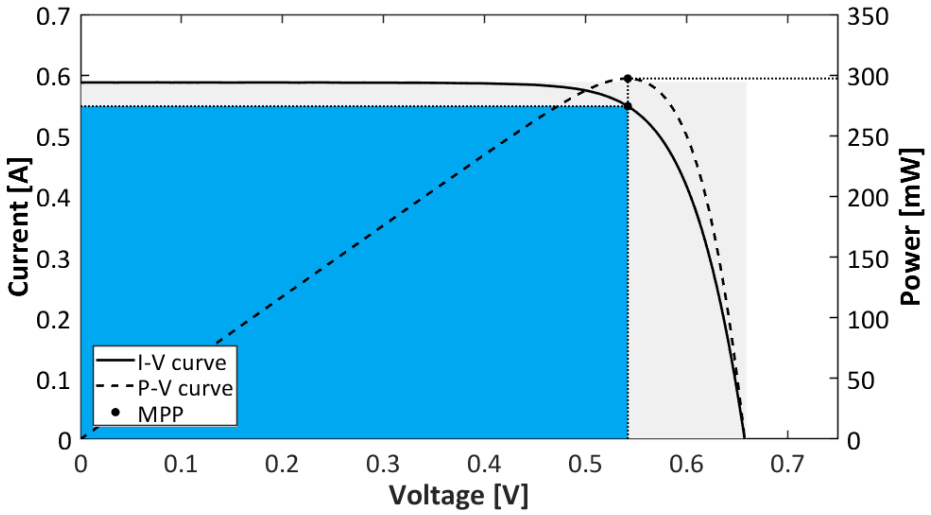

Figure 6.3: *Measured I-V and P-V curve of the mini solar cell.*

The external solar cell parameters are derived from the I-V curve. These are listed in Table 6.1. Each mini solar cell produces around 0.3 W under standard test conditions. The current density of these cells is almost identical to the value used in the earlier simulations.

Table 6.1: *Measured external solar cell parameters.*

Parameter	Symbol	Value
Open-circuit voltage	V_{OC}	0.66 V
Short-circuit current	I_{SC}	0.59 A
Power in MPP	P_{MPP}	297 mW
Voltage in MPP	V_{MPP}	0.54 V
Current in MPP	I_{MPP}	0.55 A
Fill factor	FF	0.77
Efficiency	η	19.5%

In order to compare the measurements with the simulation results, the mini solar cells must be parameterized. The parameters in an equivalent solar cell model are obtained by fitting both the illuminated and dark I-V curve. The dark I-V curve of the mini solar cell is shown in Figure 6.4 on both a linear and semi-logarithmic scale. The shunt resistance, saturation current and ideality factor describe the slope and curvature in the low current region, whereas the series resistance dictates the slope at high current levels [56].

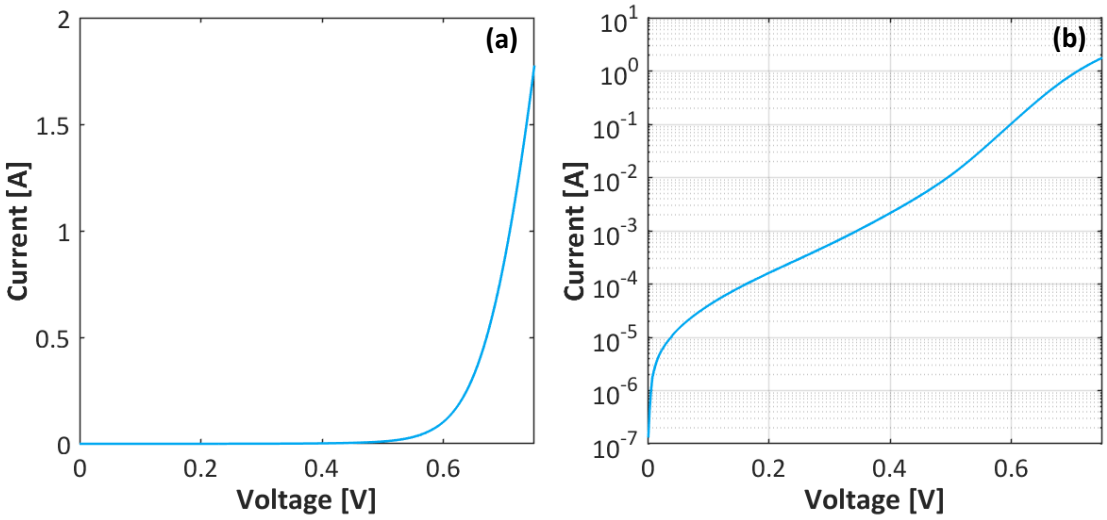

Figure 6.4: *Dark I-V curve of a mini solar cell on a (a) linear and (b) semi-logarithmic scale.*

To increase the accuracy of the fits, a more advanced double diode model is used. This solar cell model takes the junction recombination losses into account by placing an additional diode in parallel to the one in the single diode model in Figure 2.2 [16]. The resulting parameters are listed in Table 6.2.

Table 6.2: *Parameters in the double diode solar cell model.*

Parameter	Symbol	Value
Series resistance	R_{S}	37.2 mΩ
Shunt resistance	R_{SH}	19.7 kΩ
Saturation current	$I_{0,1}$	28.2 nA
Ideality factor	n_1	1.2
Saturation current	$I_{0,2}$	0.12 µA
Ideality factor	n_2	3.0
Photogenerated current	I_{PH}	0.59 A
Saturation current (reverse)	$I_{0,\mathrm{RB}}$	0.01 A
Ideality factor (reverse)	n_{RB}	200
Reverse bias voltage	V_{RB}	-3 V

Before interconnecting the mini solar cells to form subgroups and eventually the module, several tests are performed. First, several electroluminescence images are taken. Electroluminescence is both an optical and electrical phenomenon in which a material emits light in response to the flow of an electric current or a strong electric field. Here, current is fed into the cell in forward bias and radiative recombination of charge carriers causes light emission. Electroluminescence images provide information about the uniformity of solar cells as well as possible damage on the cells. Figure 6.5a shows an image of an undamaged cell. Solar cells with serious damage such as cracks or relatively large inactive areas have not been used in the prototype.

When a solar cell operates in forward bias, the cell temperature is uniform. The temperature of a solar cell was measured during the electroluminescence test with a thermal infrared camera. The temperature distribution when a current of 0.6 A is fed into the solar cell is shown in Figure 6.5b. It can be observed that the tabbing wire appears much colder than the solar cell, although their actual temperature is equal. The reason is the difference in emissivity between the two materials. The small gradient in the cell temperature is caused by the view angle of the camera. Note that the solar cell is not yet laminated and that the cell temperature in the assembled PV module will be higher.

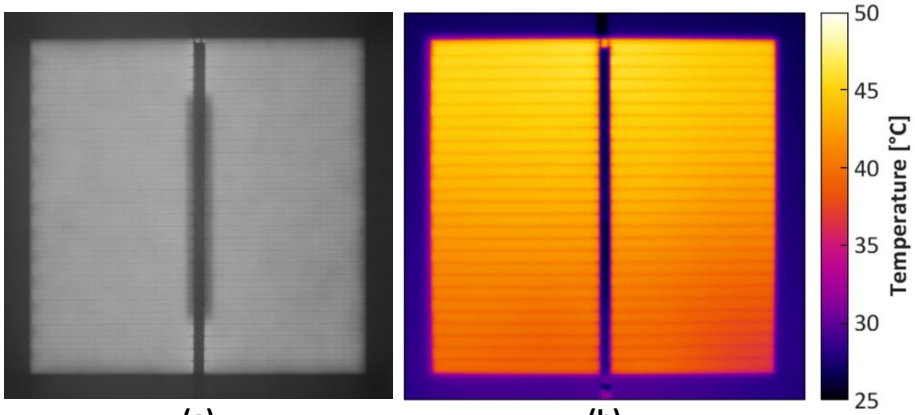

Figure 6.5: *(a) Electroluminescence and (b) thermal image of a mini solar cell when a current of 0.6 A is fed into the cell in forward bias.*

Next, a hot-spot test is performed. When current is fed into the mini solar cell in reverse bias, the cell starts dissipating power. As explained earlier, avalanche multiplication in conventional solar cells leads to localized hot-spot heating. This might result in permanent damage to the solar cell. The current in reverse bias can never exceed the short-circuit current of an unshaded solar cells. Hence, the hot-spot test is performed at a current of 0.6 A. An electroluminescence image after the hot-spot test is shown in Figure 6.6a. It clearly shows that a hot-spot is formed in the top-left side of the solar cell. This hot-spot reduces the active area of the solar cell and therefore leads to a lower current and hence a lower performance. The temperature distribution during the formation of this hot-spot is shown in Figure 6.6b. There was a tremendous increase in the temperature at the position of the hot-spot. The temperature rose to 400°C and the solar cell started smoking.

Solar cells only operate in high reverse bias in very specific circumstances. The reconfigurable PV module must be connected in its series configuration and only one or two cells must be shaded. This scenario could occur due to bird droppings or fallen leaves. In all other cases, the reverse bias voltage is not sufficient to cause hot-spots. To prevent the formation of hot-spot in the reconfigurable module, solar cells with a soft breakdown must be used. In the prototype, solar cells with a high reverse breakdown voltage are used.

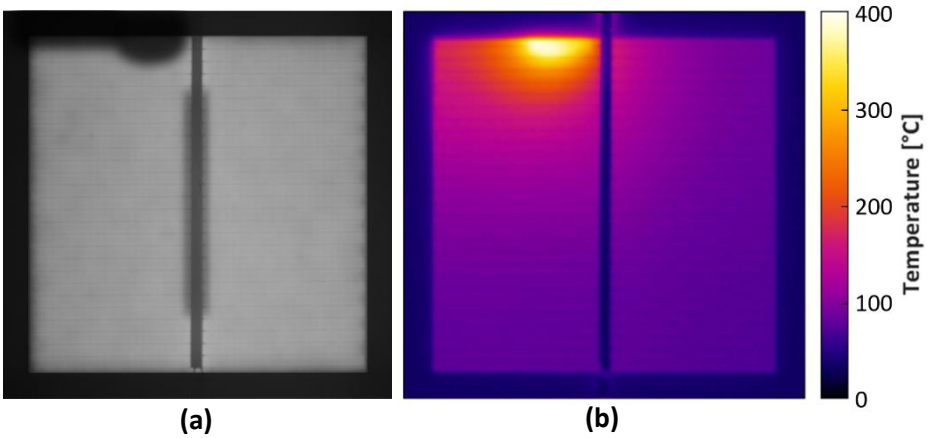

Figure 6.6: *(a) Electroluminescence and (b) thermal image of a mini solar cell when a current of 0.6 A is fed into the cell in reverse bias and resulted in a hot-spot.*

Each subgroup in the prototype contains 12 mini solar cells which are connected in series. Solar cells are tied together by soldering a tabbing wire between the front contact of one cell and the rear contact of another cell. Note that wide tabbing wires are used for interconnections between side-to-side strings. An electroluminescence image is made of each subgroup and the poorest performing cells are replaced. The subgroups are then laminated between two layer of ethylene vinyl acetate with a 4 mm thick glass plate on top and a white back sheet underneath to protect the solar cells. The prototype has a size of 60 by 40 cm^2 and the spacing between cells is 5 mm. Each subgroup is connected through the back sheet to its own junction box with an integrated smart bypass diode. Wires with a cross-sectional area of 2.5 mm^2 with banana plugs on one side are then used to switch between the *6 series*, *6 parallel* and *6 reconfigurable* module topologies. The main advantage of using a single prototype is that the solar cell characteristics and alignment in each architecture are identical. The ultimate prototype is shown in Figure 6.7 together with an electroluminescence image. It is clear that no cracks are created in the lamination process.

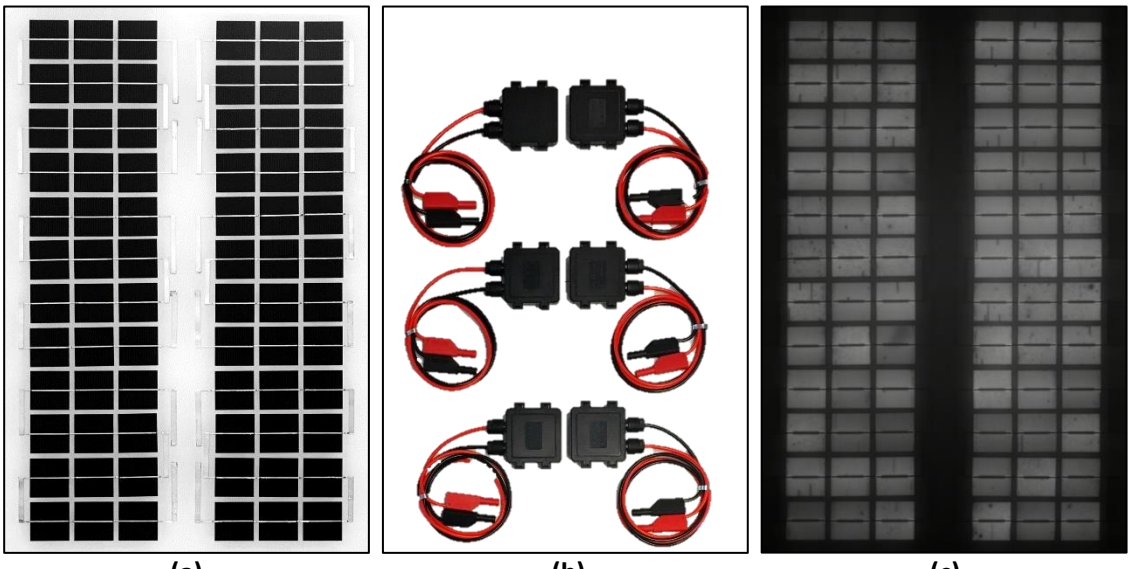

Figure 6.7: *(a) Frontside, (b) backside and (c) electroluminescence image of the prototype.*

6.2. MEASUREMENT SET-UP

The I-V curves of the three different module architectures of the prototype will be traced under a large area solar simulator (LASS) for multiple static shading scenarios. The LASS contains gas discharge and halogen lamps to mimic natural sunlight. Mirrors are used to ensure an uniform irradiation of approximately 1000 W/m^2 is incident on the PV module. In the experiments, thin sheets of plastic are stacked to shade parts of the prototype. It is obvious that a thicker layer of sheets results in a lower transmissivity. To determine the number of sheets required to obtain a certain shading factor, the spectral irradiance of the LASS is measured when the spectrometer is covered with different layer thicknesses as shown in Figure 6.8. The ratio between the irradiation (i.e. integral of the spectral irradiance over the relevant wavelengths) when the spectrometer is covered with the stack of plastic sheets and the unobstructed irradiation gives the shading factor. The relevant wavelengths correspond to photons with an energy higher than the bandgap energy of silicon. It was found that a typical shading factor of 0.8 requires a stack of around 38 plastic sheets.

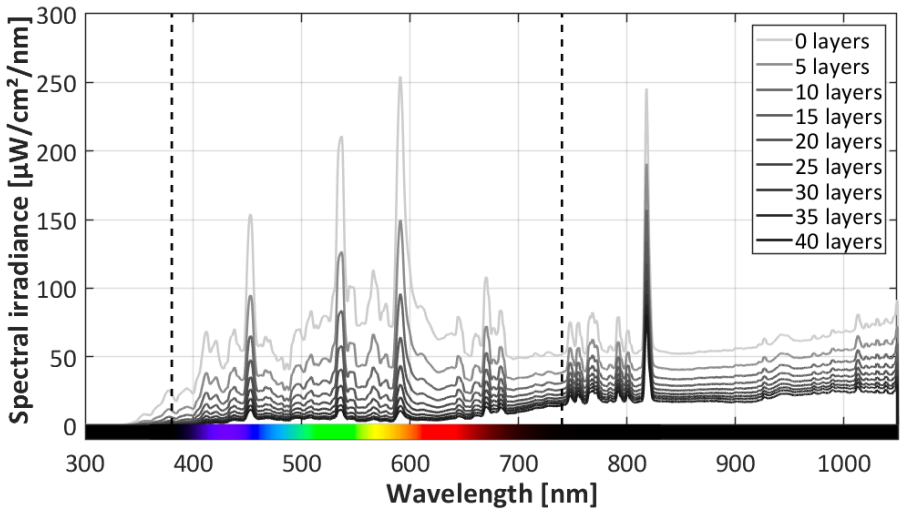

Figure 6.8: *Spectral irradiance when the spectrometer is shaded by a various stacks of plastic sheets. The dashed lines mark the boundaries of the visible spectrum.*

The measurements also show that the plastic sheets affect the spectral irradiance distribution. To quantify the uniformity, the irradiation is calculated between several smaller consecutive wavelength intervals and is compared with the irradiation over the entire spectrum as shown in Table 6.3. It is clear that the absorption of photons with lower wavelengths is significantly higher.

Table 6.3: *Measured irradiation and transmittance for different wavelength ranges when the spectrometer is shaded by a range of plastic layers in a stack.*

Wavelength range	0 layers	10 layers	20 layers	30 layers	40 layers
300 < λ < 1050 nm	465.0 W/m^2	51.7%	33.8%	24.3%	18.6%
300 < λ < 450 nm	36.5 W/m^2	34.1%	14.9%	6.7%	3.1%
450 < λ < 600 nm	138.4 W/m^2	39.9%	19.8%	10.1%	5.7%
600 < λ < 750 nm	95.8 W/m^2	48.8%	30.0%	20.1%	14.0%
750 < λ < 900 nm	94.0 W/m^2	63.4%	47.6%	38.6%	32.0%
900 < λ < 1050 nm	98.9 W/m^2	66.8%	51.0%	41.3%	34.1%

Due to the change in spectral distribution, the equivalent shading factor differs slightly. This corrected shading factor depends on the spectral response of the solar cell, the spectrum of the LASS and the transmittance of the stack of plastic sheets. The spectral response (SR) is given by

$$SR(\lambda) = EQE(\lambda)\frac{q\,\lambda}{h\,c} \tag{6.1}$$

where EQE is the external quantum efficiency of the solar. This is the ratio between the number of carriers collected by the solar cell and the number of photons with a given wavelength incident on the solar cell. Furthermore, q is the charge of an electron, λ is the wavelength, h is Planck's constant and c is the speed of light. The equivalent shading factor (ESF) is then given by

$$ESF = \frac{\int_{\lambda_{\min}}^{\lambda_{\max}} \tau(\lambda)\, SR(\lambda)\, G(\lambda)\, \mathrm{d}\lambda}{\int_{\lambda_{\min}}^{\lambda_{\max}} SR(\lambda)\, G(\lambda)\, \mathrm{d}\lambda} \tag{6.2}$$

where τ is the transmittance and G is the spectral irradiance of the LASS. Using the external quantum efficiency of a typical solar cell gives an effective shading factor of approximately 78%. This factor is equal to the ratio of the short-circuit current of the shaded and unshaded solar cell.

The simulation framework is updated to include the double diode model with the parameters of the mini solar cells as well as the modified subgroup interconnections and the relatively long wires to the measurement equipment. Before tracing the I-V curves of the three different PV module architectures of the prototype, each subgroup is measured individually and compared with the simulations as shown in Figure 6.9. The subgroups share almost the same open-circuit voltage, while the short-circuit current differs per subgroup. The main reason is that the irradiance under the LASS is not perfectly uniform. Furthermore, the short-circuit current of a subgroup depends on the active area of the worst performing cell within a subgroup. In Figure 6.7c, it can be seen that each subgroup is slightly different.

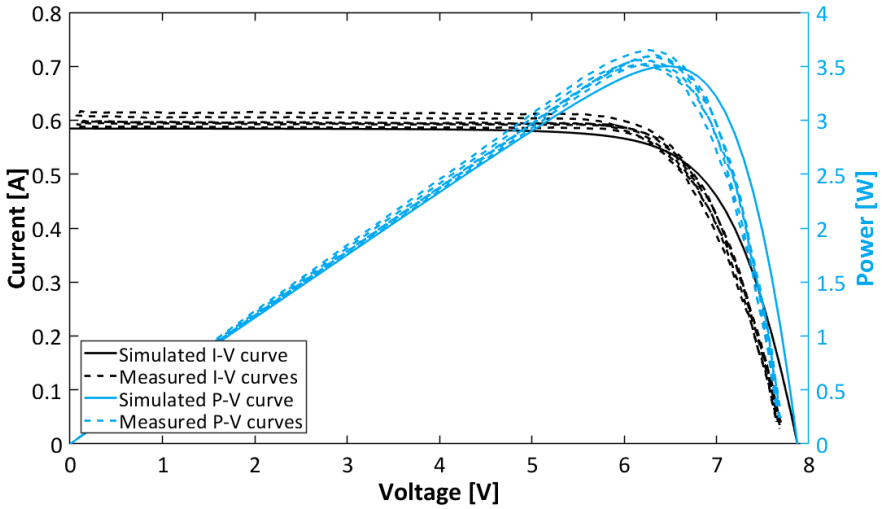

Figure 6.9: *Simulated and measured I-V and P-V curves of the six subgroups in the prototype.*

The current of the measured I-V curves is higher in comparison with the simulated I-V curves, whereas the voltage is lower. The reason is that all simulations are performed at a solar cell temperature of 25°C which corresponds to the standard test conditions. The temperature under the LASS can easily exceed this value. The impact of the cell temperature on the performance of solar cells has already been discussed in section 2.4. The temperature of each subgroup is measured with temperature probes on the backside of the prototype. Since conduction is a relatively slow process compared to radiation, the actual subgroup temperature will be slightly underestimated. The I-V curves are traced from open-circuit to short-circuit conditions. Although each trace only takes a couple of seconds, the temperature rises a few degrees throughout the measurement. It should be noted that the temperature cycle is kept constant between different

measurements. According to the datasheets of typical monocrystalline silicon PV modules, the temperature coefficient of the open-circuit voltage is -0.30%/°C, whereas the coefficient of the short-circuit current is around +0.06%/°C. If the module temperature is around 30°C at the start of the measurement, the reduction in open-circuit voltage is completely due to the temperature difference. The probes indicates that this is realistic. The increase in the short-circuit current is significantly higher than the temperature coefficient suggests. The higher measured current is also a consequence of the optical gains which are neglected in the simulations. The prototype has a white back sheet and a relatively large cell spacing. Therefore, internal reflections increase the irradiation incident on the solar cells. This leads in turn to a higher photocurrent.

Similar measurements are performed at Eternal Sun using a flash solar simulator. This device is able to trace the I-V curve of a module within the time of a single flash. This prevents the module from heating up. The flash solar simulator of Eternal Sun also has a better area related uniformity which leads to more accurate measurements. The results are discussed in appendix D.

6.3. COMPARISON AND DISCUSSION

Models are approximations of real-world systems and therefore a difference between the measured and simulated values exists. Model verification and validation is the process of checking whether the model is performing as expected and if the results are sufficiently accurate. The prototype can adopt the *6 series*, *6 parallel* and *6 reconfigurable* module architectures. The I-V curves will be traced for both unshaded and partially shaded conditions and compared with the simulation results to validate the model.

The results for both the *6 series* and *6 parallel* module architectures are shown in Figure 6.10 for uniform illumination conditions. It is clear that the simulated and measured I-V and P-V curves are very similar. Due to the variation in the I-V curves of the six subgroups as shown in Figure 6.9, some current mismatch losses exist in the *6 series* topology. As a result, the I-V curve will show minor steps in the current due to the activation of bypass diodes. The effects of the temperature and optical gains are also visible. Under uniform conditions, the reconfigurable PV module is in its series configuration and therefore the I-V curve will be very similar to Figure 6.10a. However, since the reconfigurable PV module has no bypass diodes, its current will be limited by the worst performing subgroup and hence steps in the current will not occur.

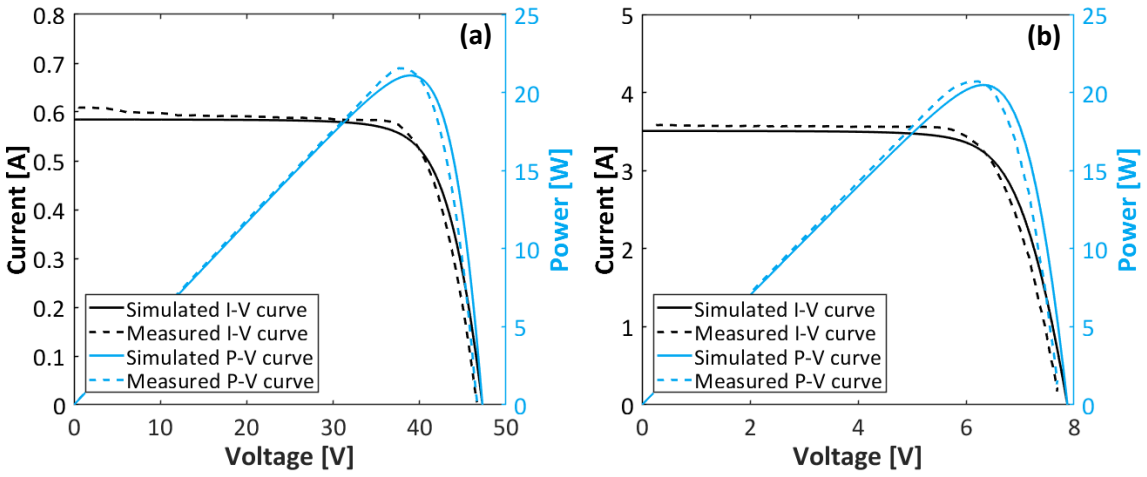

Figure 6.10: *Simulated and measured I-V and P-V curves of (a) the 6 series and (b) the 6 parallel module architecture of the prototype under uniform illumination conditions.*

Next, a comparison is performed for several static shading profiles including the row, column and corner shading scenarios introduced in section 5.3. The results for both the *6 series* and *6 parallel* module architectures are shown in Figure 6.11 when only the 'top' row is shaded with a shading factor of 0.8. The most important difference is the higher measured current when the two bypass diodes are activated in the series topology as well as the higher current in the parallel topology. This suggests that the actual shading factor within the two partially shaded subgroups is lower than used within the simulation framework.

In the experiments, only the solar cells in the top row and the margin between these cells are shaded by the plastic sheets. Optical gain can therefore arise from both sides of the shaded row. Moreover, the optical gains are relatively high, because only one side of the top row is surrounded by other solar cells which have a much lower reflectivity compared to the white back sheet. The optical gains will therefore be lower when shading a row in the centre of the module. Furthermore, due to the relatively high shading factor, optical gains contribute much more to the irradiation incident on the shaded solar cells. As a result, the effective shading factor which is based on the ratio of the short-circuit current of the shaded and unshaded subgroups is around 0.75 instead of 0.8. Another reason for this deviation is that the shaded part of a subgroups does not necessarily include the solar cell which limits the subgroup current. Because every subgroup is unique, the results will also differ slightly when the bottom rather than the top row is shaded.

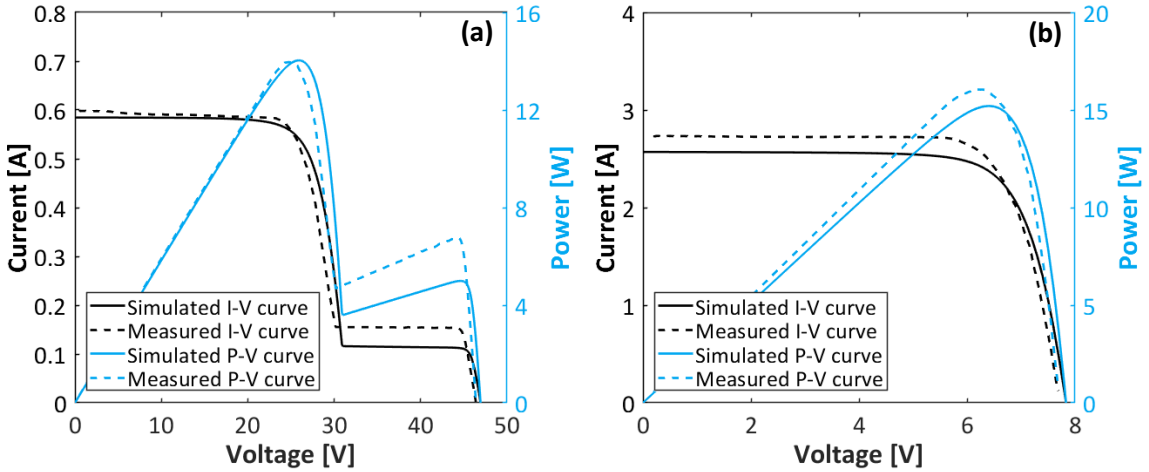

Figure 6.11: *Simulated and measured I-V and P-V curves of (a) the 6 series and (b) the 6 parallel module architecture of the prototype under row shading.*

The reconfigurable topology of the prototype can be switched manually between the 27 unique configurations reconnecting banana plugs. For further research, integrated switches, sensors and a microcontroller can be implemented to automatically select the optical configuration. As derived earlier from Figure 5.6, the 1x6 SP and three 2x3 SP configurations result in the best performance under row shading. The simulated and measured I-V and P-V curves are shown in Figure 6.12a for configuration 14 (see appendix B). Again, the performance gap is mainly due to the optical gains and temperature. According to the simulations, the curves should be identical for all three selected 2x3 SP configurations. Since each solar cell and hence each subgroups is unique, there are some minor variations observed in the short-circuit current of these configurations.

Finally, the simulation results of all three module architectures are shown in Figure 6.12b when the top row is shaded. It can be observed that the parallel and reconfigurable topologies lead to the highest shading tolerability. Furthermore, the current of the reconfigurable PV module is a factor two lower compared to the parallel topology and therefore leads to much lower resistive

power losses. An important remark is that the prototype does not contain any additional (switch) components for the reconfigurable module compared to the parallel architecture. Also, relatively long wires are used to connect the prototype to the measurement instruments which conduct the whole module current. As a result, the reconfigurable module slightly outperforms the parallel module architecture. Another advantage of the reconfigurable PV module compared to the conventional PV module is that it does not have local maxima in the P-V curve and hence requires a much simpler and faster maximum power point tracker.

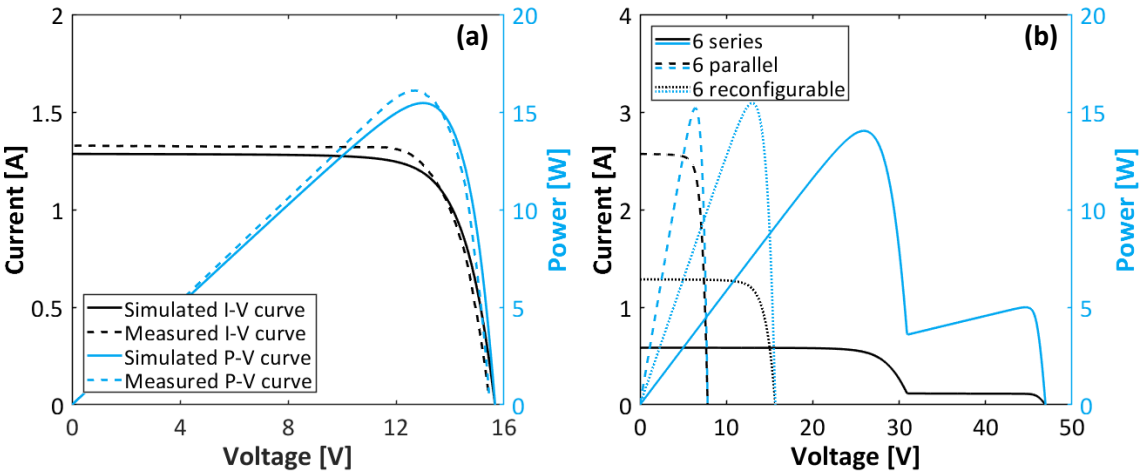

Figure 6.12: *(a) Simulated and measured I-V and P-V curves of the reconfigurable module architecture under row shading when the module is in its optimal configuration. (b) Comparison of the simulated I-V and PV curves of the three module architectures of the prototype under row shading.*

Similar conclusions are valid for the other shading scenarios and will therefore not be discussed in detail. To summarize, the performance gap between the simulations and measurements is small and can be explained by means of the temperature, optical gains and uniqueness of subgroups which are not taken into account in the simulation framework.

7

CONCLUSIONS AND FUTURE WORK

The aim of the research was to evaluate the potential and performance of reconfigurable PV modules in urban landscapes and to find the optimal module configuration. A reconfigurable PV module architecture changes its electrical configuration depending on the shading profile. The smallest group of solar cells in a PV module which can be electrically relocated is known as a *reconfigurable unit*. The potential of reconfigurable modules and their optimal unit size can be determined by estimating the maximum amount of solar radiation that a module can convert as a function of its layout.

For a case study, a PV system is modelled on a rooftop facing south with a tilt of 30 degrees. The rooftop is often partially shaded by a nearby building. Using a module with 72 solar cells, it was found that six series-parallel connected reconfigurable units is the optimal trade-off between a high shading tolerability and a simple module design. In this case, the reconfigurable PV module requires 25 switches to support 27 unique configurations. Simulations showed that the most partially shaded module can capture up to 15% more irradiation in comparison with conventional PV modules. The gain is higher for locations further away from the equator.

The put the performance of the reconfigurable PV module into perspective, it is compared with static series and parallel connected PV module layouts. An electrical simulation framework was developed to trace the current-voltage (I-V) characteristics of each architecture. For a typical urban landscape location in Rotterdam, the annual energy yield of the most partially shaded PV module can increase by around 9% when switching from a conventional to a reconfigurable PV module. Reconfigurable PV modules require additional electrical components, but the negative effect on the power output under uniform illumination conditions is marginal.

Compared to a module with six subgroups in a static parallel connection, the reconfigurable PV module has a slightly lower annual yield. This is mainly due to the presence of switches. However, the current of the reconfigurable PV module is generally much lower, leading to significantly lower power losses on the *system level*. An extensive sensitivity analysis showed that replacing the central switchboard with distributed switches will lead to a slight increase of the module output. However, the annual energy yield will significantly decrease if the dimensions of wires for subgroup interconnections are too small.

The reconfigurable PV module does not outperform the *optimal* static module architecture for a certain shading location. However, its marginal power losses at uniform illumination conditions and its high shading-tolerability, makes complex shading analysis for the design of building added or building integrated PV systems superfluous. Consequently, reconfigurable PV modules allow plug-and-play installations. Another advantage is the smaller seasonal fluctuation in energy yield. This has a positive effect on energy storage requirements. Additionally, the reconfigurable PV module does not contain any bypass diodes and therefore only shows one maximum in the P-V curves. This makes maximum power point tracking both simpler and faster. The disadvantage of the reconfigurable module is the increased complexity due to the required switches, sensors and microcontroller. This leads in turn leads to a lower reliability and higher module cost. A detailed cost-benefit analysis must point out whether the reconfigurable module is economically viable.

Finally, a small-scale prototype of the reconfigurable PV module was manufactured to validate the simulation framework. The prototype also serves as a proof of concept. Deviations between the simulation results and the measurements are mainly caused by the optical gains, module temperature and mismatch between solar cells which are not taken into account in the model. Experiments showed that to prevent the formation of hot-spots in all possible partial shading conditions, solar cells with a soft breakdown must be used.

Recommendations and prospects

The conclusions in this report are based on simulations of a single PV system. The shape, duration and intensity of shadows differ per location. Alternative shading scenarios in urban environments could be considered for further research. This includes building façades and rooftops which are often partially shaded by trees, chimneys, dormers or surrounding buildings. Since both the least and the most partially shaded modules in the PV system have been analysed individually, the conclusions in this report are also applicable in these alternative scenarios.

The modules in this report contain full size solar cells. However, both research and commercial applications show a trend towards the usage of half cells. Modifying the simulation framework to support half cells can easily be achieved. This allows a comparison with the DUO/Twin Peak module, one of the first commercially available shade-tolerant modules using half cells.

In partial shading conditions, the surface temperature of a module is generally non-uniform. The impact of the temperature on the performance of the module has not been taken into account in the simulations. This would drastically increase the computation time for the annual energy yield simulations. However, for static shading profiles this analysis could be performed, because the complexity is much lower. The difference in the temperature response between conventional and reconfigurable PV modules can also be investigated.

The current prototype is manually switched between configurations. A new prototype could be equipped with switches, sensors and a microcontroller that automatically determine and select the optimal configuration. For this, a more complex control algorithm needs to be developed. When full size solar cells are used in the new prototype, the impact of optical gains will become smaller. This would make it easier to compare measurements with simulation results.

BIBLIOGRAPHY

[1] V. Smil, “Energy Transitions: Global and National Perspectives,” *Praeger,* Second Edition, ISBN: 9781440853241, 2016.

[2] P. Tans and E. Dlugokencky, “Trends in Atmospheric Carbon Dioxide,” NOAA Earth System Research Laboratory, 2018. [Online]. Available: www.ourworldindata.org/co2-and-other-greenhouse-gas-emissions. [Accessed 12 December 2018].

[3] T. Boden, G. Marland and R. Andres, “Global, Regional and National Fossil-Fuel CO_2 Emissions,” CDIAC, 2017. [Online]. Available: www.ourworldindata.org/co2-and-other-greenhouse-gas-emissions. [Accessed 12 December 2018].

[4] M. Perez and R. Perez, “A Fundamental Look at Supply Side Energy Reserves for the Planet,” *IEA Solar Heating and Cooling,* vol. 62, 2015.

[5] A. Smets, K. Jäger, O. Isabella, R. van Swaaij and M. Zeman, “Solar Energy: The Physics and Engineering of Photovoltaic Conversion, Technologies and Systems,” *UIT Cambridge,* First Edition, ISBN: 9781906860325, 2016.

[6] C. Fritts, “On a New Form of Selenium Photocell,” *American Journal of Science,* vol. 26, no. 3, pp. 465-472, 1883.

[7] D. Chapin, C. Fuller and G. Pearson, “A New Silicon p-n Junction Photocell for Converting Solar Radiation into Electrical Power,” *Applied Physics,* vol. 25, no. 5, pp. 676-677, 1954.

[8] NREL, “Best Research Cell Efficiencies,” National Renewable Energy Laboratory, 2018. [Online]. Available: www.nrel.gov/pv/cell-efficiency.html. [Accessed 5 January 2019].

[9] N. Buhayar, “Musk vs. Buffett: The Billionaire Battle to Own the Sun,” Bloomberg New Energy Finance, 2016. [Online]. Available: www.bloomberg.com/features/2016-solar-power-buffett-vs-musk/. [Accessed 21 December 2018].

[10] SolarPower Europe, “Global Market Outlook for Solar Power 2018-2022,” 2018. [Online]. Available: www.solarpowereurope.org/global-market-outlook-2018-2022/. [Accessed 2 January 2019].

[11] IRENA, “Renewable Power Generation Costs in 2017,” *International Renewable Energy Agency,* ISBN: 9789292600402, 2018.

[12] IEA, “Trends in Photovoltaic Applications,” *IEA Photovoltaic Power Systems,* ISBN: 9783906042725, 2018.

[13] B. Pannebakker, A. de Waal and W. van Sark, “Photovoltaics in the Shade: One Bypass Diode per Solar Cell Revisited,” *Progress in Photovoltaics,* 2017.

[14] D. La Manna, V. Li Vigni, E. Sanseverino, V. Di Dio and P. Romano, “Reconfigurable Electrical Interconnection Strategies for Photovoltaic Arrays: A Review,” *Renewable and Sustainable Energy Reviews,* vol. 33, pp. 412-426, 2014.

[15] O. Breitenstein, J. Bauer, K. Bothe, W. Kwapil, D. Lausch, U. Rau, J. Schmidt, M. Schneemann, M. Schubert, J. Wagner and W. Warta, “Understanding Junction Breakdown in Multicrystalline Solar Cells,” *Applied Physics,* vol. 109, 2011.

[16] F. Masmoudi, F. Salem and N. Derbel, “Single and Double Diode Models for Conventional Mono-Crystalline Solar Cell with Extraction of Internal Parameters,” *13th International Multi-Conference on Systems, Signals & Devices,* 2016.

[17] H. Ibrahim and N. Anani, “Variations of PV Module Parameters with Irradiance and Temperature,” *Energy Procedia,* vol. 135, pp. 276-285, 2017.

[18] A. Bidram, A. Davoudi and R. Balog, “Control and Circuit Techniques to Mitigate Partial Shading Effects in Photovoltaic Arrays,” *IEEE Journal of Photovoltaics,* vol. 2, no. 4, pp. 532-546, 2012.

[19] P. Bauwens, J. Govaerts, M. Baka, F. Catthoor, K. Baert, G. Vandenbroeck, H. Goverde, D. Anagnotos, J. Doutreloigne and J. Poortmans, “Reconfigurable Topology for Smarter PV Modules: Simulation, Evaluation and Implementation,” *32nd European Photovoltaic Solar Energy Conference and Exhibition,* pp. 61-65, 2016.

[20] S. Golroodbari, A. de Waal and W. van Sark, “Improvement of Shade Resilience in Photovoltaic Modules Using Buck Converters in a Smart Module Architecture,” *Energies,* vol. 11, no. 1, 2018.

[21] C. Chu, L. Koduvelikulathu, V. Mihailetchi, G. Galbiati, A. Halm and R. Kopecek, “Soft Breakdown Behavior of Interdigitated-Back-Contact Silicon Solar Cells,” *Energy Procedia,* vol. 77, pp. 29-35, 2015.

[22] Texas Instruments, “Smart Bypass Diode: SM74611,” Texas Instruments, 2012. [Online]. Available: www.ti.com/lit/ds/symlink/sm74611.pdf. [Accessed 17 January 2019].

[23] S. Silvestre, A. Boronat and A. Chouder, “Study of Bypass Diodes Configuration on PV Modules,” *Applied Energy,* vol. 86, pp. 1632-1640, 2009.

[24] H. Ziar, M. Nouri, B. Asaei and S. Farhangi, “Analysis of Overcurrent Occurance in Photovoltaic Modules with Overlapped Bypass Diodes at Partial Shading,” *IEEE Journal of Photovoltaics,* vol. 4, no. 3, pp. 713-721, 2014.

[25] K. Chao, P. Lai and B. Liao, “The Optimal Configuration of Photovoltaic Module Arrays Based on Adaptive Switching Controls,” *Energy Conversion and Management,* vol. 100, pp. 157-167, 2015.

[26] R. Ramaprabha and B. Mathur, “A Comprehensive Review and Analysis of Solar Photovoltaic Array Configurations under Partial Shaded Conditions,” *International Journal of Photoenergy,* vol. 2012, 2011.

[27] C. Ramos-Paja, J. Bastidas, A. Saavedra-Montes, F. Guinjoan-Gispert and M. Goez, “Mathematical Model of Total Cross-Tied Photovoltaic Arrays in Mismatching Conditions,” *IEEE 4th Colombian Workshop on Circuits and Systems,* 2012.

[28] Y. Wang and P. Hsu, “An Investigation on Partial Shading of PV Modules with Different Connection Configurations of PV Cells,” *Energy,* vol. 36, pp. 3069-3078, 2011.

[29] S. Buddha, “Topology Reconfiguration to Improve the Photovoltaic (PV) Array Performance,” Master Thesis, 2011.

[30] H. Braun, S. Buddha, V. Krishnan, C. Tepedelenlioglu, A. Spanias, M. Banavar and D. Srinivasan, “Topology Reconfiguration for Optimization of Photovoltaic Array Output,” *Sustainable Energy, Grids and Networks,* vol. 6, pp. 58-69, 2016.

[31] G. Velasco-Quesada, F. Guinjoan-Gispert, R. Piqué-López, M. Román-Lumbreras and A. Conesa-Roca, “Electrical PV Array Reconfiguration Strategy for Energy Extraction Improvement in Grid-Connected PV Systems,” *IEEE Transactions on Industrial Electronics,* vol. 56, no. 11, pp. 4319-4331, 2009.

[32] Y. Wang, X. Lin, Y. Kim, N. Chang and M. Pedram, “Architecture and Control Algorithms for Combating Partial Shading in Photovoltaic Systems,” *IEEE Transactions on Computer-Aided Design of Integrated Circuits and Systems,* vol. 33, no. 6, pp. 917-930, 2014.

[33] J. Storey, P. Wilson and D. Bagnall, “Improved Optimization Strategy of Irradiance Equalization in Dynamic Photovoltaic Arrays,” *IEEE Transactions on Power Electronics,* vol. 28, no. 6, pp. 2946-2956, 2013.

[34] J. Roets, “Optimisation of Energy Conversion in Solar Panels using Active Cell-Reconfiguration,” Master Thesis, 2012.

[35] Z. Cheng, Z. Pang, Y. Liu and P. Xue, “An Adaptive Solar Photovoltaic Array Reconfiguration Method Based on Fuzzy Control,” *8th World Congress on Intelligent Control and Automation,* pp. 176-181, 2010.

[36] D. Nguyen and B. Lehman, “An Adaptive Solar Photovoltaic Array using Model-Based Reconfiguration Algorithm,” *IEEE Transactions on Industrial Electronics,* vol. 55, no. 7, pp. 2644-2654, 2008.

[37] M. Baka, F. Catthoor and D. Soudris, “Smart PV Module Topology with a Snake-Like Configuration.,” *31st European Photovoltaic Solar Energy Conference and Exhibition,* pp. 104-107, 2015.

[38] M. Baka, F. Catthoor and D. Soudris, “Near-Static Shading Exploration for Smart Photovoltaic Module Topologies Based on Snake-Like Configurations,” *ACM Transactions on Embedded Computing Systems,* vol. 15, no. 2, pp. 1-21, 2016.

[39] M. Baka, P. Manganiello, D. Soudris and F. Catthoor, “A Cost-Benefit Analysis for Reconfigurable PV Modules under Shading,” *Solar Energy,* vol. 178, pp. 69-78, 2019.

[40] A. Carr, M. Jansen, M. de Bruijne, L. Okel, M. Kloos and W. Eerenstein, “A High Voltage MWT Module with Improved Shadow Performance,” *40th IEEE Photovoltaics Specialists Conference,* 2014.

[41] A. Car, K. de Groot, M. Jansen, E. Bende, J. van Roosmalen, L. Okel, W. Eerenstein, R. Jonkman, R. van der Sanden, J. Bakker, B. de Gier and A. Harthoorn, “Tessera: Scalable, Shade Robust Module,” *42nd IEEE Photovoltaic Specialists Conference,* 2015.

[42] Q Cells, “Q.PEAK DUO-G5: Monocrystalline Q.ANTUM DUO TECHNOLOGY,” Q Cells, 2017. [Online]. Available: www.q-cells.co.uk/products/solar-panels/qpeak-duo-g5. [Accessed 28 March 2019].

[43] P. Vicente, T. Pimenta and E. Ribeiro, “Photovoltaic Array Reconfiguration Strategy for Maximisation of Energy Production,” *International Journal of Photoenergy,* vol. 2015, 2015.

[44] R. Santbergen, V. Muthukumar, R. Valckenborg, W. van de Wall, A. Smets and M. Zeman, “Calculation of Irradiance Distribution on PV Modules by Combining Sky and Sensitivity Maps,” *Solar Energy,* vol. 150, pp. 49-54, 2017.

[45] R. Perez, R. Seals and J. Michalsky, “All-Weather Model for Sky Luminance Distribution: Preliminary Configuration and Validation,” *Solar Energy,* vol. 50, no. 3, pp. 235-245, 1993.

[46] B. Lefevre, S. Peeters and J. Driesen, “Optimized Cell Layout of Partially Shaded PV Panels,” *29th European Photovoltaic Solar Energy Conference,* pp. 69-72, 2013.

[47] MATLAB R2017b, “Version 9.3.0.713579,” *Natick, Massachusetts: The MathWorks Inc,* 2017.

[48] A. Zegaoui, P. Petit, M. Aillerie, J. Sawicki, A. Belarbi, M. Krackai and J. Charles, “Photovoltaic Cell/Panel/Array Characterizations and Modelling Considering Both Reverse and Direct Modes,” *Energy Procedia,* vol. 6, pp. 695-703, 2011.

[49] H. Hanifi, C. Pfau, D. Dassler, S. Schindler, J. Schneider, M. Turek and J. Bagdahn, “Investigation of Cell-to-Module (CTM) Ratios of PV Modules by Analysis of Loss and Gain Mechanisms,” *Photovoltaics International,* vol. 32, pp. 91-99, 2016.

[50] M. Mittag, C. Kutter, S. Hoffmann, P. Romer, A. Beinert and T. Zech, “Electrical and Thermal Modeling of Junction Boxes,” *33rd European PV Solar Energy Conference and Exhibition,* 2017.

[51] R. Panguloori, “Achieve Bidirectional Controland Protection Through Back-to-Back Connected eFuse Devices,” Texas Instruments, 2017. [Online]. Available: www.ti.com/lit/an/slva948/slva948.pdf. [Accessed 2 March 2019].

[52] D. Paul, M. Smyth, A. Zacharopoulos and J. Mondol, “The Effects of Nonuniform Illumination on the Electrical Performance of a Single Conventional Photovoltaic Cell,” *International Journal of Photoenergy,* 2015.

[53] W. De Soto, S. Klein and W. Beckman, “Improvement and Validation of a Model for Photovoltaic Array Performance,” *Solar Energy,* vol. 80, no. 1, pp. 78-88, 2006.

[54] E. Strobach, D. Faiman, S. Bader and S. Hile, “Effective Incidence Angles of Sky-Diffuse and Ground-Reflected Irradiance for Various Incidence Angle Modifier Types,” *Solar Energy,* vol. 89, pp. 81-88, 2013.

[55] H. Obane, K. Okajima, T. Ozeki and T. Ishii, “PV System with Reconnection to Improve Output under Non-Uniform Illumination,” *IEEE Journal of Photovoltaics,* vol. 2, no. 3, pp. 341-347, 2011.

[56] E. Macabebe and E. van Dyk, “Parameter Extraction From Dark Current–Voltage Characteristics of Solar Cells,” *South African Journal of Science,* vol. 108, pp. 401-404, 2008.

[57] B. Newman, E. Bende, J. Loffler, J. Wang, J. Zhai, D. Liu, Z. Wang, Y. Chen and J. Shi, “MWT Cells for Shade-Linear, Diode-Free Modules,” *43rd IEEE Photovoltaic Specialists Conference,* 2016.

[58] S. Serna-Garcés, C. Ramon-Paja and J. Bastidas-Rodriguez, “Reconfiguration of Urban Photovoltaic Arrays Using Commercial Devices,” *Energies,* vol. 9, no. 2, 2015.

[59] S. Sze and K. Ng, “Physics of Semiconductor Devices,” *Wiley,* Third Edition, ISBN: 9780471143239, 2006.

A

HOT-SPOT PHENOMENON

Hot-spot heating occurs when a large number of series connected solar cells cause a shaded cell to operate in high reverse bias. The shaded cell will dissipate a significant amount of power which leads to localized overheating. Severe hot-spot heating results in faster degradation of the solar cell. Moreover, it can cause permanent damage such as cell cracking and melting of solder. This chapter gives a detailed explanation of the hot-spot phenomenon and describes a cell technology which mitigates power dissipation in reverse bias.

A.1. HOT-SPOT HEATING

The current of a solar cell is directly proportional to the incident irradiance and can therefore drastically be reduced when the solar cell is shaded. Since solar cells are generally connected in series, the current is limited by the worst performing cell. A heavily shaded cell cannot conduct the high current of the unshaded cells in forward bias. Consequently, the shaded cell is forced to operate in reverse bias and acts as a load which dissipates power and leads to heating of the cell. As discussed in section 2.1, there are multiple breakdown mechanisms in reverse bias. Avalanche breakdown is most dangerous, because it leads to significant local differences in charge carrier concentrations [15]. Localized or hot-spot heating is inevitable in partial shading conditions, but will only cause serious damage under specific circumstances. A solar cell in reverse bias can be divided into two categories. In low reverse bias, the solar cell acts as an insulator and will conduct a relatively small current whereas in high reverse bias (i.e. above the breakdown voltage), the solar cell becomes electrically conductive and the current increases exponentially. Permanent damage to the cells is most likely to occur at high reverse bias, because the power dissipation is significantly larger. Malfunctioning of a solar cell can also lead to hot-spot heating.

The I-V curves of unshaded and shaded solar cells can be used to visualize the power dissipation in the shaded cell(s) and to obtain the overall I-V curve. This method is only applicable in short-circuit conditions and when the shaded cells receive an equal irradiance. Consider the case where one cell is heavily shaded and is connected in series with N unshaded cells. First, the I-V curve of the shaded solar cell in both forward and reverse bias should be obtained. In short-circuit conditions, all power generated by the unshaded cells is dissipated in the shaded cell(s) and represents the worst-case scenario. Consequently, by mirroring the I-V curve of the unshaded

cells in the I-axis, the operating point of the unshaded cell is given by the intersection as shown on the left in Figure A.1. The marked area corresponds to the power dissipated in the shaded cell. Note that the unshaded solar cells have a higher current and voltage due to the higher incident irradiance and the series connection of multiple unshaded solar cells respectively. When many unshaded cells are connected in series, the shaded cell is forced to operate in high reverse bias which significantly increases the power dissipation. The temperature of the shaded cell will then rapidly rise and can lead to irreversible damage [57]. Degradation of solar cells can be observed by performing electroluminescence tests of solar cells. Bypass diodes are usually used to create an alternative path for the current to prevent operation in high reverse bias.

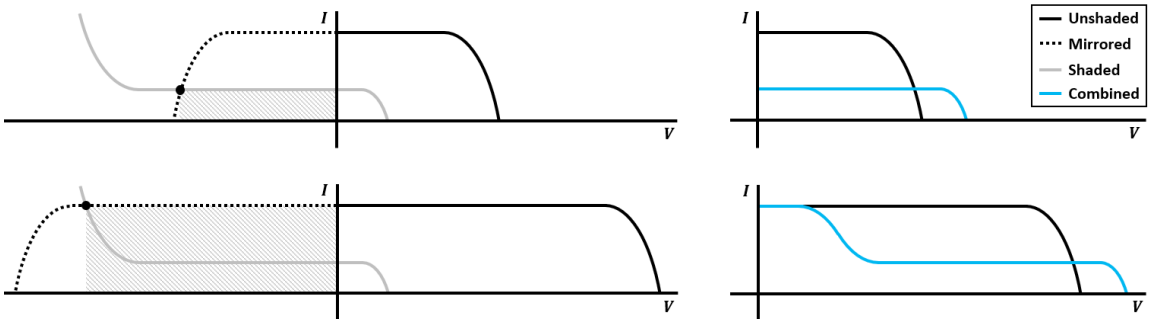

Figure A.1: *I-V curves when a shaded solar cell operates in low (top) and high (bottom) reverse bias. The marked area indicates the power dissipation in the shaded solar cell.*

Figure A.1 also shows the overall I-V curve which is obtained by combining the unshaded and shaded I-V curves and tracing the current of the shaded cell [58]. The short-circuit current is given by the intersection of the shaded and mirrored unshaded I-V curves. The open-circuit voltage in a series connection is the summation of the voltage of the unshaded and shaded cells. Note that the current can never exceed the short-circuit current of the unshaded cells.

A.2. SOFT BREAKDOWN

It is shown that the impact of reverse bias operation is dependent on the number of unshaded cells connected in series. The severity of hot-spot heating can also be tackled at the source. Cells with a lower breakdown voltage will dissipate less power at the same current. The breakdown voltage of conventional crystalline silicon solar cells is typically around -15 V and is caused by avalanche multiplication [15]. Therefore, roughly 18-25 cells can be connected in series before the shaded cell is forced to operate in high reverse bias. Interdigitated Back Contact (IBC) solar cells have both contacts on the rear side. Some of these back contacted cells benefit from a so-called soft breakdown. Chu et al. showed that breakdown then occurs around -3.7 V and can be shifted by changing the doping concentrations [21]. Their research also demonstrated that breakdown in these cells is caused by the tunnelling effect rather than avalanche multiplication and results in a more uniform thermal breakdown [59]. Consequently, the power dissipation in reverse bias is considerably lower and will be distributed more uniformly across the shaded cell. Temperature rise will be limited and therefore hot-spot formation will most likely not occur in a series connection.

B

CONFIGURATIONS OF INTEREST

A reconfigurable PV module with 6 subgroups can switch between 27 configurations. When all subgroups are connected either in parallel or series, there is only one unique configuration and are referred to as COI #1 and COI #27 respectively. However, when two or three reconfigurable units are connected in series (i.e. 2x3 SP and 3x2 SP), there are multiple configurations which can potentially result in a different output power and are shown in Figure B.1.

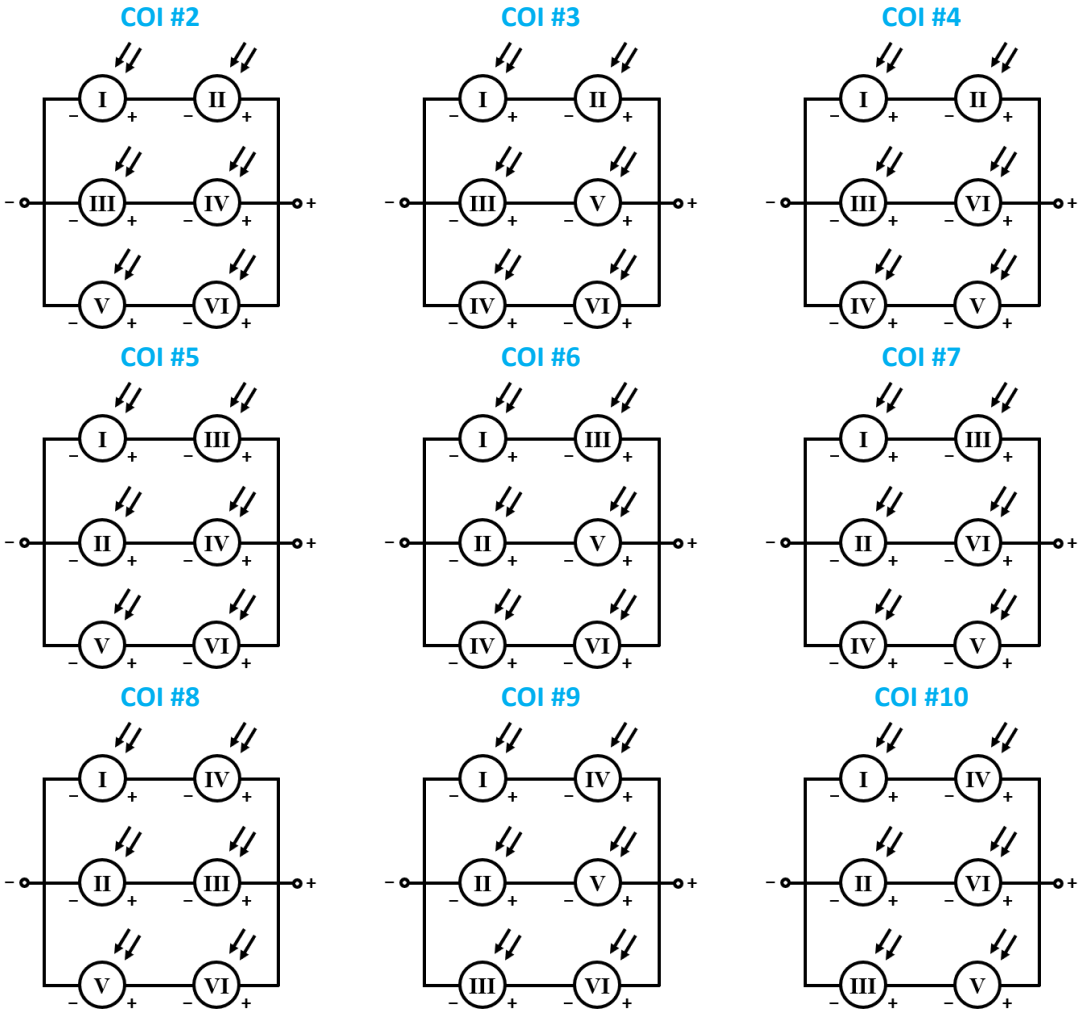

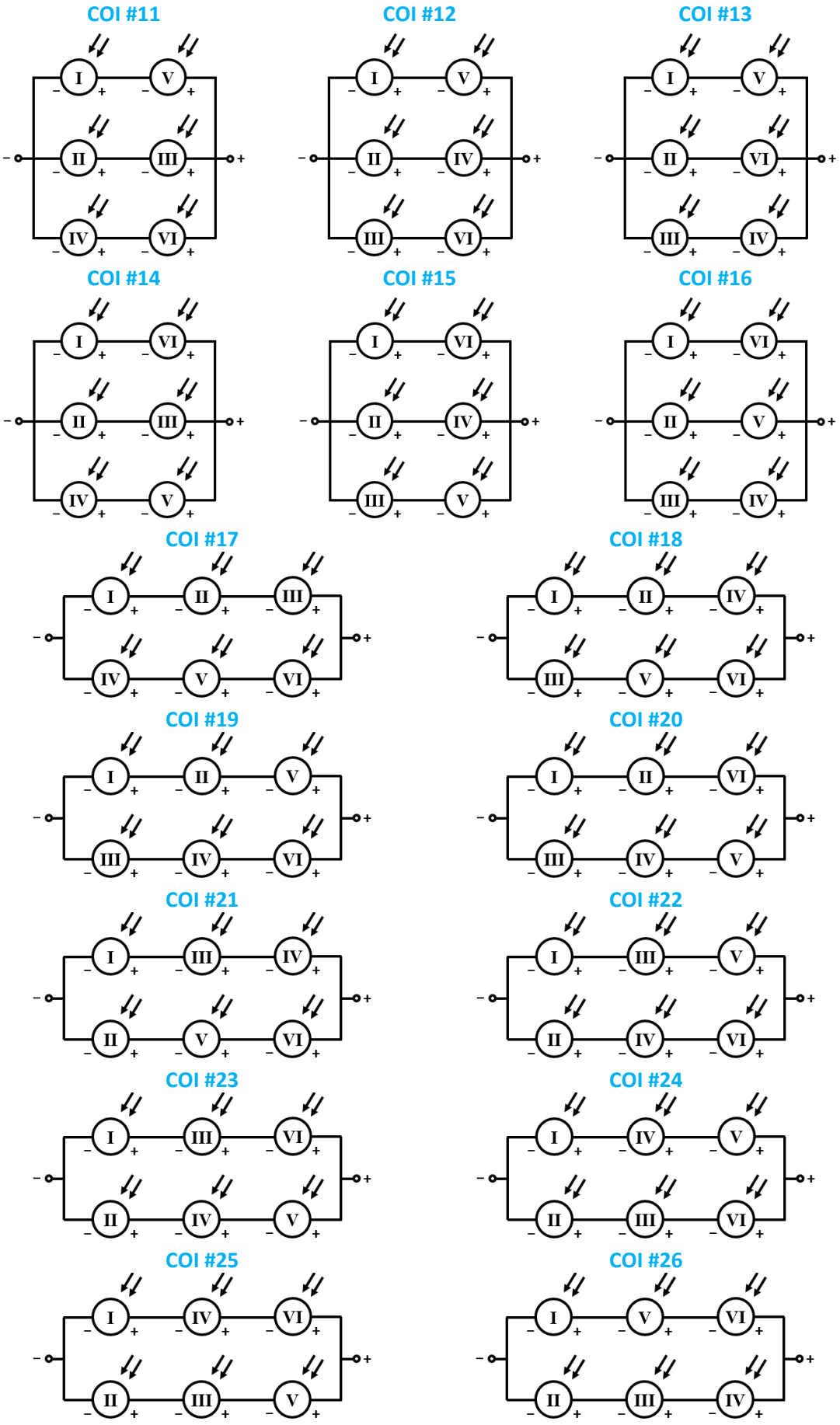

Figure B.1: *Configurations of interest of a PV module with six reconfigurable units and a 2x3 SP or 3x2 SP connection.*

C

MODULE ARCHITECTURES

To put the performance of the reconfigurable module into perspective, several series and parallel connected reference topologies are investigated. Each of these PV modules has losses which can occur due to the resistance of switches, bypass diodes, wires and contacts. A detailed overview of the implementation of these topologies in the MATLAB Simulink simulation framework is given in the figures below. Note that these figures are not drawn to scale, grey cables are assumed to be infinitely short and blue solar cells indicate the size and orientation of the subgroups.

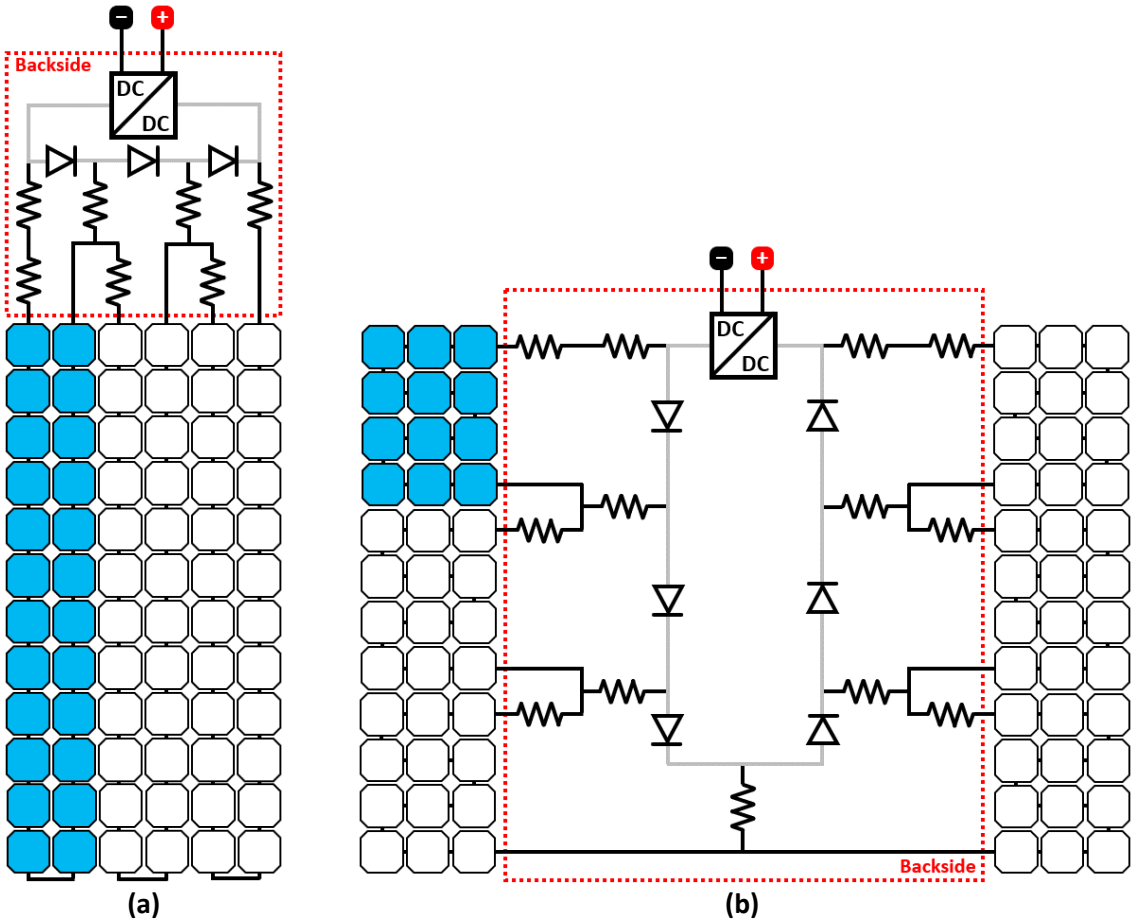

Figure C.1: *Detailed schematic overview the series connected PV module architectures with bypass diodes across each of the (a) three and (b) six subgroups.*

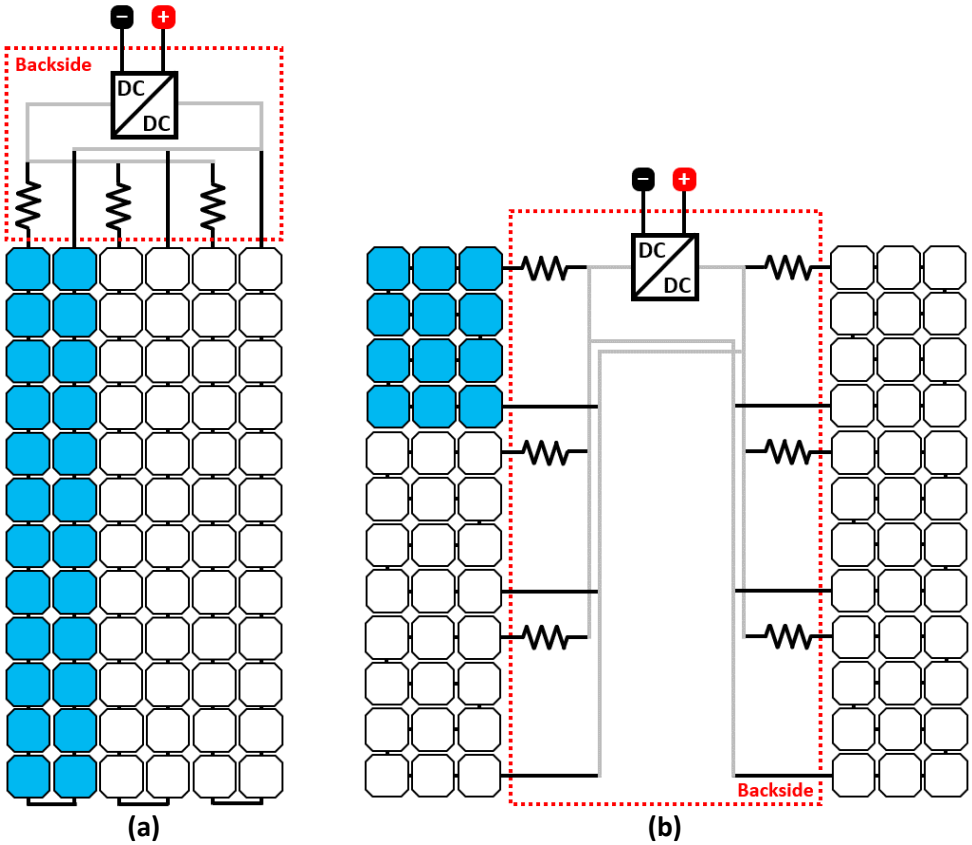

Figure C.2: *Detailed schematic overview the parallel connected PV module architectures with (a) three and (b) six subgroups.*

For simplicity, the resistance of several components are combined such as the resistance of wires and contacts. In the reconfigurable PV module, each subgroup has a current sensors connected in series which helps to determine the optimal configuration. Furthermore, a microcontroller is required. It is assumed that these additional components are lossless.

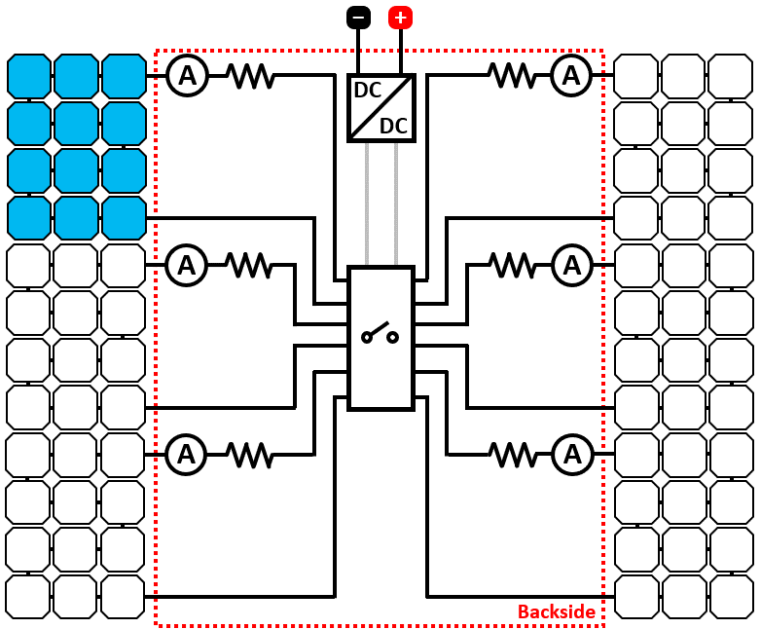

Figure C.3: *Detailed schematic overview of the reconfigurable PV module architecture.*

D

FLASH SOLAR SIMULATOR

The I-V curve measurements in section 6.2 and 6.3 are performed under a standard large area solar simulator (LASS). The main problem with this set-up is that the prototype heats up rapidly and affects the I-V curve. To mitigate temperature differences, additional measurements are performed with the 3500SLP flash simulator of Eternal Sun. This simulator produces a very short light pulse during which the I-V curve of the prototype is measured. As a result, the surface temperature remains almost the same.

The I-V and P-V curves of each subgroup of the prototype are shown in Figure D.1. The simulated curves are also shown to analyse the impact on the performance gap. The open-circuit voltage of the measurements corresponds to the simulations. It can therefore be concluded that the temperature during the measurements was kept constant at 25°C. The short-circuit current measured with the flash simulator is around 2.5% higher than the simulated current. This is comparable to the measurements with the LASS and is caused by the aforementioned optical gains. Furthermore, the measurements with the flash simulator show a much smaller variation in the short-circuit current of the subgroups. This suggests that the flash simulator has a better area related uniformity than the LASS.

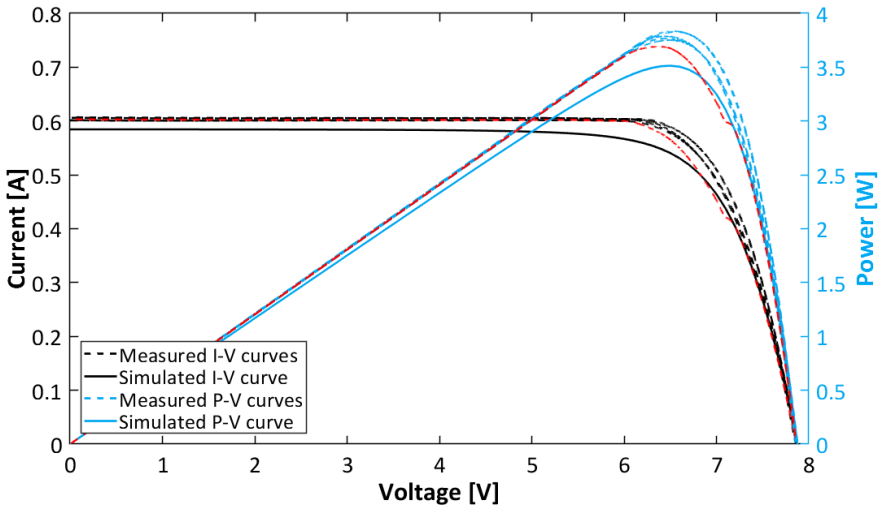

Figure D.1: *Measured and simulated I-V and P-V curves of the six subgroups in the prototype. The red lines correspond to a subgroup with a faulty solar cell.*

To minimize temperature changes under the LASS, only 150 data point were obtained during an interval or around 10 seconds. The flash solar simulator however, allows tracing the I-V curve at a rate of 3500 data points per flash which takes less than a second. Therefore, the temperature of solar cells will not change significantly. Consequently, the accuracy of the I-V curve increases. Now, a small dip in the I-V curve of one of the subgroups can be seen. This suggests that this subgroup contains a faulty solar cell. Finally, the measurements show a slightly higher fill factor than the simulations. The reason is that the tracing the I-V curve of a solar cell for parametrization is prone to errors in the series resistance of cells. This indirectly affects the fill factor.

The I-V and P-V curves for the *6 series* and *6 parallel* architectures of the prototype are shown in Figure D.2. A comparison of the measured and simulated results leads to the same conclusions about the temperature, optical gains and fill factor. Due to the better area related uniformity of the flash simulator, the minor steps in the short-circuit current of the series connected module as shown in Figure 6.10a have now disappeared.

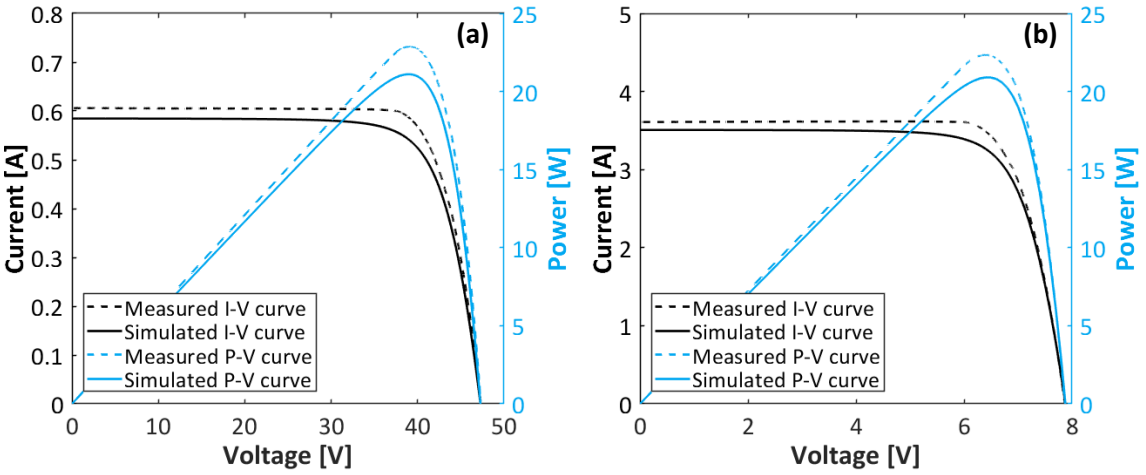

Figure D.2: *Measured and simulated I-V and P-V curves of (a) the 6 series and (b) the 6 parallel module architecture of the prototype under uniform illumination conditions.*

Measurements are performed for the *6 parallel* and reconfigurable PV module architectures. Unfortunately, the I-V curves under partial shading conditions cannot be traced for the *6 series* topology of the prototype. This is because the pulse duration of the flash simulator is too short to activate smart bypass diodes. As no new conclusions are drawn from these measurements, the results are not discussed in detail. In summary, the flash simulator increases the accuracy of the I-V and P-V curves and hence decreases the deviations between the measured and simulated results.

Delft University of Technology

Mekelweg 5
2628 CD Delft
The Netherlands

E: info@tudelft.nl
T: +31 15 278 9111

Raoul Weegink received a BSc degree in Applied Physics (*cum laude*) from Delft University of Technology, the Netherlands in 2017. During his bachelor, he participated in an exchange program with the University of British Columbia, Canada where he studied for five months with a focus on global climate change.

He is currently working towards the MSc degree in Sustainable Energy Technology with a specialisation in photovoltaic energy.